Investigating the impacts of upgrading a full-scale conventional activated sludge process with a hybrid membrane aerated biofilm reactor

by

Narasimman Lakshminarasimman Meanakshi Sekar

A thesis

presented to the University of Waterloo

in fulfilment of the

thesis requirement for the degree of

Doctor of Philosophy

in

Civil Engineering – Water

Waterloo, Ontario, Canada, 2024

Examining Committee Membership

The following served on the Examining Committee for this thesis. The decision of the Examining Committee is by majority vote.

External Examiner	Dr. Glen T. Daigger Professor of Engineering Practice, Department of Civil and Environmental Engineering, University of Michigan, MI, USA.
Supervisor	Dr. Wayne J. Parker Professor, Department of Civil and Environmental Engineering, University of Waterloo, ON, Canada.
Internal Members	Dr. Anh Pham Assistant Professor, Department of Civil and Environmental Engineering, University of Waterloo, ON, Canada.
	Dr. José R. Bicudo Adjunct Professor, Department of Civil and Environmental Engineering, University of Waterloo, ON, Canada.
Internal-external Member	Dr. Mark R. Servos Professor, Department of Biology, University of Waterloo, ON, Canada.

Author's declaration

This thesis consists of material all of which I authored or co-authored: see Statement of Contributions included in the thesis. This is a true copy of the thesis, including any required final revisions, as accepted by my examiners.

I understand that my thesis may be made electronically available to the public.

Statement of Contributions

Chapter 2 – I designed the study plan, coordinated the sampling campaigns, analyzed the samples, collected all relevant data on plant operations, performed data analysis, drafted the chapter, and incorporated revisions. Dr. Wayne Parker, my supervisor, contributed towards the study plan, interpretation of the results, and revising the chapter. This chapter will be converted into a manuscript and submitted for a peer-reviewed publication later.

Chapter 3 – I designed the study plan, harvested membrane biofilm samples, obtained biofilm scans, performed image analysis, analyzed the thickness and microbial community data, drafted the chapter, and incorporated revisions. Ms. Michelle McKnight from the University of Waterloo performed all the analytical work related to the microbial community analysis, contributed to the data analysis and interpretation, and reviewed the draft. Dr. Wayne Parker contributed towards the study plan, supervised the research, and edited the chapter. Dr. Josh Neufeld from the University of Waterloo provided input on the study design, interpretation of the results, and reviewed the chapter draft. This chapter will be converted into a manuscript and submitted for a peer-reviewed publication later.

Chapter 4 – I collected the N_2O data, simulated the full-scale plant in the simulation platform (SIMBA#), curated the input data, contributed to developing the improved N_2O model, performed simulations, analyzed the modeling results, drafted the chapter, and incorporated revisions. Mr. Michael Ogurek from ifak – Institute for Automation and Communication, modified the existing features in the SIMBA# platform and created an advanced MABR model block for this study. Mr. Oliver Schraa and Dr. Mirzaman Zamanzadeh from InCtrl Solutions contributed towards model development, interpretation of the results, and edited the chapter. Dr. Wayne Parker contributed towards the study plan, supervised the research, contributed towards model development, interpretation of the results and edited the chapter. This chapter will be converted into a manuscript and submitted for a peer-reviewed publication later.

Chapter 5 – I designed the study plan, coordinated the sampling campaigns, processed the data, drafted the chapter, and incorporated revisions. Ms. Sandra Salic and Ms. Rashne Vakharia from the University of Waterloo contributed to sample extraction, instrumental analysis, and post-processing of the chromatographic data. Ms. Leslie Bragg from the University of Waterloo developed the analytical method, supported data processing, interpretation, and analysis, and reviewed the draft of the chapter. Dr. Mark Servos provided inputs to the study plan, interpretation of the data, and reviewed the chapter. Dr. Wayne Parker contributed towards the study plan, interpretation of the results, and edited the chapter. This chapter will be converted into a manuscript and submitted for a peer-reviewed publication later.

Abstract

Membrane aerated biofilm reactors (MABR) are an emerging wastewater treatment technology that offer several process advantages such as higher aeration efficiency, simultaneous nitrification and denitrification, and reduced nitrous oxide (N_2O) emission. However, the current knowledge on MABR operations is largely based on bench- and pilot-scale systems that differ in mixing conditions, biofilm thickness control strategies, and cassette arrangement from those employed in full-scale. This study bridged this critical knowledge gap by investigating the long-term performance (20 months) of one of the largest MABR installations in North America and reported the findings on a wide range of responses related to effluent quality, electricity consumption, N_2O emissions, and biofilm characteristics.

The key performance metrics related to nitrogen removal, aeration tank operations, and electricity consumption were monitored in a full-scale conventional activated sludge (CAS) before and after upgrading with a hybrid MABR. The inclusion of the hybrid MABR process improved the seasonal nitrification observed in the CAS process before the upgrade to year-round ammonia removal. Denitrification in the hybrid MABR doubled the TN removal in the plant from 30-40% before upgrade to 70-80% afterwards. Operation at reduced MABR airflow (4.5 NL m^{-2} hr^{-1}) resulted in lower nitrification rates due to insufficient biofilm thickness control that led to diffusional limitations. Temperature was found to impact nitrification in the MABR with a 22% decrease in nitrification rate from 1.8 ± 0.2 g-N m^{-2} d^{-1} during warm weather to 1.4 ± 0.2 g-N m^{-2} d^{-1} during cold weather conditions. Operation at higher MABR airflow (6 NL m^{-2} hr^{-1}) increased the NH_4-N removal efficiency in the aeration tank during cold weather conditions suggesting increased nitrifier seeding due to enhanced sloughing of biofilm into the suspended sludge. The hybrid MABR process achieved high denitrification efficiency (80-97%) throughout the study and was not substantially impacted by ammonia loading, process airflow, or wastewater temperature. Aeration related electricity consumption, as described by volumetric energy intensity (kWh m^{-3}), decreased by 50% after the upgrade due to the efficiency of oxygen supply by the MABR and the reduction of aeration requirements downstream aeration basin. Overall, the improved N removal under reduced electricity consumption at full scale demonstrated the potential of MABR as a suitable process intensification technology.

Pollutant removal in biofilm processes such as membrane aerated biofilm reactors (MABR) is directly influenced by the biofilm thickness and microbial community functions. However, these biofilm characteristics have not been studied in full-scale MABR systems before. This study addressed this knowledge gap by characterizing the spatial and operational dynamics of key biofilm properties such as thickness, and microbial community structure and functionalities in a full-scale MABR facility. The arrangement of the MABR cassettes in an array along the length of the plug flow MABR train resulted in

a longitudinal biofilm thickness gradient. The biofilms on the front cassettes were more than twice as thick as those on cassettes at the back. Examination of biofilm thickness as a function of MABR process airflow indicated that a lower airflow (4.5 NL m^{-2} hr^{-1}) resulted in a thicker biofilm (> 1000 μm) throughout the tank. Consistent with the trends in thickness, analysis of Bray-Curtis dissimilarity index showed that there were differences in the biofilm microbial community composition along the length of the MABR tank and between operating phases. Thicker biofilms in the front cassettes of the full-scale tank were predicted to have a higher relative abundance of organisms with anaerobic functions such as fermentation and sulfur reduction and lower relative abundance of organisms with aerobic functions such as aerobic heterotrophy and nitrification. *Nitrosomonas* was identified to be the main ammonia oxidizer and *Nitrospira* and *Nitrotoga* were the main nitrite oxidizers in the biofilm samples. The 16s RNA gene profiles were strongly correlated with biofilm thickness (R^2 = 0.8) and MABR nitrification rate (R^2 = 0.4). Phases with thinner biofilm showed higher relative abundance of nitrifiers which corresponded to higher nitrification rates. Thus, optimizing the process airflow to provide adequate biofilm thickness control is key to maximizing nitrification rate in full-scale MABR.

Biological nitrogen removal often results in emission of nitrous oxide (N_2O) which is a highly potent greenhouse gas. Current published models for N_2O emissions in MABR have several simplifications that are not representative of full-scale systems. This study developed an improved MABR N_2O model that captured commonly overlooked phenomena such as back diffusion of generated N_2O into MABR lumen gas and the recirculation of the N_2O laden lumen gas for tank mixing and biofilm thickness control. The improved model was validated with measured N_2O concentrations in the lumen gas phase and bulk mixed liquor in a full-scale hybrid MABR facility. The validated model was used to obtain insights into N_2O bioconversion pathways. Model predictions revealed that all N_2O generated in the inner layers of the biofilm, which back diffused into the lumen gas, was via ammonium oxidizing organism activity. The N_2O transported to the outer biofilm layers was reduced via the heterotrophic denitrification pathway. The N_2O gas model predicted that up to 70% of the N_2O carried by the recirculated lumen gas was scrubbed into the mixed liquor which was further denitrified. An N_2O emission factor of 0.18 ± 0.01% N_2O-N/N load was estimated for the full-scale MABR process which removed up to 50% of the influent N load, highlighting the potential of this technology to mitigate N_2O emissions when compared to conventional activated sludge.

Release of organic micropollutants (OMP) such as pharmaceuticals and personal care product ingredients in the treated wastewater effluents is concerning as these compounds could have harmful effects in the aquatic ecosystem. This study monitored the removal of 16 OMPs over multiple seasons in a full-scale CAS before and after an upgrade with a hybrid MABR process. A comparison of OMP concentrations in

the plant effluent showed that 12 out of 16 target compounds were present at lower concentrations after the upgrade. An examination of plantwide removal efficiencies revealed that highly removable compounds (> 75%) such as acetaminophen, ibuprofen, naproxen, triclosan, triclocarban, and norfluoxetine and the recalcitrant carbamazepine were not impacted by the addition of the MABR process. However, six compounds namely gemfibrozil, sulfamethoxazole, trimethoprim, atorvastatin and its ortho- and para- hydroxy metabolites, that were poorly removed (< 25%) by the CAS configuration had moderate removals (25 to 75%) with the hybrid MABR/CAS configuration. After the MABR upgrade it was found that six OMPs showed higher removal under warm weather conditions (19.3 ± 1.6℃) when compared to cold weather conditions (13 ± 1.2℃). Mass balance analyses on the MABR tank revealed a broad range of compound specific responses such as complete biotransformation (acetaminophen), partial removal (naproxen), and compound formation from unmeasured precursors (sulfamethoxazole, carbamazepine). Overall, long-term monitoring of the full-scale facility before and after the upgrade revealed that upgrading of CAS to a hybrid MABR configuration can enhance the removal of some OMPs that are poorly removed by the CAS process alone.

Acknowledgements

It is a rare privilege to study an emerging technology at full-scale and an even rarer one when it is the 'first-of-its-kind'. I'm extremely grateful to my supervisor and mentor, Dr. Wayne Parker, for taking me on, creating a unique opportunity to 'poke and prod' the first full-scale MABR installation in Canada, and guiding me through this learning experience. Over the last five years, Dr. Parker has generously invested his time supervising my thesis research and other independent studies, which has helped me grow as a researcher and a wastewater engineer. He has also played a significant role in my all-round development including university teaching, public speaking, and academic writing. Joining his research group has been the best decision of my professional career. While I will miss being his PhD student, I look forward to continuing our fruitful collaboration in the future.

I am extremely thankful to Dr. Mark Servos and Ms. Leslie Bragg for generously providing all the resources I needed to study the removal of organic micropollutants. Working with their collaborative research group has been a highly rewarding experience. I would also like to acknowledge Ms. Sandra Salic and Ms. Rashne Vakharia from the Servos Lab for their diligent hard work with the analysis of organic micropollutants. Thanks to Ms. Sondus Jamal, my colleague in Parker and Servos Lab, for her support with some of the sampling activities and helpful discussions.

I am very thankful to Dr. Josh Neufeld and Ms. Michelle McKnight for their enthusiastic participation in this project to study the microbial community. A very special thanks to Michelle for guiding me through the world of microbial ecology and patiently answering all my questions.

I would also like to thank Dr. Mirzaman Zamanzadeh and Mr. Oliver Schraa from InCtrl Solutions, Canada, for their collaboration with the modeling component of this research. Mirzaman trained me to use the SIMBA# platform and offered plenty of support with setting up the full-scale plant model. The weekly meetings with Mr. Oliver Schraa and Dr. Wayne Parker during the N_2O model development were an invaluable opportunity to learn from both the modeling experts.

I would like to acknowledge Dr. João Firmino for his assistance with getting the biofilm images using OCT technology at the Center for Advanced Light Microscopy (CALM) facility at McMaster University.

Thanks to all the members of my PhD exam committee Dr. Glenn Daigger, Dr. Mark Servos, Dr. Anh Pham, Dr. Jose Bicudo, and Dr. Wayne Parker for their time and insightful feedback on my dissertation.

Finally, I would like to thank all the operational staff at the study site for providing access to the facility at the plant and sharing the operational data. Their cooperation with this study has been instrumental in achieving all our research objectives.

Dedication

To my mom, Mrs. R. Parvatha Varthini

To my dad, Mr. L. Meanakshi Sekar

Table of contents

List of figures

List of tables

List of abbreviations

ACE – Acetaminophen

AE – Aeration efficiency

AOO – Ammonia oxidizing organisms

AT – Aeration tank

ATOR – Atorvastatin

BOD – Biological oxygen demand

bON – Biodegradable organic nitrogen

bsCOD – Biodegradable soluble chemical oxygen demand

CAFF – Caffeine

CAS – Conventional activated sludge

CBZ – Carbamazepine

COD – Chemical oxygen demand

DCF – Diclofenac

DO – Dissolved oxygen

DE – Denitrification efficiency

DNR – Volumetric denitrification rate

FAPROTAX - Functional annotation of the prokaryotic taxa

FLX - Fluoxetine

GFZ – Gemfibrozil

GHG – Greenhouse gas

HRT – Hydraulic retention time

IBU – Ibuprofen

KPI – Key performance indicator

LNSE – Logarithmic Nash-Sutcliffe co-efficient of efficiency

MABR – Membrane aerated biofilm reactor

MBR – Membrane bioreactor

MBBR – Moving bed biofilm reactor

MDL – Method detection limit

MLSS – Mixed liquor suspended solids

MMT – Maximum measurable thickness

N – Nitrogen

NFLX – Norfluoxetine

NOO – Nitrite oxidizing organisms

NPX – Naproxen

NR – Nitrification rate

o-ATOR – ortho-hydroxy atorvastatin

OCT – Optical coherence tomography

OHO – Ordinary heterotrophic organisms

OMP – Organic micropollutant

p-ATOR – para-hydroxy atorvastatin

PBS – Phosphate buffer saline

PBIAS – Percentage bias

PCoA – Principal coordinates analysis

OTE – Oxygen transfer efficiency

OTR – Oxygen transfer rate

RPD – Relative percentage difference

SND – Simultaneous nitrification and denitrification

SOTE – Standard oxygen transfer efficiency

SOTR – Standard oxygen transfer rate

SRT – Solids retention time

SULF – Sulfamethoxazole

TCS – Triclosan

TCCB – Triclocarban

TKN – Total Kjeldahl nitrogen

TMP – Trimethoprim

TN – Total nitrogen

TSS – Total suspended solids

VFD – Variable frequency drive

VSS – Volatile suspended solids

WRRF – Water resource recovery facilities

Chapter 1 - Introduction

1.1 Challenges in conventional activated sludge processes

Water Resource Recovery Facilities (WRRF) are critical municipal infrastructure that treat wastewater, protect surface water quality, and ensure sanitation for communities. WRRFs are engineered systems that integrate physical, chemical, and biological unit operations to remove different constituents from the wastewater. Conventional Activated Sludge (CAS) (Figure 1.1a) is the most common design where wastewater components are broken down by a mixed consortium of microorganisms in a suspension called 'activated sludge' that is continuously aerated and recycled in the system to maintain a high population of active biomass (Metcalf and Eddy et al., 2014). Aeration provides oxygen for microbial respiration and pollutant removal and mixes the bulk phase.

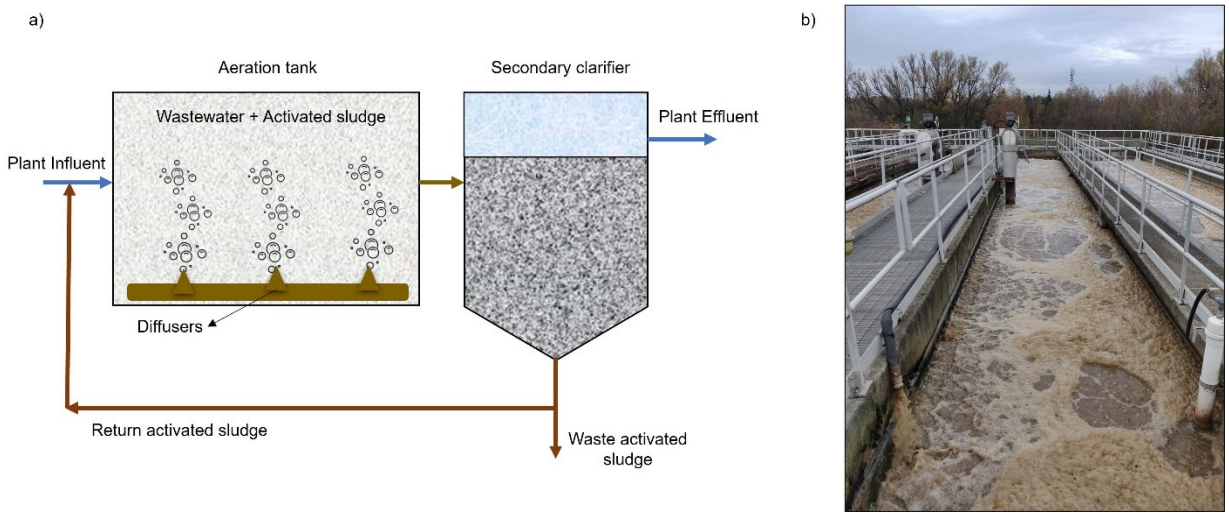

Figure 1.1 – a) Typical CAS process flow diagram and b) picture of an aeration tank with diffused aeration.

Since its development in 1914, the CAS system and its various modifications have been successfully employed to minimize the release of organic matter and nutrients into our water bodies (Jenkins & Wanner, 2014). However, the CAS process suffers from several design and operation related challenges. The main challenges are:

i) *High electricity consumption*: In Ontario, WRRFs consume about 1/3 of all the municipal electricity supplied and the aeration process represents about 60% of the total energy consumed by the WRRF (IESO, 2018). Such high demand for energy in wastewater treatment is partially due to the inefficiencies in aerator design. Typically, the aeration process in CAS systems is diffusion-based where the air from the blowers is bubbled from an array of diffusers at the bottom

of the tank (Figure 1.1). Typical fine bubble diffusers in a 4.5 m deep aeration tank can achieve only 25-35% oxygen transfer efficiency (OTE) (Metcalf and Eddy et al., 2014). This is because the bubbles reside in the bulk liquid for a relatively short period of time leading to poor gas transfer. Also, diffused aeration systems operate under relatively high pressure to overcome hydrostatic forces in the bulk liquid thereby increasing the electricity demand. Thus, the conventional mode of oxygen delivery to the activated sludge is inefficient. Improvements in process design to increase oxygen mass transfer and reduce energy requirements are desirable.

ii) *Winter nitrification*: WRRFs rely on nitrification to remove ammonia, a highly toxic nutrient, from the wastewater. The microorganisms that carry out the nitrification process are sensitive to low temperatures where their growth rate slows by 6-10% for every 1°C drop in temperature (Knowles et al., 1965). Hence nitrification in treatment plants located in temperate climates require longer solids residence time (SRT) to compensate for the slower growth kinetics during winter. However, longer SRTs typically require additional bioreactor volume, secondary clarifier capacity, and increased oxygen demand which in turn increases aeration requirements. Hence, design modifications that overcome winter nitrification challenges without significant plant capacity expansion are desirable.

iii) *Nitrous oxide emissions*: Biological nitrogen removal in the CAS process produces nitrous oxide as an intermediary product which is stripped off and emitted from the bioreactor by the aeration process (Kampschreur et al., 2009). N_2O emissions from WRRFs are concerning because it is a highly potent greenhouse gas with approximately 296 times more global warming potential than carbon dioxide (IPCC, 2007). It has been suggested that process related N_2O emissions could account for a major share of a WRRF's carbon footprint (Daelman et al., 2013; de Haas & Andrews, 2022). It is imperative to implement appropriate technologies to mitigate N_2O emissions from wastewater treatment to reduce its carbon footprint.

iv) *Discharge of organic micropollutant*: Organic micropollutants (OMP) are a broad class of anthropogenic chemicals including pharmaceuticals and personal care product ingredients that are found in trace levels (ng/L to µg/L range) in wastewaters (Stamm et al., 2016). CAS processes do not eliminate all of these compounds completely and OMPs are often discharged into receiving waters where they could have negative effects on the aquatic ecosystem (Alvarino et al., 2018). Hence, alternative treatment technologies that can minimize the release of these harmful chemicals into the environment must be evaluated.

On the whole, the CAS processes face many limitations in terms of technology footprint, electricity consumption, GHG emissions, and effluent quality. Hence, there is a critical need for alternative technologies that could alleviate these challenges and improve the overall sustainability of treatment.

1.2 MABR – An emerging alternative

The Membrane Aerated Biofilm Reactor (MABR) is a novel technology that promises energy-efficient and reliable wastewater treatment. In MABRs, oxygen is delivered to the biomass through a hollow fiber membrane which also serves as a medium for biofilm growth (Figure 1.2). Through this targeted, 'bubble-less' gas delivery, OTEs can be improved to as high as >90% with up to 6 kg of O_2 transferred per kWh of energy consumed (Côté et al., 2015). When compared to conventional aeration designs (1.2-1.6 kg O_2/kWh), membrane aeration can provide up to 5 times more gas transfer per unit of energy consumed. This improvement is in part due to the delivery of oxygen through the membranes that reduces the hydrostatic back pressure that is prevalent in conventional diffused aeration. Thus, the blowers for MABRs can be operated under relatively lower pressures and high OTEs can be achieved with reduced airflow.

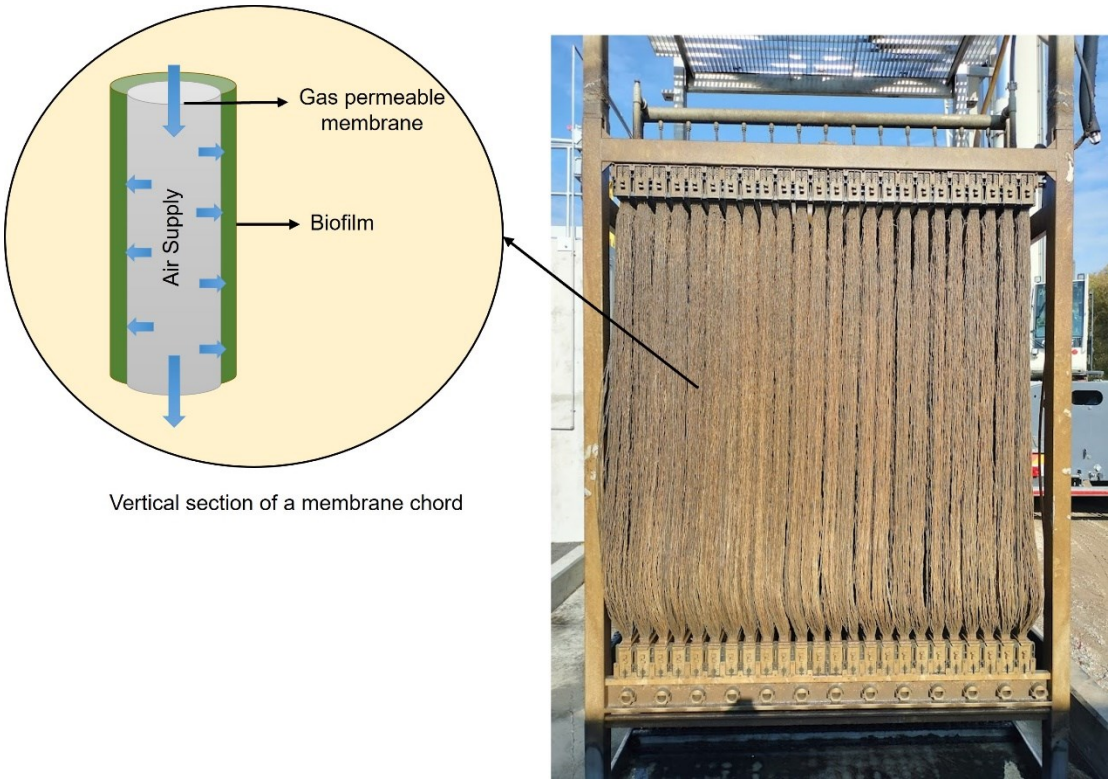

Figure 1.2 – Oxygen delivery in MABRs

The MABR process offers several other process benefits in addition to improved aeration.

- Traditional nitrogen removal in WRRFs involves a multistep biochemical pathway that typically requires two different operating zones: Conversion of NH_3 into nitrite (NO_2^-) and subsequent oxidation of nitrite into nitrate (NO_3^-) occurs under oxic conditions, while nitrate is reduced to nitrogen gas (N_2) in the absence of oxygen. MABRs, with their unique layering of microbes of

different nutrient removal functions in the biofilms can support simultaneous nitrification denitrification (SND) in the same reactor. SND offers two advantages- i) total N removal can be achieved through short cut nitrogen removal to reduce aeration requirements ii) the need for two separate zones with associated recycle streams is eliminated thereby reducing the technology footprint and pumping costs. Further hybrid configurations that combine MABR with suspended sludge can be employed for simultaneous removal of carbon and nutrients (Peeters et al., 2017).

- The presence of biofilms in MABR decouples the hydraulic retention time (HRT) from the solids retention time (SRT). This enables the immobilization of slow growing microorganisms on the membrane biofilms that can enhance nutrient removal without the need for long bulk phase SRTs and associated increased secondary clarifier capacity.
- MABRs can be easily retrofitted into existing systems and provide 'process intensification' of the plant. With proper membrane packing MABRs can provide a high specific surface area for gas transfer and biomass attachment increasing the system capacity to handle high pollutant loadings while maintaining stable operations (Duvall, 2017).

Owing to these advantages, the MABR technology has been successfully applied for the treatment of surface water (Li et al., 2016b), pharmaceutical wastewater (Wei et al., 2012b), landfill leachate (Syron et al., 2015), high strength industrial wastewater (Li et al, 2016; Stricker et al., 2011), and municipal wastewater (Côté et al., 2015; Downing et al., 2010; Houweling et al., 2016; Kunetz et al, 2016; Peeters et al., 2016). Since its initial development, the feasibility of MABR for municipal wastewater treatment has been well established in bench-scale units operated under laboratory conditions (Bunse et al., 2020; Downing & Nerenberg, 2008c; Hibiya et al., 2003; Lackner et al., 2010; Mehrabi et al., 2020; Terada et al., 2006). There have been a few pilot-scale MABR studies that have demonstrated simultaneous carbon and nitrogen removal from municipal wastewater over relatively short operational periods(Corsino & Torregrossa, 2022a; Long, et al., 2020; Peeters et al., 2017; Ravishankar et al., 2022a; Uri-Carreño et al., 2021). However, the performance of the MABR system has not been investigated in detail at full-scale with multiple MABR cassettes under varying operating conditions. It is unclear whether the potential observed at small-scale can be maintained for extended periods in full-scale applications with real wastewater and dynamic operating conditions.

1.3 Objectives of the research

The overarching goal of this study was to conduct a comprehensive assessment of the performance of a full-scale hybrid MABR process in terms of its effluent quality, energy consumption, and N_2O emissions. In line with that, the specific objectives of the research are to:

O1. Compare key performance indicators related to carbon and nitrogen removal and electricity consumption at a full-scale WRRF before and after an MABR upgrade.

O2. Evaluate the impact of MABR airflow, influent loading, and wastewater temperature on the nitrification and denitrification performance of a full-scale hybrid MABR.

O3. Characterize spatial and operational variations in biofilm thickness in a full scale MABR to obtain insights into factors affecting process performance.

O4. Characterize the microbial community in the MABR biofilm as a function of location and operating conditions and correlate the community profile with MABR performance.

O5. Develop and validate an improved model to describe the spatial and diurnal dynamics of N_2O emissions from a full-scale hybrid MABR process.

O6. Evaluate whether upgrading a full-scale WRRF with a hybrid MABR enhanced removal of OMPs during different seasons.

1.4 Thesis outline

This dissertation is organized into six chapters and the contents in each of these chapters are summarized below:

Chapter 1 introduces the problem statement, background on MABR systems, and the objectives of this research.

Chapter 2 presents a long-term study addressing carbon and nitrogen removal and energy consumption at a full-scale WRRF before and after an MABR upgrade. This chapter addresses research objectives O1 and O2.

Chapter 3 describes a study of biofilm thickness and the biofilm and suspended sludge microbial community profiles over the study period. Chapter 3 pertains to research objectives O3 and O4.

Chapter 4 presents the formulation, validation, and application of an improved process model to describe the spatial and temporal trends in N_2O emissions from a full-scale hybrid MABR process addressing the research objective O5.

Chapter 5 reports on a study of the fate of OMP in the WRRF across multiple seasons that spanned the MABR upgrade and the answers the research question in O6.

Chapter 6 provides a summary of the main conclusions from this research work, outlines the impact of the study, and lists suggestions for future research.

Chapter 2 - Long term performance evaluation of a full-scale hybrid membrane aerated biofilm reactor (MABR) facility

Abstract

Membrane aerated biofilm reactors (MABR) are emerging to be a popular alternative for intensifying wastewater treatment. However, the performance of the technology has not yet been investigated at full-scale where mixing conditions and biofilm thickness control strategies differ from those employed in smaller-scale MABRs. This study investigated the long-term performance (20 months) of one of the largest MABR installations in North America and reported key performance metrics related to nitrogen removal, aeration tank operations, and electricity consumption. Prior to the addition of the hybrid MABR upstream of the aeration tank the plant was only capable of seasonal nitrification. After upgrading with the MABR the plant achieved high levels of ammonia removal year-round. Denitrification in the hybrid MABR doubled the TN removal in the plant from 30-40% before upgrade to 70-80% afterwards. Operation at reduced MABR airflow (4.5 NL m^{-2} hr^{-1}) resulted in lower nitrification rates due to insufficient biofilm thickness control that led to diffusional limitations. Temperature was found to impact nitrification in the MABR with a 22% decrease in nitrification rate from 1.8 ± 0.2 g-N m^{-2} d^{-1} during warm weather to 1.4 ± 0.2 g-N m^{-2} d^{-1} during cold weather conditions. Operation at higher MABR airflow (6 NL m^{-2} hr^{-1}) increased the NH_4-N removal efficiency in the aeration tank during cold weather conditions suggesting increased nitrifier seeding due to enhanced sloughing of biofilm into the suspended sludge. The hybrid MABR process achieved high denitrification efficiency (80-97%) throughout the study and was not substantially impacted by ammonia loading, process airflow, or wastewater temperature. Aeration related electricity consumption, as described by volumetric energy intensity, decreased by 50% after the upgrade due to the efficiency of oxygen supply by the MABR and the reduction of aeration requirements downstream aeration basin. Overall, the improved N removal under reduced electricity consumption at full scale demonstrated the potential of MABR as a suitable process intensification technology.

Keywords: MABR, simultaneous nitrification and denitrification, electricity consumption, aeration efficiency

2.1 Introduction

Aeration of activated sludge is highly energy intensive, typically consuming over half of all the electricity used in wastewater treatment (IESO, 2018). This is because of high backpressures, poor aeration efficiency and low oxygen transfer rates of diffused aeration (Metcalf and Eddy et al., 2014). The membrane aerated biofilm reactor (MABR) process is a bubbleless aeration technology capable of high oxygen transfer rates (Perez-Calleja et al., 2017; Syron & Casey, 2008) with significantly lower electricity consumption (Aybar et al., 2015). MABRs consist of a bundle of gas permeable, dense membranes that diffuse oxygen directly to the biofilm grown on the membrane surface (Casey et al., 1999). The oxygen demand exerted by the biofilm bioactivity further increases the gas transfer rate (Pellicer-Nàcher et al., 2013). Counter diffusion of substrates such as oxygen from membrane side and BOD or ammonia from the bulk liquid side results in unique microbial stratification that can potentially achieve simultaneous nitrification and denitrification (SND) in the same reactor (Martin & Nerenberg, 2012). SND can also be achieved with MABRs in a hybrid configuration with an anoxic mixed liquor for high denitrification rates (Downing et al., 2010; Downing & Nerenberg, 2008b). Thus, MABRs are an attractive alternative for process intensification, and it is critical to investigate their real-world performance to promote wider adoption.

Factors influencing MABR performance have been investigated previously to identify optimal operational conditions to achieve maximum SND. Studies on bench-scale MABR systems with installed membrane surface areas between 0.1-15 m^2 have evaluated the impact of intra-membrane pressure (Dong et al., 2009; Terada et al., 2006), hydraulic retention time (Wei et al., 2012), ammonia and BOD loading (Downing & Nerenberg, 2008c), influent C/N ratio (H. Liu et al., 2010a) and wastewater temperature (Clements et al., 2024; Németh et al., 2023). However, early investigations with lab-scale MABR designs were challenged by membrane clumping, biofilm detachment, condensate accumulation, packing density, and inadequate biofilm scouring that adversely impacted the MABR performance (Downing et al., 2010; LaPara et al., 2006; Semmens et al., 2003; Terada et al., 2006). Recommendations have been made to investigate larger, representative MABR cassettes to assess the performance at scale (Lu et al., 2020; Martin & Nerenberg, 2012). Subsequently, with the development of full-scale commercial MABR products, larger-scale systems with one or two MABR cassettes and installed surface areas in the range of 1920-4400 m^2 have been employed in studies that have examined the impact of bulk phase oxidation-reduction potential (Uri-Carreño et al., 2023), ammonia loading (Houweling et al., 2017), wastewater temperature (Long et al., 2020), and C/N ratio (Ravishankar et al., 2022). However, studies of full-scale systems with an array of MABR cassettes have not been reported. Understanding the performance, at scale, under dynamic operating conditions is critical in establishing conditions that maximize the effectiveness of MABR systems.

Membrane air supply is an important process control variable in MABR operations as it influences the dissolved oxygen profile through the biofilm. Bench-scale studies have shown that higher intra-membrane air pressure increases the dissolved oxygen (DO) concentration at the membrane biofilm interface (Downing & Nerenberg, 2008a), enhances DO penetration in the biofilm (Wang et al., 2016), and increases the nitrification rate (Perez-Calleja et al., 2017). However, the mixing and air scouring configurations in these bench-scale studies differed from those employed in full-scale MABR systems. Commercial MABR cassettes such ZeeLung™, OxyMem™ recirculate the process air exiting the membrane lumen into the bulk to shear excess biofilm and maintain a desired biofilm thickness. Hence any changes in air supply to the MABR biofilm could potentially influence the biofilm thickness and its nitrification performance. Thus, the impact of airflow on MABR performance must be evaluated in its full-scale aeration design.

MABRs are often integrated within existing CAS processes for intensified treatment (Underwood et al., 2018). MABR upgrades can significantly impact the aeration tank performance in several ways. In this regard, the seeding of nitrifying organisms from the MABR biofilms into suspended sludge biomass and the resulting nitrification below 'washout SRT' is viewed as a major process benefit (Houweling & Daigger, 2019). Experimental investigations with lab-scale MABR/CAS systems have shown substantial nitrification in the aeration basin with solids retention times (SRT) as low as 3 days (Corsino & Torregrossa, 2022b; Houweling et al., 2018). However, the extent of the seeding effect in full-scale systems has not been investigated before. Moreover, the inclusion of an upstream MABR and the resulting reduction in loading can have other impacts on downstream aeration tank operations. The impact of MABR addition on the airflow and DO requirements in the CAS process has not been investigated before. Thus, process evaluations should consider a plantwide perspective to understand the overall impact of MABR technology.

Overall, the knowledge base on MABR performance is largely limited to investigations in lab-scale or full-scale systems with single cassette installations. There are major gaps in knowledge of the performance of full-scale MABRs when an array of cassettes is employed and the subsequent impact on plantwide operations. Hence, the objective of this study was to evaluate the treatment performance of a full-scale CAS process before and after upgrading with an array of MABR cassettes in one of the largest installations in North America. In this regard, carbon and nitrogen removal, airflow and DO requirements, and electricity consumption in the MABR and CAS process were monitored over three years. The extensive dataset generated was used to obtain insights into the impact of process airflow, wastewater loading, and seasonal temperature on the N removal performance of the MABR.

2.2 Methodology

2.2.1 Study Site

The study site initially consisted of a conventional activated sludge (CAS) configuration with an average rated capacity of 9,320 m^3 d^{-1}. The treatment sequence consisted of preliminary treatment with a 2 mm fine screen and grit removal in the headworks followed by secondary treatment in the aeration tanks (Figure 2.1). The CAS process consists of two aeration tanks (total volume = 2,404 m^3) that are equipped with fine bubble diffusers. The mixed liquor after aeration is treated with coagulants for chemical P removal. Three secondary clarifiers provide solids separation after which the secondary effluent is disinfected by chlorination. The plant was upgraded at the end of August 2022 to include an MABR process located in an upstream anoxic tank with return activated sludge recycled to it. The MABR tank has four parallel treatment trains (21.4 m long x 2.4 m wide x 3.1 m deep x 4 tanks = 637 m^3) with nine ZeeLung™ cassettes (Veolia Water Solutions and Technologies) in each train yielding a total membrane surface area of 69,120 m^2. The exhaust from the membranes is recycled to the integral diffuser at the base of the cassettes to provide mixing and sparging to shear off excessive biofilm growth.

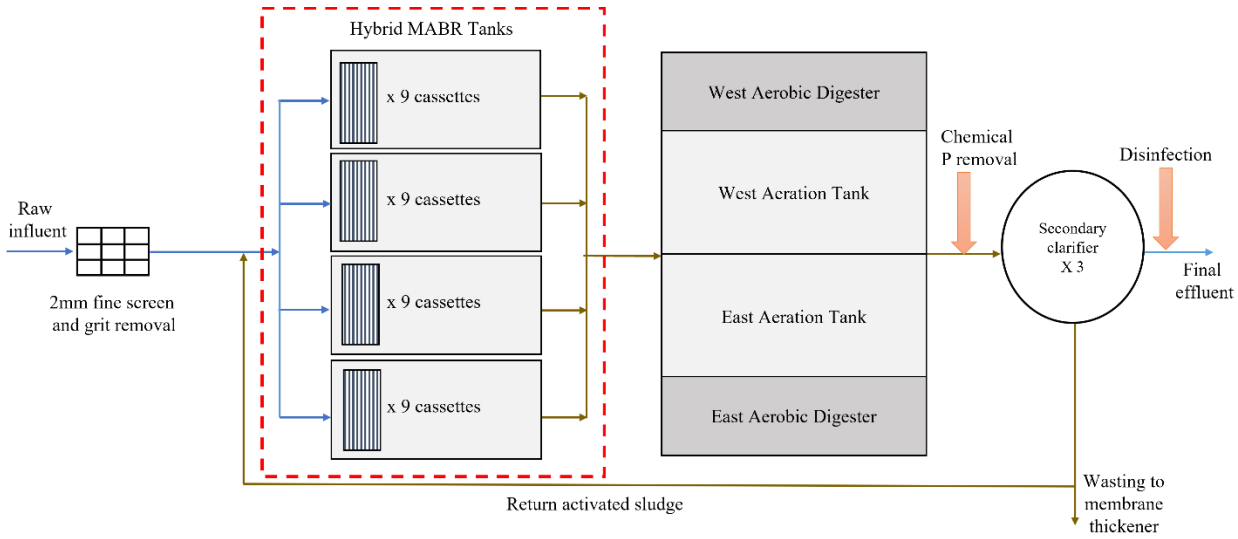

Figure 2.1 - Layout of the study site (not to scale). MABR is shown inside red dotted box.

2.2.2 Plant operating conditions post upgrade

The performance of the upgraded plant was assessed under 5 different operational conditions (Phases: Table 2.1) to support an assessment of the impact of MABR airflow, loading, and seasonality of wastewater temperature on SND performance. Over the 18-month test period (Sep 2022- Apr 2024, the mixed liquor temperature went through two full cycles of winter (12-15°C) and summer (15-20°C) temperatures. The air flow to the MABR was a primary operating variable controlling oxygen supply to

the membranes and the biofilm thickness as it supports scouring. Operation with air flows at 4.5, 5.5 and 6 NL m^{-2} hr^{-1} was examined. The loading of wastewater to the MABR was also expected to impact MABR performance as it impacts the HRT in the tanks as well as the loading of substrates (BOD and NH_4-N) to the biofilm. The impact of loading on the MABR performance was evaluated by removing one of the four MABR tanks from service during phase 2 such that the remaining three MABRs received an elevated NH_4-N loading of 3.9 ± 0.7 gN m^{-2} d^{-1}.

Table 2.1 – Operational conditions in the plant after upgrade. Values are average ± standard deviation.

Operational parameter	Phase 1	Phase 2	Phase 3	Phase 4	Phase 5
No. of days of operations	71	61	78	224	76
Temperature range (°C)	17.0 ± 1.0	14.0 ± 0.3	12.0 ± 0.7	19.0 ± 1.5	13.0 ± 0.44
MABR air flow (NL m^{-2} hr^{-1})	6.1 ± 0.1	5.4 ± 0.2	4.5 ± 0.2	5.9 ± 0.2	6.3 ± 0.2
No. of tanks	4	3	4	4	4
NH_4-N loading (gN m^{-2} d^{-1})	2.5 ± 0.3	3.9 ± 0.7	3.3 ± 0.4	2.9 ± 0.3	3.5 ± 0.3

2.2.3 Sampling and analytical methods

Before the MABR upgrade, 24-hour composite samples of the plant influent and final effluent were collected once a week using refrigerated autosamplers that were maintained at 2°C to minimize any biological activity. After the MABR upgrade, 24-hour composite samples of the plant influent, MABR influent, MABR effluent, and final effluent were collected three times a week (Monday, Wednesday, and Friday). Grab samples of the aeration tank and MABR mixed liquor, and the waste activated sludge were collected once a week. Where soluble species were analyzed, the samples were filtered using 0.45 µm nylon syringe filters. The NH_4-N concentrations in the filtered samples were measured using Hach TNT 832 and 830 methods depending on the concentration range. The NO_2^- and NO_3^- concentrations in the filtered samples were measured using ion chromatography (Dionex ICS 1100, Thermo Fisher Scientific) following Standard Method 4110. The TKN and BOD_5 in the total samples of the plant influent and effluent were measured following Standard Method - 4500-Norg D, Block Digestion and Flow Injection Analysis and modified APHA 5210 B, respectively. Total (TSS) and volatile (VSS) suspended solids in the plant influent, MLSS, and WAS streams were measured following Standard Methods 2540 D. The plant influent, effluent, RAS, and WAS flows, temperature, airflows, and dissolved oxygen concentration in the aeration basins were obtained from online sensors in the plant. The oxygen concentration in exhaust lumen gas was measured for each MABR train in a slip stream that received process air from all the

cassettes within the train. The exhaust lumen gas O_2 was measured continuously in each train using an online oxygen purity meter (Panametrics Oxy.IQ #31100, USA).

2.2.4 Plant performance metrics

The data on wastewater quality and the plant operational data were used to calculate various performance metrics for the MABR and aeration tank separately and for the overall plant.

Overall plant performance: The overall plant performance was primarily evaluated based on the concentrations of key N species and BOD_5 in the plant effluent, and the total nitrogen (TN) and BOD_5 removal. TN concentrations were calculated as the sum of TKN+NO_2-N+NO_3-N concentrations and mass flows were computed as the product of measured flows and concentrations. Plantwide removal efficiencies for BOD_5 and TN were calculated as shown in equation 2.1.

$$Removal\ efficiency\ (\%) = \frac{M_{Plant\ Inf} - M_{Plant\ Eff}}{M_{Plant\ Inf}}\ x\ 100\ \% \quad \text{.....(2.1)}$$

$M_{Plant\ Inf}$ = BOD_5 or TN mass flow in influent (kg-BOD d^{-1} or kg-N d^{-1})

$M_{Plant\ Eff}$ = BOD_5 or TN mass flow in effluent (kg-BOD d^{-1} or kg-N d^{-1})

Oxygen transfer in MABR: Two oxygen transfer metrics (oxygen transfer efficiency (OTE) and oxygen transfer rate (OTR)) were calculated using the average measured exhaust O_2 concentrations of the MABR trains as shown in equations (2.2) and (2.3), respectively (Houweling et al., 2017).

$$OTE_{MABR} = \frac{0.209 - O_{2,E} * (\frac{1-0.209}{1-O_{2,E}})}{0.209} \quad \text{.....(2.2)}$$

$$OTR_{MABR} = \frac{OTE * Q_{air} * 0.209 * 32}{22.414 * A_{MABR}} \quad \text{.....(2.3)}$$

$O_{2,E}$= Daily average fraction of O_2 in MABR lumen exhaust (Average of 3 or 4 tanks)

Q_{air} = Daily average of air flow to lumen (NL hr^{-1})

A_{MABR} = Membrane surface area (m^2)

Nitrification rate in MABR: The area-specific nitrification rate was estimated using two different calculations that have different inherent assumptions. Method 1 (NR_{NHx}) was based on ammonia concentrations measured in the MABR influent and effluent composite samples using equation 2.4. NR_{NHx} does not include NH_4-N oxidized from the biodegradable organic nitrogen fraction (bON) of TKN. Hence, NR_{NHx} is considered to be a minimum estimate of nitrification rate, and the actual nitrification rate may be higher depending on the extent of bON hydrolysis in the MABR process.

$$NR_{NH_x} = \frac{Q_{Blend} * (M_{NH_4,MABR\ in} - M_{NH_4,MABR\ out})}{A_{MABR}} \quad \text{.....(2.4)}$$

NR_{NH_x}= Nitrification rate based on measured ammonia concentrations (g-N m^{-2} d^{-1})

Q_{Blend} = Blended raw influent and RAS flow (m^3 d^{-1})

$M_{NH_4,MABR\ in}$ = NH_4-N concentration in MABR influent (mg-N L^{-1})

$M_{NH_4,MABR\ out}$ = NH_4-N concentration in MABR effluent (mg-N L^{-1})

A_{MABR} = Total membrane surface area available for biofilm growth (m^2)

In Method 2 (NR_{OTR}) was calculated from oxygen transfer using the stoichiometric oxygen requirement for ammonia oxidation (Metcalf and Eddy, 2014). NR_{OTR} assumes that all the oxygen supplied is used only for ammonia oxidation and all the nitrite formed is further oxidized to nitrate. Hence, NR_{OTR} can be considered as an upper bound for the nitrification rate.

$$NR_{OTR} = \frac{OTR}{4.57 \frac{g-O_2}{g\ NH_4-N\ oxidized}} \quad \text{.....(2.5)}$$

NR_{OTR} = Nitrification rate based on oxygen transfer rate (g-N m^{-2} d^{-1})

Denitrification in MABR: The volumetric denitrification rate (DNR in kg-N m^{-3} d^{-1}) and the denitrification efficiency (DE in %) were calculated to characterize denitrification in the MABR tank using equations 2.6 and 2.7, respectively. The DNR and DE values are considered as minimum estimates of denitrification as they do not include nitrate generated by oxidation of organic nitrogen in the MABR.

$$DNR = \frac{M_{NO_3,MABR\ in} + M_{NO_3,gen} - M_{NO_3,MABR\ out}}{V_{MABR}} \quad \text{.....(2.6)}$$

$$DE = \frac{M_{NO_3,MABR\ in} + M_{NO_3,gen} - M_{NO_3,MABR\ out}}{M_{NO_3,MABR\ in} + M_{NO_3,gen}} * 100\ \% \quad \text{..... (2.7)}$$

$M_{NO_3,MABR\ in}$ = Mass flow of nitrate-N in MABR influent (kg-N d^{-1})

$M_{NO_3,MABR\ out}$ = Mass flow of nitrate-N in MABR effluent (kg-N d^{-1})

$M_{NO_3,gen}$ = Mass flow of nitrate-N generated through nitrification

$= M_{NH_4,MABR\ in} - M_{NH_4,MABR\ out}$ (kg-N d^{-1})

V_{MABR} = Volume of MABR basins (m^3)

The ratio of soluble biodegradable carbon (bsCOD) to nitrogen in the influent wastewater was calculated as an indicator of readily biodegradable carbon availability for denitrification in the MABR.

$$\frac{bsCOD}{N} = \frac{M_{sCOD,Inf} - M_{sCOD,Eff}}{M_{TN,Inf}} \quad \text{.....(2.8)}$$

$M_{sCOD,Inf}$ = Mass flow of soluble COD in the plant influent (kg-COD d^{-1})

$M_{sCOD,Eff}$ = Mass flow of soluble COD in the plant effluent (kg-COD d^{-1})

$M_{TN,Inf}$= Mass flow of total nitrogen in the plant effluent (kg-N d^{-1})

The oxygen credit per unit of wastewater treated that was obtained through anoxic BOD consumption in the hybrid MABR was calculated using Equation (2.9) (Metcalf and Eddy et al., 2014) to quantify the potential savings in aeration in the downstream aeration tank.

$$Oxygen\ credit\ \left(\frac{kg\ O_2}{m^3}\right) = \frac{2.86\ kg\ O_2}{kg\ NO_3{-}N} * \left(M_{NO_3,\ MABR\ in} + M_{NO_3,\ gen} - M_{NO_3,\ MABR\ out}\right) * Q_{Inf} \quad \text{.....(2.9)}$$

$\frac{2.86\ kg\ O_2}{kg\ NO_3-N}$ = Oxygen equivalence of using nitrate as electron acceptor.

Q_{Inf} = Plant influent flow ($m^3\ d^{-1}$)

<u>*Nitrification in aeration tank:*</u> The mass flow of TKN oxidized in the aeration tank post MABR upgrade was quantified through a nitrogen mass balance on the overall plant using equation (2.10)

$$M_{Nit,AT} = M_{TKN,Inf} - M_{Nit,MABR} - M_{TKN,Eff} - M_{N,WAS} \quad \text{.....(2.10)}$$

$M_{Nit,AT}$ = Mass flow of nitrification in aeration tank (kg-N d^{-1})

$M_{Nit,MABR}$ = Mass flow of nitrification in MABR = $M_{NH_4,MABR\ in} - M_{NH_4,MABR\ out}$ (kg-N d^{-1})

$M_{N,WAS}$ = Mass flow of N in WAS = $Q_{WAS} * X_{WAS,VSS} * f_N$ (kg-N d^{-1})

Q_{WAS} = Waste activated sludge flow

$X_{WAS,VSS}$ = VSS concentration in the WAS stream (mg-VSS L^{-1})

f_N = Fraction of nitrogen in WAS solids (g-N g-VSS^{-1})

Additionally, the removal efficiency of NH_4-N in the aeration tank was calculated to ascertain the extent of nitrification in the aeration tank across different phases of MABR operation post upgrade.

$$Removal\ efficiency\ (\%) = \frac{M_{NH_4,AT\ in} - M_{NH_4,AT\ out}}{M_{NH_4,AT\ in}}\ x\ 100\ \% \quad \text{.....(2.11)}$$

$M_{NH_4,AT\ in}$ = Mass flow of NH_4-N entering the aeration tank (kg-N d^{-1})

$M_{NH_4,AT\ out}$ = Mass flow of NH_4-N leaving the aeration tank (kg-N d^{-1})

2.2.5 Electricity consumption

Aeration-related electricity consumption was monitored to support estimation of the impact of MABR addition on energy use. The electricity demand by the turbo blowers used for the aeration tank was obtained directly from a continuous power monitor that was integrated into the blower instrumentation. In the case of the MABR facility, a Fluke energy logger (Model #1730) was installed on the electrical feed to the blowers to continuously monitor the electricity demand. The combined daily electricity consumption (kWh) for the MABR and aeration tanks was used to calculate two KPIs as per equations 2.12 and 2.13:

$$Volumetric\ energy\ intensity\ (\frac{kWh}{m^3}) = \frac{Daily\ electricity\ consumption\ (\frac{kWh}{day})}{Daily\ average\ flow\ (\frac{m^3}{d})} \quad \ldots\ldots (2.12)$$

$$Aeration\ efficiency\ \ (\text{kg}\ O_2/\text{kWh}) = \frac{Oxygen\ transfer\ rate\ (\frac{kg\ O_2}{d})}{Daily\ electricity\ consumption\ (\frac{kWh}{day})} \quad \ldots\ldots (2.13)$$

The oxygen transfer rates in MABR and aeration tank were calculated using different approaches. The MABR oxygen transfer rate (OTR_{MABR}) was calculated as per equation 2.3. The oxygen transfer rate in the aeration tank (OTR_{AT}) was estimated according to Metcalf and Eddy (2014) as per Equation 2.14. The values for the various correction factors in Equation 2.14 were assumed from literature. These assumptions could contribute to some degree of uncertainty with the OTR_{AT} estimation. The implication of the uncertainty on the findings is discussed later in the results section.

$$OTR_{AT} = \alpha * F * SOTR * \ \theta^{(T-20)} * (\frac{\beta C^*_{S,T,H} - C}{C_{S,20}}) \quad \ldots.. (2.14)$$

where,

α = Correction term for mass transfer co-efficient in wastewater = 0.44 (Calculated based on Rosso et al. (2005))

F= Fouling factor = 0.9 (Assumed based on Metcalf and Eddy (2014))

$SOTR$ = Standard oxygen transfer rate = $Q_{air} * SOTE * f_{oxy}$ (kg O_2 d^{-1})

Q_{air} = Airflow in aeration tank (m^3 d^{-1})

$SOTE$ = Standard oxygen transfer efficiency = 0.28 (Obtained from diffuser manufacturer)

f_{oxy} = concentration of oxygen in air (kg O_2 m^{-3}air)

Θ = Temperature correction factor = 1.024

T = Aeration tank operational temperature

β = Correction term for oxygen saturation concentration in wastewater = 0.9 (Assumed based on Metcalf and Eddy (2014))

$C^*_{S,T,H}$ = Saturation oxygen concentration in clean water at operational temperature and elevation (mg L^{-1})

C = Average dissolved oxygen concentration in the aeration tank (mg L^{-1})

$C_{S,20}$= Saturation dissolved oxygen concentration in clean water at 20°C and 1 atm (mg L^{-1})

2.2.6 Statistical analysis

The calculated performance indicators were compared between the different phases to assess the impact of operational variables on MABR performance. Since the number of sampling days and the variance in measurement differed between the phases, the non-parametric Kruskal-Wallis Test was used for analysis of variation between the groups. Dunn's post-hoc test was used for multiple comparisons of the

performance metrics between the five phases of operation. The P value was adjusted using a Bonferroni correction (α/number of comparisons (10)) from the standard 0.05 value to P*=0.005 to minimize the risk of Type I error when making multiple comparisons (Armstrong, 2014).

2.3 Results and discussion

2.3.1 Plant operations

The influent wastewater loadings and solids parameters in the plant were examined to establish the overall operational conditions in the plant throughout the study. Table 2.2 shows the influent loading and plant operations before and after the upgrade. The average influent flow and the BOD_5 and TKN loadings were similar between the pre- and post- upgrade period as seen in Table 2.2. The waste activated sludge (WAS) flows were also similar with averages of 278 ± 82 and 247 ± 59 m^3 d^{-1}, before and after the upgrade, respectively. The underflow solids concentration did not change either. The consistent solids wasting rate translated into similar aeration tank solids residence times of approximately 5 days with an MLSS concentration of ~3000 mg/L throughout the study period. Although the operating MLSS did not change, it could be anticipated that biomass likely changed in composition. The increased anoxic tank volume would shift some growth from the aeration basin and increase the overall SRT leading to increased endogenous decay of biomass relative to the period before the MABR upgrade. The MLSS would also include sloughed biofilm biomass that could have influenced the aeration tank nitrification performance because of nitrifier seeding (Corsino & Torregrossa, 2022b; Houweling & Daigger, 2019). Overall, the influent loading and aeration tank operations remained similar in the plant before and after the MABR upgrade. Thus, any observed changes in the plant performance post-upgrade were attributed to the addition of MABR and its various operational conditions.

Table 2.2 – Plant operations before and after MABR upgrade. Values shown as average ±standard deviation.

Parameter	Before upgrade (CAS)	After upgrade (MABR/CAS)
Monitoring period	Jan 2021 – Aug 2022	Sep 2022 – Mar 2024
Raw influent flow (m^3d^{-1})	6110 ± 620	6150 ± 592
BOD_5 loading (kg BOD d^{-1})	1910 ± 1508	1640 ± 445
TKN loading (kg N d^{-1})	304 ± 55	297 ± 39
WAS flow (m^3d^{-1})	278 ± 82	247 ± 59
MLSS concentration (mg L^{-1})	2998 ± 179	3053 ± 209
Aeration tank SRT (days)	5.35 ± 2.07	5.12 ± 0.99

2.3.2 Overall plant performance

The impact of the MABR upgrade on carbon and nitrogen removal across the overall plant was assessed based on BOD_5 and N species concentrations in the final effluent, respectively. The BOD_5 concentrations measured in the plant influent and final effluent alongside its removal efficiency are shown in Figure 2.2 The BOD_5 concentration in the plant effluent was in the range of 7 ± 6 mg/L throughout the study period (Figure 2.2) and did not change substantially after the upgrade. Correspondingly, the plantwide BOD_5 removal efficiencies were also similar with values of 96 ± 3% over the three-year monitoring period (Figure 2.2). The results were consistent with anticipated BOD_5 removals for CAS systems that are operated with an MLSS in the range of 2000-3000 mg/L and a 5-day SRT (Metcalf and Eddy, 2014). Overall, there was satisfactory year-round BOD_5 removal in the plant before the upgrade and the MABR addition did not alter the plantwide BOD_5 removal.

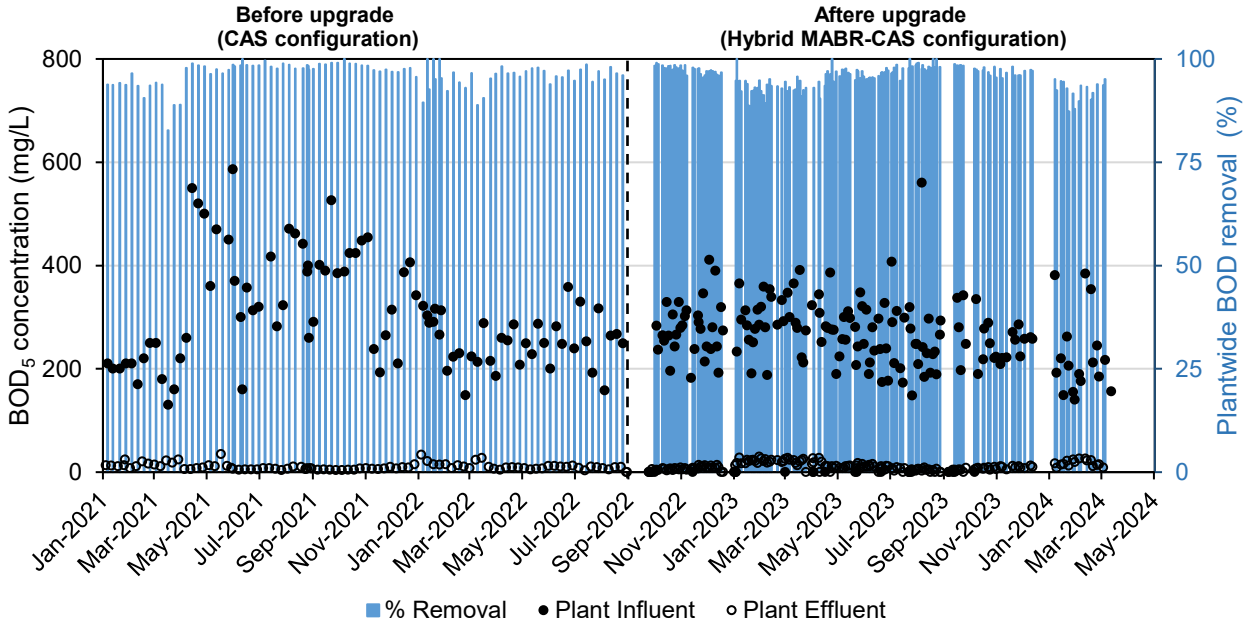

Figure 2.2 – BOD_5 concentrations and plantwide BOD_5 removal through study

The nitrogen species concentrations and the aeration tank temperature data were initially evaluated to assess the state of nitrification before the upgrade. The wastewater temperature in the plant fluctuated seasonally between 22°C in the Sep-Oct period to 11°C in Feb-Mar each year (Figure 2.3a). The original CAS configuration showed a strong seasonality in nitrogen conversions. During warm weather months (T > 15°C), effluent NH_4-N concentrations were below 1 mg/L while NO_3-N concentrations were elevated (15-35 mg-N/L) indicating good nitrification (Figure 2.3a). However, when the aeration tank temperature was between 10-15°C (Jan-Apr) high effluent NH_4-N (15-35 mg-N/L) concentrations and

correspondingly low NO_3-N concentrations (Figure 2.3a) were observed. This was attributed to the 5d SRT that was maintained during the winter conditions that led to wash-out of nitrifiers (Houweling & Daigger, 2019). The results indicate that the original plant configuration was capable of nitrification during the warm period of the year, but not during the colder periods.

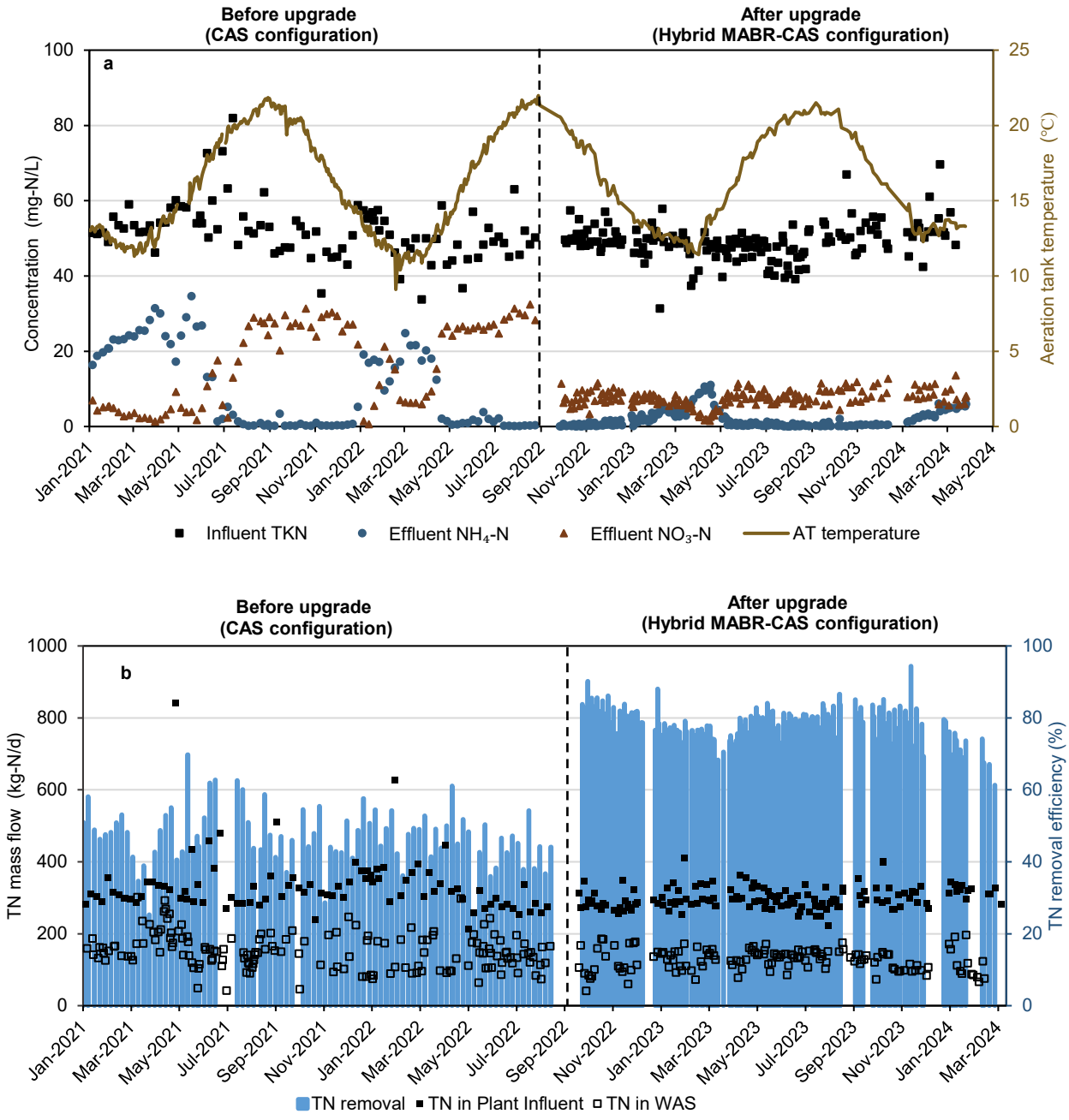

Figure 2.3 – a) N species concentrations and b) N mass flows and TN removal before and after MABR

The TN mass flows and removal efficiencies were examined to understand the TN removal mechanisms that were active in the plant before upgrade. The CAS process showed TN removal efficiencies in the range of 45-60% (Figure 2.3b). In this configuration TN removal was largely attributed to growth of biomass as nitrification does not contribute to TN removal. The N flow in the wasting mass flow was in the range of 150-200 kg-N/d, about 50-60% of the influent mass flow and was consistent with the overall TN removals. Overall, the plant in its CAS configuration reported moderate TN removal attributed solely towards biomass wasting.

The impact of the MABR upgrade on nitrification was assessed on the basis of the plant effluent N concentrations during the low temperature operating periods. As seen in Figure 2.3a, during the first winter season after MABR upgrade (Jan-Feb 2023), the effluent ammonia concentrations were found to be consistently less than 5 mg/L but increased to 10 mg-N/L during Mar-Apr 2023. These concentrations were lower than the winter averages seen before upgrade (Figure 2.3a). With subsequent changes in MABR operations (discussed further in section 2.3), the final effluent NH_4-N concentration was consistently less than 5 mg-N/L during Jan-Apr 2024. The results indicate that the MABR upgrade substantially reduced the impact of seasonality on nitrification by enhancing nitrification under cold weather conditions. It was concluded that the presence of nitrifying organisms in the MABR biofilms increased the 'effective SRT' in the plant thereby overcoming the nitrifier biomass limitations during winter operations (Figure 2.3a). The impact of MABR addition on aeration tank nitrification is further discussed further in Section 2.3.3.

The plant effluent nitrate concentrations were also examined as they can provide an additional line of evidence regarding nitrification and total N removal. The effluent nitrate concentrations decreased after the upgrade with concentrations of 5-10 mg-N/L during summer months and less than 5 mg-N/L during winter months. Correspondingly, the TN removal in the plant after the upgrade increased to values in the range of 75-90%. while the TN mass flow in the WAS stream remained steady (Figure 2.3b). The elevated TN removal observed alongside low effluent nitrate concentrations was attributed to denitrification in the MABR (discussed further in Section 2.3.4). Overall, addition of the MABR improved effluent quality in terms of TN and substantially reduced the seasonally high ammonia concentrations in the plant effluent.

2.3.3 Nitrification in MABR

The improved plant performance observed post upgrade was investigated further by examining several performance metrics that were calculated for MABR and aeration tank. The MABR oxygen transfer metrics are presented in the Supplemental Information. The subsequent discussion addresses nitrification in the MABR for the different operating conditions.

Nitrification rates quantified based on NH_4-N removal (NR_{NHx}) and oxygen transfer (NR_{OTR}) (Equations 2.4 and 2.5) were initially compared to investigate the active microbial metabolisms in the biofilm based on the inherent assumptions of the two indicators. Figure 2.4 shows estimated NR_{OTR} and NR_{NHx} values along with key operational variables including ammonia loading, MABR airflow, and wastewater temperature. The NR_{OTR} values were in the range of 1.7-2.8 g-N m^{-2} d^{-1}, whereas the NR_{NHx} values were in the range of 0.7-2.2 g-N m^{-2} d^{-1} and were consistently lower than the NR_{OTR} values. The NR_{OTR} calculation assumes all oxygen transferred from the gas phase is consumed by nitrification. However, oxygen can also be taken up by other metabolisms such as aerobic heterotrophy. In addition, oxygen can be consumed to nitrify ammonia released from the decay of organic matter. Hence, the difference between the two nitrification rate estimates could be an indicator of the relative extent of aerobic carbon oxidation in the biofilm (Uri-Carreño et al., 2021) and nitrification of organic N. Overall, the data indicates that the MABR biofilm supported aerobic microbial metabolisms like heterotrophic activity in addition to nitrification.

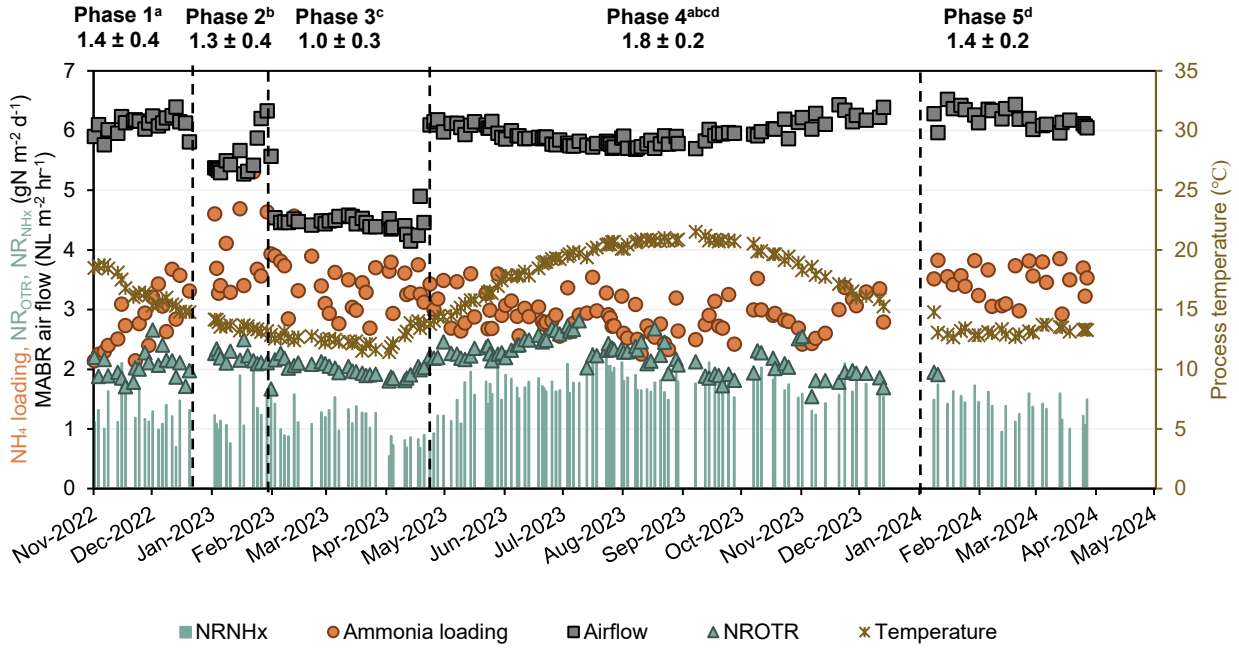

Figure 2.4 – Estimated nitrification rates and key operating conditions. Values below the phase heading shows the mean ± standard deviation of the NR_{NHx} calculated for each phase. Superscripts on the phase titles indicate that averages of the corresponding phases were significantly different (P* < 0.005). NR_{OTR} values were not available for Phase 5.

One of the objectives of this study was to evaluate the influence of ammonia loading, airflow, and operational temperature on MABR nitrification. Though all three variables could influence nitrification

rates, the reality of operating a full-scale plant did not allow us to implement a full factorial experimental design where each variable could be adjusted while others were held constant. Nevertheless, the dataset obtained from the operational conditions tested could still be leveraged to study the effect of the variable on a case-by-case basis. NR_{NHx} was chosen as the primary indicator for this discussion as it is based on actual ammonia removal as opposed to NR_{OTR} that is based on assumptions about ammonia removal.

Impact of temperature: The estimated nitrification rates were compared between the warm and cold weather phases to investigate the impact of mixed liquor temperature. The nitrification performance of phases 4 and 5 representing summer/fall 2023 and winter 2024 were directly compared as they had similar airflows and ammonia loadings (Table 2.1). It was found that the average NR_{NHx} values significantly ($P^* < 0.005$) decreased by 22% from 1.8 ± 0.2 g-N m^{-2} d^{-1} during Phase 4 to 1.4 ± 0.2 g-N m^{-2} d^{-1} in Phase 5 (Figure 2.3) that represented a 6°C decrease in the average temperature from 19°C to 13°C. Thus, there was a modest but significant impact of temperature on MABR nitrification rates.

Sustained nitrification under winter temperatures is considered one of the major process advantages of MABR (Long, et al., 2020). Hence, the magnitude of the temperature sensitivity of nitrification was compared with relevant studies from the literature. Prior studies of full-scale MABR installations have shown similar nitrification rates over temperatures ranging from 10 to 20°C (Long et al., 2020; Uri-Carreño et al., 2021). The lack of impact of temperature on MABRs has been assumed to be masked by changes in the biofilm thickness (Long et al., 2020; Uri-Carreño et al., 2021). Similarly, a low temperature dependence of the nitrification rate in bench-scale MABR activity tests was attributed to slower substrate diffusion at lower temperature (Németh et al., 2023). Moreover, bench-scale MABR systems have reported significantly thicker biofilms at 10°C when compared to 30°C despite increased microbial growth at the latter temperature (Clements et al., 2024). While the increased biofilm thickness at cold temperature increases diffusion limitation, the additional biomass can sustain nitrification in biofilms albeit at a slower rate (Hoang et al., 2014; Zhang et al., 2014). Overall, the MABR achieved substantial ammonia removal at temperatures as low as 11°C with a minor decrease in performance when compared with warm weather operations.

Impact of airflow: The impact of airflow on nitrification was examined to assess whether the observed changes in NR_{NHx} across the phases could be explained by this factor. The nitrification rate in Phase 4 (1.8 ± 0.2 g-N m^{-2} d^{-1}) that had an airflow of 5.9 ± 0.2 NL m^{-2} hr^{-1} was significantly higher ($P^* < 0.005$) than all the other phases. Phases 1 and 5, that had similar airflows around 6 NL m^{-2} hr^{-1}, showed about a 20% decrease in NR_{NHx} with an average of about 1.4 g-N m^{-2} d^{-1}. When the airflow was lowered to 5.5 and 4.5 NL m^{-2} hr^{-1} (Phases 2 and 3 respectively) the NR_{NHx} values decreased to 1.3 ± 0.4 g-N m^{-2} d^{-1} and 1.0 ± 0.3 g-N m^{-2} d^{-1}, respectively. The low airflow operations reported about 27% and 44% decrease in

NR_{NHx} when compared to high airflow operations. Viewed collectively, the highest and lowest NR_{NHx} values corresponded to the highest and lowest process airflow. This trend suggested that nitrification in MABR was strongly influenced by the airflow.

The MABR nitrification rate has been reported to have a strong dependence on the biofilm thickness (Semmens et al., 2003). In the full-scale MABR, the biofilm thickness control is achieved through recirculating the process airflow into the bulk to create shearing conditions and control excessive growth. Hence the observed trends in NR_{NHx} and the process airflow were examined in the context of biofilm thickness. Thickness measurements in biofilms harvested from full-scale cassettes at different phases of the study revealed that the average biofilm thickness in the rear cassettes had a higher average thickness of 819 ± 69 µm under lower airflow setting at Phase 3 (4.5 NL m^{-2} hr^{-1}) when compared to Phases 1 and 4 where the average range was 285 and 440 µm, respecively, under a higher airflow (6 NL m^{-2} hr^{-1}) (Discussed further in Chapter 3). These trends coincide with nitrification rates where higher thickness in Phase 3 coincided with a lowest nitrification rate range of 1.1 ± 0.2 g-N m^{-2} d^{-1} in this study. Phases with relatively thinner biofilms (Phases 1,4) reported the highest NR_{NHx} values (Figure 2.4). Thus, the process airflow in full-scale MABR systems influences nitrification through its ability to control the biofilm thickness.

The nitrification rates estimated by the two different methods were compared between low airflow (Phases 2,3) and higher airflow phases (Phases 4) to assess the extent of competition for oxygen from heterotrophic activity. Phases 2 and 3, that had lower airflows and higher loading (Table 2.1), were marked by a wider difference between NR_{OTR} and NR_{NHx} (Figure 2.4) suggesting that there was a higher competition for oxygen supply by aerobic heterotrophy because of a thicker biofilm. The close values observed during phase 4 with higher airflow (Figure 2.4) indicates that a higher proportion of the oxygen consumed by the biofilm is utilized for ammonia oxidation and the heterotrophic competition seen in the previous phases has been reduced. Thus, the process airflow that provided biofilm thickness control influences the relative extents of carbon and nitrogen removal metabolisms in the MABR.

In prior studies process air supply has been used as a control variable to suppress nitrite oxidation and achieve N removal via either nitrite-shunt (Mehrabi et al., 2020) or partial nitritation-anammox (Bunse et al., 2020) activities in MABR biofilms through limiting oxygen supply by either intermittent aeration (Ma et al., 2022; Ukaigwe et al., 2023) or lowering intramembrane lumen gas pressure (Gilmore et al., 2012; Terada et al., 2006). The current dataset was investigated to assess whether any of the process airflow conditions resulted in short cut N removal. The nitrite concentrations measured in the 24-hour composite samples in the MABR effluent were consistently below detection (< 0.03 mg-N/L; data not shown) and nitrate was found to be the predominant oxidation product in all phases. The prevalence of nitrate over

nitrite suggests that NOB activity was significant under these conditions. The results indicate that the dual purpose design of the MABR process aeration system which provides oxygen, bulk mixing and biofilm thickness control necessitates a higher airflow that results in high OTRs (8-10 g-O_2 m^{-2} d^{-1}) than that which is suitable for partial nitritation (Ravishankar et al., 2022a). Future MABR designs could consider decoupling process air and mixing and scouring air to obtain a finer control over oxygen supply for the biofilm or operate at a lower airflow and intermittently increase the airflow for biofilm thickness control if partial nitritation is desired in full-scale systems.

Impact of ammonia loading: The average ammonium loadings and the nitrification rates were compared between phases to understand the impact of loading on ammonia oxidation in the MABR tanks. Phase 2 of the study simulated high loading conditions in the plant by diverting the influent flow into only three of four MABR trains. This resulted in a higher ammonia loading in phase 2 with 3.9 ± 0.7 g-N m^{-2} d^{-1} while the remaining phases (1,3,4,5) had lower averages between 2.5 and 3.5 g-N m^{-2} d^{-1}. An increase in NR_{NHx} with the increase in ammonia loading was expected in Phase 2 (Côté, et al., 2015; Downing et al., 2010; Houweling et al., 2017; Long, et al., 2020). However, the average NR_{NHx} values did not differ significantly between phases (P* > 0.005). The absence of an effect of loading suggests that the nitrification rate during phase 2 was limited by other variables such as lower wastewater temperature (14°C) and reduced process airflow (5.5 NL m^{-2} hr^{-1}) during phase 2. The presence of a relatively thicker biofilm combined with lower temperatures appears to have limited the diffusion of ammonia into the biofilm during phase 2. Overall, the absence of a relationship between ammonia loading and nitrification rate suggests that biofilm thickness could be a limiting factor for nitrification under a higher carbon loading if the process airflow is not optimized.

On the whole, investigating the impacts of different operating conditions on MABR nitrification rate, we find that the process airflow that provided biofilm thickness control had a strong influence followed by operating temperature that had a relatively smaller effect. In case of increased influent loading to the MABR, the process airflow must be increased to control excessive biofilm growth and maintain a higher nitrification rate.

2.3.4 Denitrification in MABR

The performance metrics related to denitrification were compared across the different phases to examine whether operational conditions impacted nitrate reduction in the hybrid MABR process. The volumetric denitrification rate (DNR) and the denitrification efficiency (DE) values after the upgrade are shown in figure 2.5. The average DNR in Phase 1 was 142 ± 22 g-N m^{-3} d^{-1} and it then decreased to 106 ± 15 g-N m^{-3} d^{-1} and 118 ± 29 g-N m^{-3} d^{-1} during phases 2 and 3, respectively and subsequently increased in phases 4 and 5 to 173 ± 44 g-N m^{-3} d^{-1} and 210 ± 14 g-N m^{-3} d^{-1}, respectively. The trends in DNR were consistent

with the in the previously discussed NR_{NHx} values (Figure 2.4) indicating that nitrate reduction was dictated by the extent of ammonia oxidation in the process.

Examining the denitrification response in terms of DE, the average DE was observed to be over 85% in all the phases except during phase 1. Phase 1 had a relatively small but significantly lower DE of 80 ± 10 % (P* < 0.005) when compared to all the other phases. The slightly lower DE could be because phase 1 data reflected the operations after only two months of MABR start up. During this period the heterotrophic biomass inventory was likely developing as indicated by the general upward trend in DE during Phase 1 and thin biofilm (discussed later in Chapter 3). A comparison of DE values among the remaining phases showed that the values were statistically similar Phase 2 and 3 and then DE values progressively increased through phases 4 and 5. Though the DE values in phase 4 were generally high (92%), it was slightly lower than Phase 5 (P* < 0.005). The increase in Phase 5 relative to Phase 4 was attributed to the relatively lower NO_3-N loading from the return stream in Phase 5 (cold weather with reduced nitrification) when compared to Phase 4 (warm weather). On the whole, the DE was generally high (> 80%) with very little impact of operational conditions.

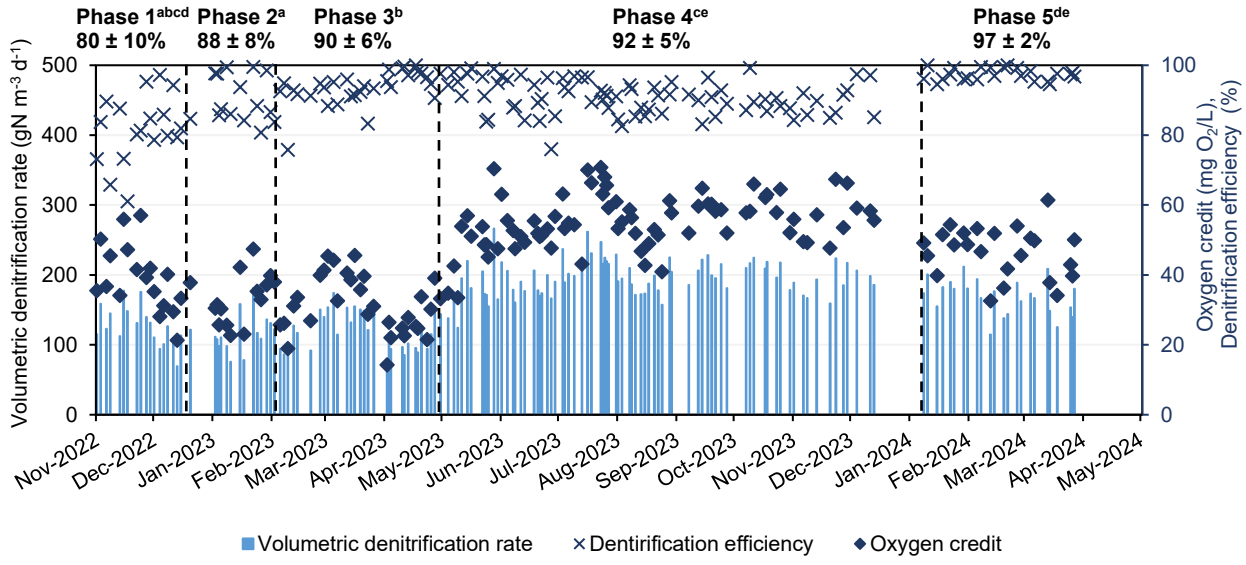

Figure 2.5 – Denitrification metrics versus time. Values below the phase heading shows the mean ± standard deviation of the denitrification efficiency calculated for each phase. Superscripts on the phase titles indicates that corresponding phases are significantly different (P* < 0.005)

The literature on bench and pilot scale hybrid MABR studies was reviewed to assist in further interpreting the observed results. While some pilot scale hybrid MABR studies have observed some degree of denitrification, they did not quantify nitrate/nitrite removal (Kunetz et al., 2016, Côté et al., 2015). Even

the few reports that evaluated denitrification reported TN removals. TN removal efficiencies of 77% to 100% have been reported for lab-scale hybrid MABR treating synthetic wastewater (Downing et al., 2010; Downing & Nerenberg, 2008c). Similarly high TN removals (78-95%) have been reported for small-scale biofilm-only MABRs with careful control of biofilm through gas sparging in the bulk (Semmens et al., 2003; Timberlake et al., 1988). The high DE values observed in the current study are consistent with the high rates of TN removal reported in the literature.

While MABRs report high denitrification, the denitrification efficiency could be impacted by availability of readily biodegradable carbon as electron donors for denitrification. Denitrification limitation due to lack of carbon has been reported for both biofilm-only (LaPara et al., 2006) and hybrid MABRs (Corsino & Torregrossa, 2022b). Prior studies that involved either bench-scale experiments or modeling studies of biofilm-only MABRs have recommended a C/N ratio between 3 and 5 in the influent to achieve high levels of SND (Liu et al., 2010; Matsumoto et al., 2007; Semmens, 2005; Zhong et al., 2023). Ravishankar et al. (2022) observed a decrease in denitrification efficiency in a pilot-scale biofilm-only MABR from about 95% to 15% when the sbCOD/N ratio in the influent decreased from 3.4 to 1.3. In the current study, the influent sbCOD/N ratio (calculated using Equation 2.8) over the entire study was 3.3 ± 1.5 (shown in Figure S2.2 in supplemental information) suggesting that there was sufficient carbon available for denitrification and hence the previously described DE values were not limited in this regard.

The MABR process airflow could influence denitrification efficiency because of the variations in oxygen supply and thickness control in the biofilm. In the current study the average denitrification efficiency for the hybrid MABR process remained stable between 80-92% over the process airflow range of 4.5-6 NL during the 5 phases (Figure 2.4). The stable denitrification efficiency with different oxygen transfer rates and shearing intensities observed in this study was contrary to reports from other studies investigating biofilm only MABRs. Dong et al. (2009) observed a decrease in TN removal from 78% to 26% when the intra-membrane oxygen pressure was increased from 140 to 170 kPa due to a reduction in the anoxic region in the biofilm. Ravishankar et al. (2022) observed inhibition of denitrification in a biofilm only MABR when the oxygen supply was more than the combined demand for COD and TN removal. Similarly, Bunse et al. (2023) observed accumulation of nitrate and decrease in TN removal when the scouring intensity was increased in a biofilm-only MABR. The reduced sensitivity of denitrification efficiency in the current study could be because of nitrate reduction in the anoxic suspended sludge. It appears that any reduction in denitrification in the biofilm due to excess oxygen supply or shearing was buffered by nitrate reduction in the bulk phase. Thus, hybrid MABR processes benefit from the presence of the anoxic bulk phase that renders the denitrification efficiency less sensitive to variations in biofilm oxygen transfer rate and shearing intensity.

Carbon removal through MABR denitrification was considered one of the process advantages of the upgrade as it could reduce the oxygen requirements in the downstream aeration tank. Hence, the oxygen credit obtained through denitrification (equation 2.9) in the MABR tank was examined. From figure 2.5, the oxygen credit was in the range of 15-70 mg-O_2 L^{-1} indicating a corresponding amount of oxygen consumption was avoided in the aeration tank due to anoxic carbon removal. Moreover, the oxygen credit followed a similar trend as the nitrification rate. There was a reduction in oxygen credit (20-40 mg-O_2 L^{-1}) during phases 2 and 3 when the nitrification rate decreased (Figure 2.3) but the increase in nitrification rate Phase 4 led to an increased credit of 70 mg-O_2 L^{-1}. Thus, the hybrid MABR process provided considerable oxygen credit, with the extent of savings determined by the nitrification rate.

Overall, based on the analysis of the denitrification metrics, it was concluded that though the denitrification rate was limited by nitrification rate, the denitrification efficiency in the hybrid MABR was not impacted by external factors if sufficient carbon is available. The denitrification process also provided substantial oxygen credit through anoxic BOD consumption thereby reducing the organic loading to the aeration tank.

2.3.5 Nitrification in aeration tank

As previously discussed, prior to the MABR upgrade nitrification in the aeration tank was limited under low temperatures (Figure 2.3a). Integrating the MABR with the existing CAS was anticipated to enhance nitrification in the aeration tank because of the nitrifier seeding effect. Hence the NH_4-N removal efficiency in the aeration tank was examined to assess the extent of the seeding effect. Figure 2.6 shows NH_4-N removal efficiency in the aeration tank (Equation 2.11) during each phase. Phases that had warm temperatures namely Phase 1 (17.0 ± 1.0 ℃) and Phase 3 (19 ± 1.5 ℃) had very high NH_4-N removals of 93 ± 5% and 94 ± 5%, respectively by the CAS (Figure 2.5). High levels of ammonia removal in these temperature ranges is not surprising as the 5 days aerobic SRT is higher than wash-out limit (Houweling & Daigger, 2019). The impact of seeding from the biofilm was mainly anticipated in Phases 3 and 5, which represented the cold weather operations with average temperatures of 12.0 ± 0.7 ℃ and 13.0 ± 0.44 ℃, respectively. Contrary to the expectation, there was a substantial drop in aeration tank nitrification to 53 ± 16% during Phase 3 indicating minimal seeding of nitrifiers. However, in Phase 5, a higher nitrification efficiency (73 ± 9%) in the aeration tank was observed suggesting a positive impact of nitrifier seeding. The differing nitrification performance between the two cold weather periods suggests that the MABR operations influenced the extend of nitrifier seeding into the aeration tank.

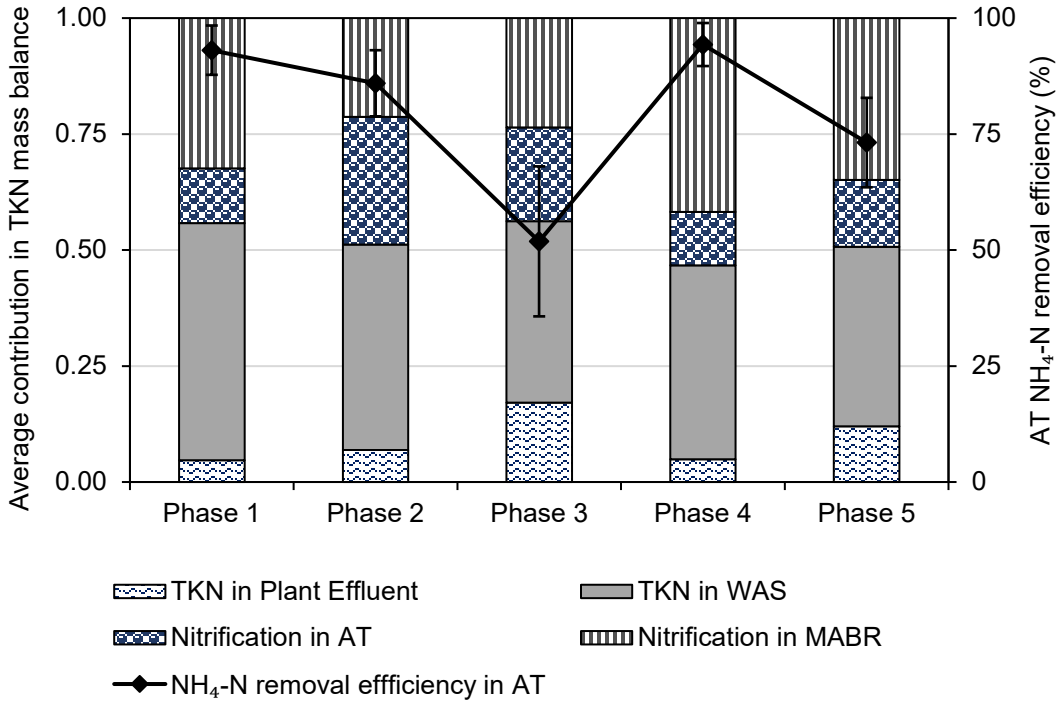

Figure 2.6 – TKN balance for the overall plant and NH4-N removal efficiency in the aeration tank measured during different phases of MABR operation. The left side y-axis shows the average contribution of the different terms to the plantwide TKN balance. The right side y axis shows the percentage removal of NH4-N entering aeration tank.

The nitrification performance of the aeration tank was examined further through a plantwide TKN mass balance to understand the role of the MABR operations, specifically the process air flow rate in seeding. Figure 2.6 presents the average contributions of different pathways of TKN removal in the plant. As seen from figure 2.6, biomass wasting removed about half of the influent TKN mass load across all the phases. The fraction of TKN removed through MABR nitrification was variable as discussed previously through nitrification rate. Focusing specifically on the cold weather phases, the average fraction of TKN nitrified by the MABR was higher in Phase 5 (35%) than phase 3 (25%). The difference in performance between the two winters was attributed to differences in the MABR airflow that provided thickness control. Through process modeling, Houweling & Daigger (2019) proposed that NH_4-N removal in the biofilm and nitrifier sloughing are the main factors influencing aeration tank nitrification at SRT values below traditional wash-out values. In this study, the lower airflow of 4.5 NL m^{-2} hr^{-1} in Phase 3 that limited the nitrification rate, appears to have limited the sloughing of nitrifier biomass to the aeration tank. In contrast, in Phase 5 with a higher airflow rate 6 NL m^{-2} hr^{-1}, a higher nitrification rate and apparently led

to a higher rate of biomass shearing into the suspended sludge. Thus, MABR biofilm thickness control appears to have a role in achieving enhanced low temperature nitrification in the aeration tank.

2.3.6 Impact of MABR on aeration tank operations

The previously discussed nitrification, BOD removal through denitrification and aerobic heterotrophy in the MABR was expected to reduce the oxygen demand exerted in the downstream aeration tank. The air supply for the aeration tank was supplied by a turbo blower with a variable frequency drive (VFD) to vary the airflow with a target of 2 mg/L DO at the front of the tank. Hence, any changes in oxygen demand in the wastewater after MABR addition was expected to be reflected in the aeration tank airflow and dissolved oxygen concentration. The aeration tank operations were studied before and after the upgrade to assess the extent of this impact. The analysis was done for operations under warm weather conditions when the aeration demand was expected to be maximum.

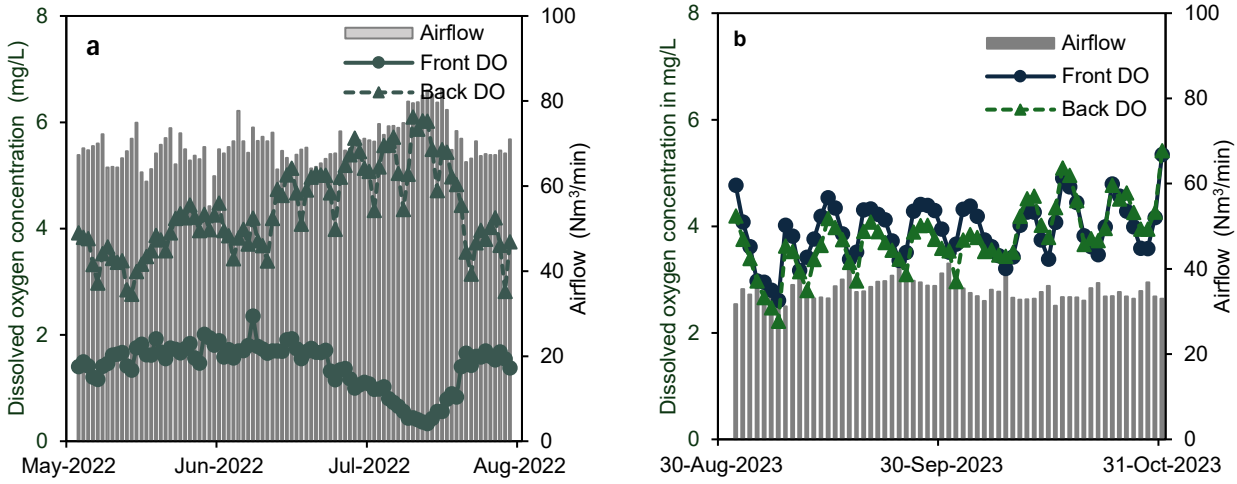

Figure 2.7 – Daily average airflow and DO profile in aeration tank during warm weather conditions a) before and b) after MABR upgrade.

The daily average airflow supplied to the aeration tank was compared between pre- and post-upgrade (Figure 2.7) to determine the impact of MABR. The daily average airflow for the same DO set point in the aeration tank decreased from 71 ± 6 $Nm^3\,min^{-1}$ before the upgrade to 35 ± 2 $Nm^3\,min^{-1}$ after the upgrade (Figure 2.7). The 50% reduction in airflow was attributed to the significant loading reduction by the MABR as discussed previously (Figure 2.6). The observed airflow post upgrade was limited by the lowest blower setting to provide adequate mixing and the actual oxygen requirements for the prevailing loading were lower than that indicated by the air flow. Thus, the lower oxygen demand combined with the dynamic aeration control resulted in substantial reduction in air supply in the post upgrade aeration tank.

The DO concentrations in the aeration tank were compared before and after upgrade to obtain further insights into the impact of loading reduction by the MABR. The aeration tank had DO sensors at the front and the back sections of the tank to enable a DO based aeration control and monitor the oxygen availability in the tank. The daily average concentrations of the dissolved oxygen in the aeration tank are shown in Figure 2.7. The regular peaks and troughs in DO (Figure 2.7) every seven days indicated a weekly loading pattern with high loading on the weekends leading to a lower daily average DO. The DO control by the VFD drive maintained a DO level around 2 mg/L in the front section of the tank before the upgrade as seen in Figure 2.7a. With decreasing oxygen demand along the length of the tank, the mixed liquor DO at the back section increased to 4-6 mg/L. After the upgrade, the DO concentrations were similar in the front and back sections of the aeration tank (Figure 2.7b). Moreover, the DO in the front section of the aeration tank (3-5 mg/L as seen in Figure 2.7b) after MABR upgrade was above the 2 mg/L DO set point for aeration control indicating a higher oxygen supply compared to the demand. After the MABR upgrade, the lower oxygen demand of the wastewater entering the aeration tank resulted in a turn down of the turbo blower to its minimum speed. Even at the minimum airflow setting, the airflow was higher than the requirements for the DO set point and the mixed liquor reached 3-5 mg/L DO. The prevailing DO levels suggest that the plant will be able to operate at the minimum speed until loadings increase in the future.

The shift in aeration tank DO profile observed after the MABR addition likely reflected changes in wastewater composition entering the aeration tank. Before upgrade, the relatively lower DO in the front of the aeration tank was attributed to the high oxygen demand exerted by the readily biodegradable substrates entering the tank. The longitudinal increase in DO towards the back (Figure 2.7a) indicated depletion of readily biodegradable substrates and utilization of slowly biodegradable substrates towards the end of the tank. Contrarily, the uniform and relatively high DO concentration (3-5 mg/L) in the aeration tank after the upgrade, suggests that most of the readily degradable substrates were taken up by the upstream MABR process and the wastewater entering aeration tank was mostly composed of more slowly degradable substrates. Thus, the upstream MABR not only reduced the loading but also likely shifted the aeration tank influent substrates to more slowly degradable fractions. Future designs should consider these impacts in the design and operation of the CAS aeration system.

In conclusion, the sequential arrangement of hybrid MABR-CAS process had profound impacts on the downstream aeration tank operations. The MABR upgrade substantially lowered the airflow requirements and effected a more uniform DO profile across the aeration tank due to reduction in loading and shift in wastewater characteristics. Analysis of the aeration tank operations also demonstrated that it is imperative to have an appropriate aeration control in the downstream aeration tank to reap all the potential savings in

aeration after an MABR upgrade. The reduction in airflow will have corresponding savings in aeration related electricity consumption which is discussed further in the following section.

2.3.7 Electricity consumption for aeration

MABRs have been promoted on the basis of being more energy efficient with respect to oxygen supply than traditional aeration. Hence, the key performance indicators for aeration electricity consumption were compared before and after the MABR upgrade to evaluate its impact on energy efficiency. Figure 2.8a shows the volumetric energy intensity (Equation 2.12) before and after MABR upgrade while Figure 2.8b shows the aeration efficiencies (Equation 2.13) calculated for the aeration tank (Equation 2.14) and the MABR. The monitoring period for these two performance indicators spanned over the three years (2021 to 2023) including all the seasonal and operational changes.

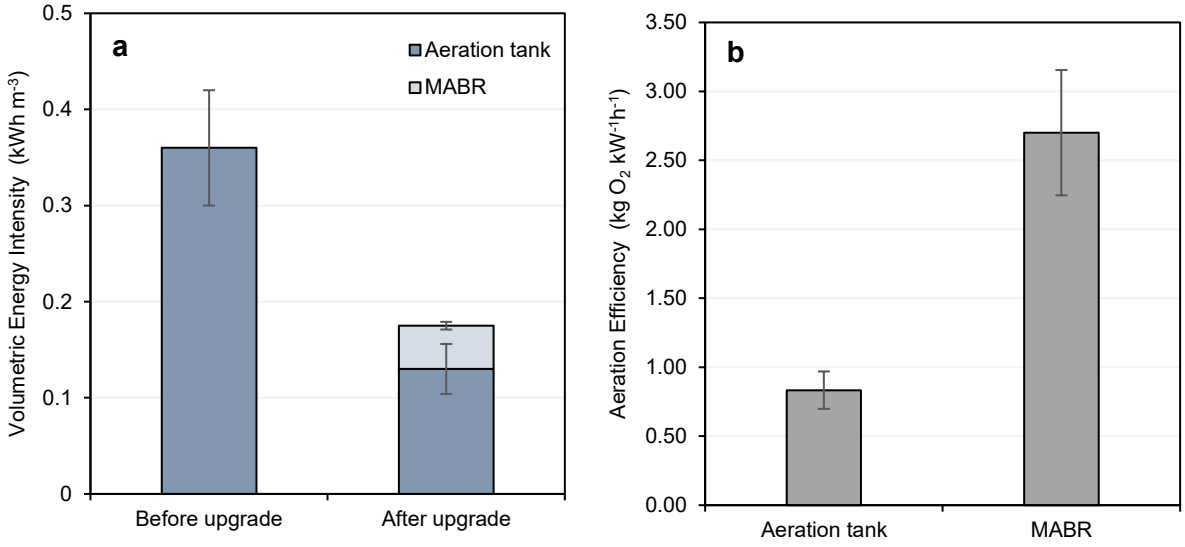

Figure 2.8 - a) Comparison of volumetric energy intensity in the full-scale facility before and after MABR upgrade. b) Comparison of aeration efficiency estimated for the aeration tank and MABR. Error bars indicate the standard deviation between different measurement days.

The volumetric energy intensity which quantifies the aeration related electricity consumption per unit volume of wastewater was 0.37 ± 0.06 kWh m^{-3} (Figure 2.8) when the plant was in the CAS configuration before the upgrade. After the upgrade, this value decreased to 0.17 ± 0.02 kWh m^{-3} revealing an average of 54% energy savings. The decrease in electricity consumption was partly achieved by a 33% reduction in average electricity consumption by the aeration tank (0.37 to 0.13 kWh m^{-3}) (Figure 2.8a) due to the considerable TKN removal (Figure 2.6) and denitrification related oxygen credit provided by the upstream hybrid MABR process.

The observed reduction in electricity usage associated with different modes of aeration in the MABR and CAS was further examined. The aeration efficiency that describes the quantity of oxygen supplied per unit of electricity consumed was selected as the indicator for this comparison. As seen in Figure 2.8a, the aeration efficiency of the MABR process (2.7 kg O_2 $kW^{-1}h^{-1}$) was 3.25 times higher than the 0.83 kg O_2 $kW^{-1}h^{-1}$ estimated for the aeration tank. There was some degree of uncertainty in this comparison, as values calculated for the aeration tank included several assumptions regarding the various correction factors for field conditions (Equation 2.14). Nevertheless, comparing the volumetric energy intensity of the MABR and aeration tank post upgrade provided a second line of evidence. The average electricity consumed for aeration of the MABR process (0.05 kWh m^{-3}) was about 2.5 times lower than the 0.13 kWh m^{-3} consumed for aeration through the conventional diffused aeration in the aeration tank. A comparison of both the indicators in terms of oxygen delivered and wastewater treated revealed that the hybrid MABR process removed a substantial part of the influent loading with a lower electricity consumption when compared to the aeration tank. Thus, through a combination of energy efficient treatment in the MABR and reduced aeration requirements in the energy intensive diffused aeration process, the MABR upgrade reduced the electricity consumed for the aeration in the plant by approximately 50%.

The KPIs estimated in this study were compared with values from the literature to benchmark them against electricity monitoring studies in other full-scale facilities. The volumetric energy intensity calculated before upgrade in this study compared well with the range of 0.25-0.4 kWh m^{-3} reported in the literature for CAS plants with BOD and ammonia removal in Canada (Ontario Ministry of Environment, 2016*)*. The aeration efficiency calculated for fine bubble diffused aeration in the aeration tank (0.83 kg O_2 $kW^{-1}h^{-1}$) was within the range of reported values (0.2-6 kg O_2 $kW^{-1}h^{-1}$) (Ashley et al., 1991; Huibregtse et al., 1983). Data on KPIs for MABR process based on field monitoring was not available in the literature. However, several studies have reported KPIs and energy savings from MABR upgrades based upon process modeling. Peeters et al., (2017) predicted an MABR aeration efficiency of 2.2-2.5 kg O_2 $kW^{-1}h^{-1}$ at a process airflow rate of 4.5 NL m^{-2} hr^{-1} which was comparable to the observations in this study. Modeling studies that compare MABR processes with conventional designs have predicted energy savings of 40% (Peeters et al., 2016) to 86% (Aybar et al., 2015) for CAS, 50% for Modified Ludzack Ettinger (He & Daigger 2023) and 50 % for A2O/Bardenpho (Flores-Alsina et al., 2023) process. The overall 54% energy savings calculated using actual electricity consumption data in this current study is therefore consistent with predicted literature estimates. To our knowledge, this is the first study to report KPIs based on long term power monitoring in a full-scale MABR that included a cascade of MABR cassettes in a hybrid configuration.

2.4. Conclusion

This study evaluated pollutant removal and electricity consumption in a large MABR installation (69000 m^2 installed membrane surface area). Three years of intensive sampling monitored the plant performance when it was in its CAS configuration and CAS/MABR configurations under different MABR airflow, seasons, and loading conditions. The findings from this full-scale study showed that:

- The MABR process enabled year-round nitrification in the plant with low effluent NH_4-N concentrations below 1 mg-N/L and 5 mg-N/L in summer and winter conditions, respectively. The MABR upgrade doubled the TN removal in the plant with high denitrification efficiencies (80-92%).
- The MABR nitrification rate can be limited by the thickness control provided by the airflow. The MABR nitrification rate had a low sensitivity to operational temperature with a 22% decrease in nitrification rate for an average temperature differential of 6℃ between warm and cold weather operations.
- The MABR achieved high DE (< 80%) and was insensitive to wastewater temperature, loading, MABR airflow. The DNR and associated oxygen credit through anoxic carbon removal were limited by the nitrification rate in the MABR.
- The nitrification efficiency in the aeration tank post upgrade was impacted by the MABR operations. Higher rates of biomass scouring that were enabled by higher MABR airflow improved the NH_4-N removal in the aeration tank when the suspended SRT (5 d) was below typical washout values for cold weather (13℃) conditions.
- The volumetric electricity consumption for plantwide aeration decreased by 50% after the MABR upgrade because of substantial loading reduction achieved in that MABR that had higher aeration efficiency and reduced aeration requirements for the conventional diffused aeration that had a relatively lower aeration efficiency.
- The overall improved N removal under a reduced electricity consumption demonstrates the promising intensification potential of MABR technology.

2.5 Supplemental information

2.5.1 Oxygen transfer in MABR

Oxygen transfer from the lumen gas to the biofilm is considered a key factor determining the performance of MABRs. The quantity of oxygen transferred to the biofilm could be influenced by the air supply from the lumen side and the demand from the biofilm side. Hence the two oxygen transfer metrics calculated using Equations 2.2 and 2.3 were studied as a function of the different airflows maintained in the MABR (Figure S2.1) to assess the relative roles of the lumen gas and biofilm activity on the oxygen supply. The first indicator, oxygen transfer efficiency (OTE), measured the fraction of the supplied oxygen that is utilized by the biofilm (Houweling et al., 2017). The daily average OTE exhibited a downward trend from 28% to 23-21% when the airflow set point was increased from 4.5 to 6 NL m^{-2} $hr^{-1}$with increasing airflow (Figure S2.1). Lower airflow has a longer gas residence time in the membrane lumen which in turn allowed a greater fraction of oxygen to diffuse through a membrane and hence a higher OTE. Thus, the variations in OTE are largely controlled by the process airflow.

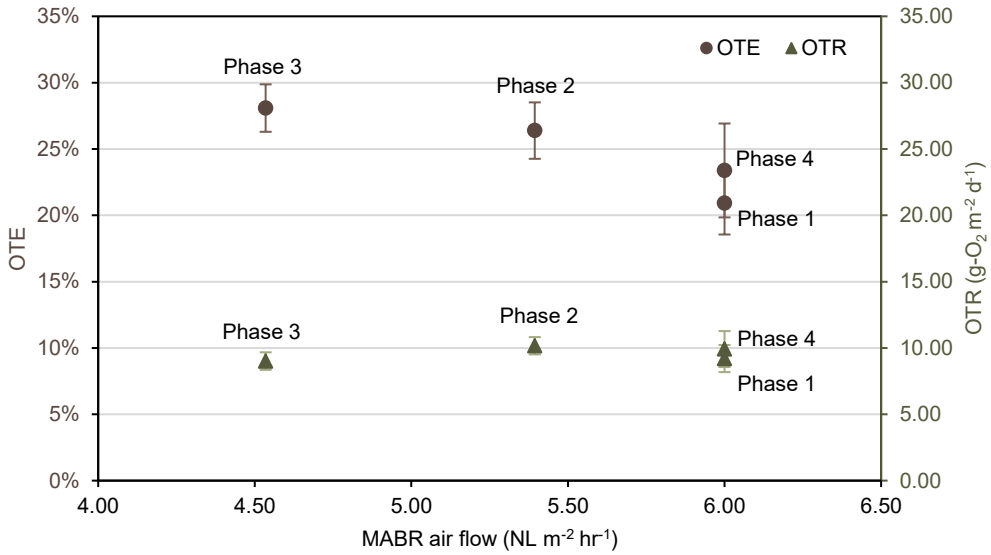

Figure S2.1 – Daily averages of OTE and OTR measured at different airflows set points. Error bars indicate standard deviations observed within phases. Oxygen transfer metrics were not available for Phase 5.

The same analysis was done using oxygen transfer rate (OTR) as the indicator. OTR at different airflows was examined to assess the impacts of seasonal and loading conditions. OTR is the rate at which the supplied oxygen is utilized by the biofilm. With a higher airflow, a higher OTR would be expected. However, the average OTR observed for different airflows remained stable between 9-10 g-O_2 $m^{-2}d^{-1}$. The

flat oxygen response indicates that there was a steady oxygen consumption in the biofilm during all the phases. This could be due to the steady oxygen consumption by heterotrophs alongside nitrifiers that makes it insensitive to conditions like temperature and loading.

The oxygen transfer metrics observed in this study were compared with reports from other smaller scale studies to evaluate the effect of scaling up of MABR systems on oxygen transfer. In the current study, the average OTR ranged between 8.8-10.1 $gO_2\,m^{-2}d^{-1}$ and average OTE values between 20-28% were observed. These values were consistent with OTRs and OTEs reported for smaller scale installations with similar airflows (Houweling et al., 2017; Long, et al., 2020; Uri-Carreño et al., 2021). Corssino and Torregrossa (2022) reported a higher OTR range of 15-30 $gO_2\,m^{-2}d^{-1}$ but the airflow in their system was considerably higher (10.5 NL $m^{-2}\,hr^{-1}$). The results suggest that oxygen transfer metrics scale up well to large scale MABR systems if the air flow rates are similar.

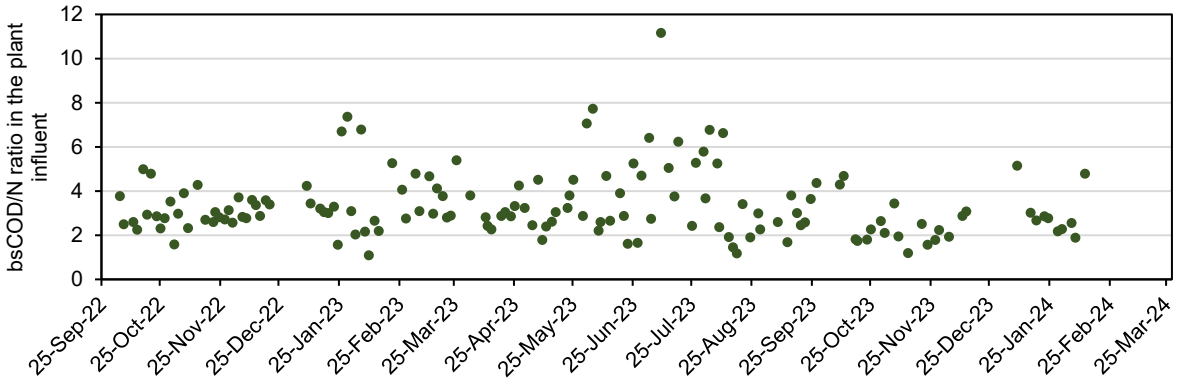

Figure S2.2 – bsCOD/N measured in the plant influent over the study period.

2.6 References

Ashley, K. I., Hall, K. J., & Mavinic, D. S. (1991). Factors influencing oxygen transfer in fine pore diffused aeration. *Water Research*, *25*(12), 1479–1486. https://doi.org/10.1016/0043-1354(91)90178-S

Aybar, M., Pizarro, G., Boltz, J. P., Downing, L., & Nerenberg, R. (2014). Energy-efficient wastewater treatment via the air-based, hybrid membrane biofilm reactor (hybrid MfBR). Water Science and Technology, 69(8), 1735–1741. https://doi.org/10.2166/wst.2014.086

Bunse, P., Orschler, L., Pidde, A. V., & Lackner, S. (2023). Effects of scouring on membrane aerated biofilm reactor performance and microbial community composition. *Bioresource Technology*, *369*, 128441. https://doi.org/10.1016/j.biortech.2022.128441

Casey, E., Glennon, B., & Hamer, G. (1999). Oxygen mass transfer characteristics in a membrane-aerated biofilm reactor. *Biotechnology and Bioengineering*, *62*(2), 183–192. https://doi.org/10.1002/(SICI)1097-0290(19990120)62:2<183::AID-BIT8>3.0.CO;2-L

Clements, E., Nahum, Y., Pérez-Calleja, P., Kim, B., & Nerenberg, R. (2024). Effects of temperature on nitrifying membrane-aerated biofilms: An experimental and modeling study. *Water Research*, *253*, 121272. https://doi.org/10.1016/j.watres.2024.121272

Corsino, S. F., & Torregrossa, M. (2022). Achieving complete nitrification below the washout SRT with hybrid membrane aerated biofilm reactor (MABR) treating municipal wastewater. *Journal of Environmental Chemical Engineering*, *10*(1), 106983. https://doi.org/10.1016/j.jece.2021.106983

Côté, P., Peeters, J., Adams, N., Hong, Y., Long, Z., & Ireland, J. (2015). A New Membrane-Aerated Biofilm Reactor for Low Energy Wastewater Treatment: Pilot Results. WEFTEC 2015. https://www.accesswater.org/publications/proceedings/-277906/a-new-membrane-aerated-biofilm-reactor-for-low-energy-wastewater-treatment--pilot-results

Dong, W., Wang, H., Li, W., Ying, W., Gan, G., & Yang, Y. (2009). Effect of DO on simultaneous removal of carbon and nitrogen by a membrane aeration/filtration combined bioreactor. *Journal of Membrane Science*, *344*(1), 219–224. https://doi.org/10.1016/j.memsci.2009.08.007

Downing, L. S., Bibby, K. J., Esposito, K., Fascianella, T., Tsuchihashi, R., & Nerenberg, R. (2010). Nitrogen Removal from Wastewater Using a Hybrid Membrane-Biofilm Process: Pilot-Scale Studies. *Water Environment Research*, *82*(3), 195–201. https://doi.org/10.2175/106143009X426103

Downing, L. S., & Nerenberg, R. (2008a). Effect of oxygen gradients on the activity and microbial community structure of a nitrifying, membrane-aerated biofilm. *Biotechnology and Bioengineering*, *101*(6), 1193–1204. https://doi.org/10.1002/bit.22018

Downing, L. S., & Nerenberg, R. (2008b). Sustainable nitrogen removal from wastewater with the hybrid membrane biofilm process (HMBP): Bench-scale studies. *Water Science and Technology*, *58*(9), 1715–1720. https://doi.org/10.2166/wst.2008.550

Downing, L. S., & Nerenberg, R. (2008c). Total nitrogen removal in a hybrid, membrane-aerated activated sludge process. *Water Research*, *42*(14), 3697–3708. https://doi.org/10.1016/j.watres.2008.06.006

Flores-Alsina, X., Uri-Carreno, N., Nielsen, P. H., & Gernaey, K. V. (2023). Modelling the impacts of operational conditions on the performance of a full-scale membrane aerated biofilm reactor. *Science of The Total Environment*, *856*, 158980. https://doi.org/10.1016/j.scitotenv.2022.158980

Gilmore, K. R., Terada, A., Smets, B. F., Love, N. G., & Garland, J. L. (2012). Autotrophic Nitrogen Removal in a Membrane-Aerated Biofilm Reactor Under Continuous Aeration: A Demonstration. *Environmental Engineering Science*, *30*(1), 38–45. https://doi.org/10.1089/ees.2012.0222

He, H., & Daigger, G. T. (2023). The hybrid MABR process achieves intensified nitrogen removal while N2O emissions remain low. *Water Research*, *244*, 120458. https://doi.org/10.1016/j.watres.2023.120458

Hoang, V., Delatolla, R., Abujamel, T., Mottawea, W., Gadbois, A., Laflamme, E., & Stintzi, A. (2014). Nitrifying moving bed biofilm reactor (MBBR) biofilm and biomass response to long term exposure to 1 °C. *Water Research*, *49*, 215–224. https://doi.org/10.1016/j.watres.2013.11.018

Houweling, D., & Daigger, G. (2019). *Intensifying Activated Sludge Using Media-Supported Biofilms*. CRC Press. https://doi.org/10.1201/9780429260278

Houweling, D., Long, Z., Peeters, J., Adams, N., Côté, P., Daigger, G., & Snowling, S. (2018). Nitrifying below the "Washout" SRT: Experimental and Modelling Results for a Hybrid MABR / Activated Sludge Process. 1250–1263. https://www.accesswater.org/publications/proceedings/-299455/nitrifying-below-the--washout--srt--experimental-and-modelling-results-for-a-hybrid-mabr-/-activated-sludge-process

Houweling, D., Peeters, J., Côté, P., Long, Z., & Adams, N. (2017). Proving Membrane Aerated Biofilm Reactor (MABR) Performance and Reliability: Results from Four Pilots and a Full-Scale Plant. WEFTEC 2017. https://www.accesswater.org/publications/proceedings/-279607/proving-membrane-aerated-biofilm-reactor-mabr-performance-and-reliability-results-from-four-pilots-and-a-full-scale-plant

Huibregtse, G. L., Rooney, T. C., & Rasmussen, D. C. (1983). Factors Affecting Fine Bubble Diffused Aeration. *Journal (Water Pollution Control Federation)*, *55*(8), 1057–1064.

IESO. (2018). *Market Characterization & Conservation Potential for Ontario's Drinking Water & Wastewater Treatment Plants*. http://www.ieso.ca/en/Sector-Participants/IESO-News/2019/02/Water-and-wastewater-treatment-report

LaPara, T. M., Cole, A. C., Shanahan, J. W., & Semmens, M. J. (2006). The effects of organic carbon, ammoniacal-nitrogen, and oxygen partial pressure on the stratification of membrane-aerated biofilms. *Journal of Industrial Microbiology and Biotechnology*, *33*(4), 315–323. https://doi.org/10.1007/s10295-005-0052-5

Liu, H., Yang, F., Shi, S., & Liu, X. (2010). Effect of substrate COD/N ratio on performance and microbial community structure of a membrane aerated biofilm reactor. *Journal of Environmental Sciences*, *22*(4), 540–546. https://doi.org/10.1016/S1001-0742(09)60143-1

Liu, H., Yang, F., Wang, T., Liu, Q., & Hu, S. (2007). Carbon membrane-aerated biofilm reactor for synthetic wastewater treatment. *Bioprocess and Biosystems Engineering*, *30*(4), 217–224. https://doi.org/10.1007/s00449-007-0116-1

Long, Z., Oskouie Ali K., Kunetz Thomas E., Peeters Jeff, Adams Nick, & Houweling Dwight. (2020). Simulation of Long-Term Performance of an Innovative Membrane-Aerated Biofilm Reactor. *Journal of Environmental Engineering*, *146*(6), 04020041. https://doi.org/10.1061/(ASCE)EE.1943-7870.0001705

Lu, D., Bai, H., Kong, F., Liss, S. N., & Liao, B. (2020). Recent advances in membrane aerated biofilm reactors. *Critical Reviews in Environmental Science and Technology*, *0*(0), 1–55. https://doi.org/10.1080/10643389.2020.1734432

Ma, Y., Piscedda, A., Veras, A. D. L. C., Domingo-Félez, C., & Smets, B. F. (2022). Intermittent aeration to regulate microbial activities in membrane-aerated biofilm reactors: Energy-efficient nitrogen removal and low nitrous oxide emission. *Chemical Engineering Journal*, *433*, 133630. https://doi.org/10.1016/j.cej.2021.133630

Martin, K. J., & Nerenberg, R. (2012). The membrane biofilm reactor (MBfR) for water and wastewater treatment: Principles, applications, and recent developments. *Bioresource Technology*, *122*, 83–94. https://doi.org/10.1016/j.biortech.2012.02.110

Matsumoto, S., Terada, A., & Tsuneda, S. (2007). Modeling of membrane-aerated biofilm: Effects of C/N ratio, biofilm thickness and surface loading of oxygen on feasibility of simultaneous nitrification and

denitrification. *Biochemical Engineering Journal*, *37*(1), 98–107. https://doi.org/10.1016/j.bej.2007.03.013

Mehrabi, S., Houweling, D., & Dagnew, M. (2020). Establishing mainstream nitrite shunt process in membrane aerated biofilm reactors: Impact of organic carbon and biofilm scouring intensity. *Journal of Water Process Engineering*, *37*, 101460. https://doi.org/10.1016/j.jwpe.2020.101460

Metcalf and Eddy Inc., George Tchobanoglous, H. Stensel, Ryujiro Tsuchihashi, & Franklin Burton. (2014). *Wastewater Engineering: Treatment and Resource Recovery* (5th Edition). McGraw Hill.

Németh, A., Ainsworth, J., Ravishankar, H., Lens, P. N. L., & Heffernan, B. (2023). Temperature dependence of nitrification in a membrane-aerated biofilm reactor. *Frontiers in Microbiology*, *14*. https://www.frontiersin.org/articles/10.3389/fmicb.2023.1114647

Ontario Ministry of Environment. (2016). *Energy Conservation Measures | Water and Energy Conservation Guidance Manual for Sewage Works.* ***ontario.ca*****.** Retrieved February 26, 2024, from http://www.ontario.ca/document/water-and-energy-conservation-guidance-manual-sewage-works/energy-conservation-measures.

Peeters, J., Adams, N., Long, Z., Côté, P., & Kunetz, T. (2017). Demonstration of innovative MABR low-energy nutrient removal technology at Chicago MWRD. *Water Practice and Technology*, *12*(4), 927–936. https://doi.org/10.2166/wpt.2017.096

Peeters, J., Vicevic, G., Koops, G. H., & Côté, P. (2016). The role of innovative technologies in achieving energy-neutral wastewater treatment. *Water Practice and Technology*, *11*(4), 691–701. https://doi.org/10.2166/wpt.2016.074

Pellicer-Nàcher, C., Domingo-Félez, C., Lackner, S., & Smets, B. F. (2013). Microbial activity catalyzes oxygen transfer in membrane-aerated nitritating biofilm reactors. *Journal of Membrane Science*, *446*, 465–471. https://doi.org/10.1016/j.memsci.2013.06.063

Perez-Calleja, P., Aybar, M., Picioreanu, C., Esteban-Garcia, A. L., Martin, K. J., & Nerenberg, R. (2017). Periodic venting of MABR lumen allows high removal rates and high gas-transfer efficiencies. *Water Research*, *121*, 349–360. https://doi.org/10.1016/j.watres.2017.05.042

Ravishankar, H., Nemeth, A., Massons, G., Puig, D., Zardoya, D., Carpi, N., Lens, P. N. L., & Heffernan, B. (2022). Factors impacting simultaneous nitrification and denitrification in a membrane aerated biofilm reactor (MABR) system treating municipal wastewater. *Journal of Environmental Chemical Engineering*, *10*(5), 108120. https://doi.org/10.1016/j.jece.2022.108120

Rosso, D., Iranpour, R., & Stenstrom, M. K. (2005). Fifteen Years of Offgas Transfer Efficiency Measurements on Fine-Pore Aerators: Key Role of Sludge Age and Normalized Air Flux. *Water Environment Research*, *77*(3), 266–273. https://doi.org/10.2175/106143005X41843

Semmens, M. (2005). *Membrane Technology: Pilot Studies of Membrane-Aerated Bioreactors*. https://doi.org/10.2166/9781843397045

Semmens, M. J., Dahm, K., Shanahan, J., & Christianson, A. (2003). COD and nitrogen removal by biofilms growing on gas permeable membranes. *Water Research*, *37*(18), 4343–4350. https://doi.org/10.1016/S0043-1354(03)00416-0

Syron, E., & Casey, E. (2008). Membrane-Aerated Biofilms for High Rate Biotreatment: Performance Appraisal, Engineering Principles, Scale-up, and Development Requirements. *Environmental Science & Technology*, *42*(6), 1833–1844. https://doi.org/10.1021/es0719428

Terada, A., Yamamoto, T., Igarashi, R., Tsuneda, S., & Hirata, A. (2006). Feasibility of a membrane-aerated biofilm reactor to achieve controllable nitrification. *Biochemical Engineering Journal*, *28*(2), 123–130. https://doi.org/10.1016/j.bej.2005.10.001

Timberlake, D. L., Strand, S. E., & Williamson, K. J. (1988). Combined aerobic heterotrophic oxidation, nitrification and denitrification in a permeable-support biofilm. *Water Research*, *22*(12), 1513–1517. https://doi.org/10.1016/0043-1354(88)90163-7

Ukaigwe, S., Zhang, Y., Lee, K., & Liu, Y. (2023). Structural and Microbial Dynamics Analyses of MABR Biofilms. *Journal of Environmental Engineering*, *149*(12), 04023085. https://doi.org/10.1061/JOEEDU.EEENG-7438

Underwood, A., McMains, C., Coutts, D., Peeters, J., Ireland, J., & Houweling, D. (2018). *Design and Startup of the First Full-Scale Membrane Aerated Biofilm Reactor in the United States*. 1282–1296. https://www.accesswater.org/publications/proceedings/-299457/design-and-startup-of-the-first-full-scale-membrane-aerated-biofilm-reactor-in-the-united-states

Uri-Carreño, N., Nielsen, P. H., Gernaey, K. V., & Flores-Alsina, X. (2021). Long-term operation assessment of a full-scale membrane-aerated biofilm reactor under Nordic conditions. *Science of The Total Environment*, *779*, 146366. https://doi.org/10.1016/j.scitotenv.2021.146366

Uri-Carreño, N., Nielsen, P. H., Gernaey, K. V., Wang, Q., Nielsen, U. G., Nierychlo, M., Hansen, S. H., Thomsen, L., & Flores-Alsina, X. (2023). The effects of low oxidation-reduction potential on the

performance of full-scale hybrid membrane-aerated biofilm reactors. *Chemical Engineering Journal*, *451*, 138917. https://doi.org/10.1016/j.cej.2022.138917

Wang, R., Xiao, F., Wang, Y., & Lewandowski, Z. (2016). Determining the optimal transmembrane gas pressure for nitrification in membrane-aerated biofilm reactors based on oxygen profile analysis. *Applied Microbiology and Biotechnology*, *100*(17), 7699–7711. https://doi.org/10.1007/s00253-016-7553-1

Wei, X., Li, B., Zhao, S., Qiang, C., Zhang, H., & Wang, S. (2012). COD and nitrogen removal in facilitated transfer membrane-aerated biofilm reactor (FT-MABR). *Journal of Membrane Science*, *389*, 257–264. https://doi.org/10.1016/j.memsci.2011.10.038

Zhang, S., Wang, Y., He, W., Wu, M., Xing, M., Yang, J., Gao, N., & Pan, M. (2014). Impacts of temperature and nitrifying community on nitrification kinetics in a moving-bed biofilm reactor treating polluted raw water. *Chemical Engineering Journal*, *236*, 242–250. https://doi.org/10.1016/j.cej.2013.09.086

Zhong, H., Dong, L., Tang, Y., Qi, L., & Wang, M. (2023). The C/N Ratio's Effect on a Membrane-Aerated Biofilm Reactor (MABR): COD and Nitrogen Removal, Biofilm Characteristics, and Microbial Community Structure. *Water*, *15*(24), Article 24. https://doi.org/10.3390/w15244298

Chapter 3 - Characterizing biofilm thickness, microbial community, and functionality in a full-scale hybrid membrane aerated biofilm reactor

Abstract

Pollutant removal in biofilm processes such as membrane aerated biofilm reactors (MABR) is directly influenced by the biofilm thickness and microbial community functions. However, these biofilm characteristics have not been studied in full-scale MABR systems before. This study addressed this knowledge gap by characterizing the spatial and operational dynamics of key biofilm properties such as thickness, and microbial community structure and functionalities in a full-scale MABR facility. The arrangement of the MABR cassettes in an array along the length of the plug flow MABR train resulted in a longitudinal biofilm thickness gradient. The biofilms on the front cassettes were more than twice as thick as those on cassettes at the back. Examination of biofilm thickness as a function of MABR process airflow indicated that a lower airflow (4.5 NL m^{-2} hr^{-1}) resulted in a thicker biofilm (> 1000 μm) throughout the tank. Consistent with the trends in thickness, analysis of Bray-Curtis dissimilarity index showed that there were differences in the biofilm microbial community composition along the length of the MABR tank and between operating phases. Thicker biofilms in the front cassettes of the full-scale tank were predicted to have a higher relative abundance of organisms with anaerobic functions such as fermentation and sulfur reduction and lower relative abundance of organisms with aerobic functions such as aerobic heterotrophy and nitrification. *Nitrosomonas* was identified to be the main ammonia oxidizer and *Nitrospira* and *Nitrotoga* were the main nitrite oxidizers in the biofilm samples. The 16s RNA gene profiles were strongly correlated with biofilm thickness (R^2 = 0.8) and MABR nitrification rate (R^2 = 0.4). Phases with thinner biofilm showed higher relative abundance of nitrifiers which corresponded to higher nitrification rates. Thus, optimizing the process airflow to provide adequate biofilm thickness control is key to maximizing nitrification rate in full-scale MABR.

Keywords: MABR, biofilm thickness, nitrification rate, microbial community analysis

3.1 Introduction

Biofilms are complex and dynamic biostructures where a variety of microorganisms and their associated products are embedded in a matrix of extracellular polymeric surfaces (EPS) and immobilized on a surface (Boltz et al., 2017). Biofilm reactors such as membrane aerated biofilm reactors (MABR) are engineered to have high surface area to volume ratios to maximize attached biomass and thereby increase reaction rates and reduce the process footprint (Qureshi et al., 2005). The redox gradients and microbial stratification within the MABR biofilm created by counter-diffusion of substrates enables simultaneous nitrification and denitrification for concurrent carbon and nitrogen removal (Martin & Nerenberg, 2012). The extent of macroscale carbon and nitrogen removal can be influenced by both substrate transport and biological activity in biofilms. Hence, linking macro-scale MABR performance with the meso-scale biofilm features and microbial community composition will help us to better understand the biofilm processes and support efforts to purposefully influence the biofilm development for an optimized treatment process (Morgenroth and Milferstedt, 2009).

Biofilm thickness control is critical for the effective operation of biofilm reactors as excessively thin biofilms will be biomass limited while excessively thick biofilms can limit substrate diffusion (Sørensen & Morgenroth, 2023). Co-diffusional biofilm treatment systems such as moving bed biofilm reactors (MBBR) have reported that biofilm thicknesses in the range of 200-500 μm achieved similar ammonium removal (Piculell et al., 2016). This is because nitrification occurs in the outer layers of the biofilm which has direct contact with the oxygen and ammonium supply from the bulk. On the contrary, nitrification in MABRs can be influenced by the biofilm thickness because of its counter-diffusional biofilm geometry where nitrification occurs in the inner layers. Low nitrification rates and process failures have been reported in bench-scale MABRs that have high biofilm thickness (Semmens et al., 2003). Similarly, bench-scale biofilm-only MABRs have reported a reduction in TN removal rate when high scouring rates were employed (Bunse et al., 2023; Mehrabi et al., 2020). Thus, air scouring in MABR has profound impacts on biofilm thickness and the resulting pollutant removal performance. Full scale MABR technologies recirculate the process air for to create shearing conditions in the bulk, and agitate the membrane fibers to slough off excess biofilm growth (Peeters et al., 2017). However, the impact of airflow on full-scale biofilm thickness has not been investigated before.

Biofilm thickness can also indirectly impact reactor performance by shaping the microbial community structure and functions. The biofilm impacts diffusion of substrates such as oxygen, chemical oxygen demand (COD), and various nitrogen (N) species, thereby creating substrate gradients that serve as unique niches for microbial stratification (Stewart & Franklin, 2008). Thus, thicker biofilms could potentially harbor a more diverse microbial community with heterogeneous functions. The role of biofilm thickness

has been studied well in MBBR processes using biofilm carriers with specific grid wall height that determine the maximum possible thickness (Piculell et al., 2016). Experiments with carriers of different biofilm thicknesses have shown that thicker biofilms had increased richness, evenness, and Shannon index when compared to thinner biofilms (Suarez et al., 2019; Torresi et al., 2016; Zhao et al., 2022). In terms of biofilm functions, thin biofilms with a higher aerobic fraction and high DO have been shown to provide a competitive advantage for ammonia oxidizing organisms over nitrite oxidizing organisms for partial nitritation in MBBR reactors (Piculell et al., 2016). However, it is unclear whether biofilm thickness plays the same role on community diversity and functions in MABR biofilms with counter diffusional design. While prior studies have characterized the MABR biofilm microbial community under intermittent aeration (Pellicer-Nàcher et al., 2014), and with different influent loading (Tian et al., 2015) and C/N ratio (Liu et al., 2010), the impact of biofilm thickness on MABR microbial community diversity, composition, and functionalities remains unexplored.

In summary, the current knowledge on biofilm characteristics is largely based on co-diffusional biofilm systems. The few studies that have focused on MABR utilized small-scale systems fed with synthetic wastewaters that do not represent the actual mixing and shearing hydrodynamics or the substrate complexity of full-scale systems. No study so far has characterized the degree of heterogeneity in biofilm properties in full-scale MABR systems that have long membrane cords (up to 2 m), large membrane surface areas (10^4 to 10^5 m^2) and are arranged within a plug flow tank. Hence, to address these knowledge gaps, this study had three objectives: i) characterize biofilm thickness as a function of location and operating conditions ii) characterize microbial community composition and functionality in the MABR biofilms over similar conditions; and finally, iii) examine relationships between MABR nitrification performance, biofilm thickness, and microbial community composition and functionality. These objectives were achieved by harvesting membranes at selected locations and operating conditions of a full scale MABR facility.

3.2 Methodology

3.2.1 Sampling strategy

The study site has been described in Chapter 2 Section 2.2.1. The MABR process at the study site consisted of 4 parallel operating tanks that received influent wastewater and return activated sludge (RAS) streams. Each of the 4 tanks housed nine ZeeLung MABR cassettes arranged in a row. Membrane harvesting was enabled by lifting the full-scale cassettes using a crane in November 2022 (middle of phase 1), April 2023 (end of phase 3), May 2023 (beginning of phase 4) and October 2023 (end of phase 4). Hence the sampling spanned a range of air flow, temperature, and biofilm maturity conditions. During each membrane harvesting campaign, cassettes representing the front, middle, and rear sections were

lifted to capture the longitudinal profile of the biofilm. The details of the membrane harvesting are shown in Table 3.1. The average operating temperature, MABR process airflow, and nitrification rate (Equation 2.4 in Chapter 2) for the sampling week are also shown in Table 3.1.

After lifting, the cassettes were placed on the ground to drain excess water (Figure 3.1a) and then sprayed with secondary effluent to remove any loosely held material. Sampled cords were selected after visual inspection to ensure they were representative of their respective cassette and then snipped at the top and bottom using scissors. The remaining cords were knotted off to prevent air leakage from the cassettes (Figure 3.1 b). The harvested cord was cut into five equivalent sections namely top, mid-top, mid, mid-bottom, and bottom (Figure 3.1c). Each of the five sections was further cut into two for biofilm thickness and microbial community analyses, respectively. The cut sections designated for biofilm thickness analysis were placed inside sterile vials that contained phosphate buffer saline (PBS) solution to preserve the structural integrity of the biofilms and then stored at 2℃ in a refrigerator until analysis. The biofilm samples designated for microbial community analysis were placed inside empty snap cap tubes and stored in a -20℃ freezer until analysis.

Table 3.1 – Sampling scheme and operating conditions during biofilm harvesting. Cells highlighted in green show the cassettes lifted during a sampling event.

Operational conditions		**Phase 1**	**Phase 3**	**Phase 4a**			**Phase 4b**	
T (℃)		16.9	13.4	17.4			19.6	
$Q_{Air, MABR}$ (NL m^{-2} hr^{-1})		6	4.5	6			6	
NR_{NHx} (g-N m^{-2} d^{-1})		1.44	0.78	1.7			1.9	
Location	**Cassette #**	**Tank 4**	**Tank 4**	**Tank 2**	**Tank 3**	**Tank 4**	**Tank 4**	**Tank 3**
Front	C1							
	C2							
	C3							
Middle	C4							
	C5							
	C6							
Rear	C7							
	C8							
	C9							

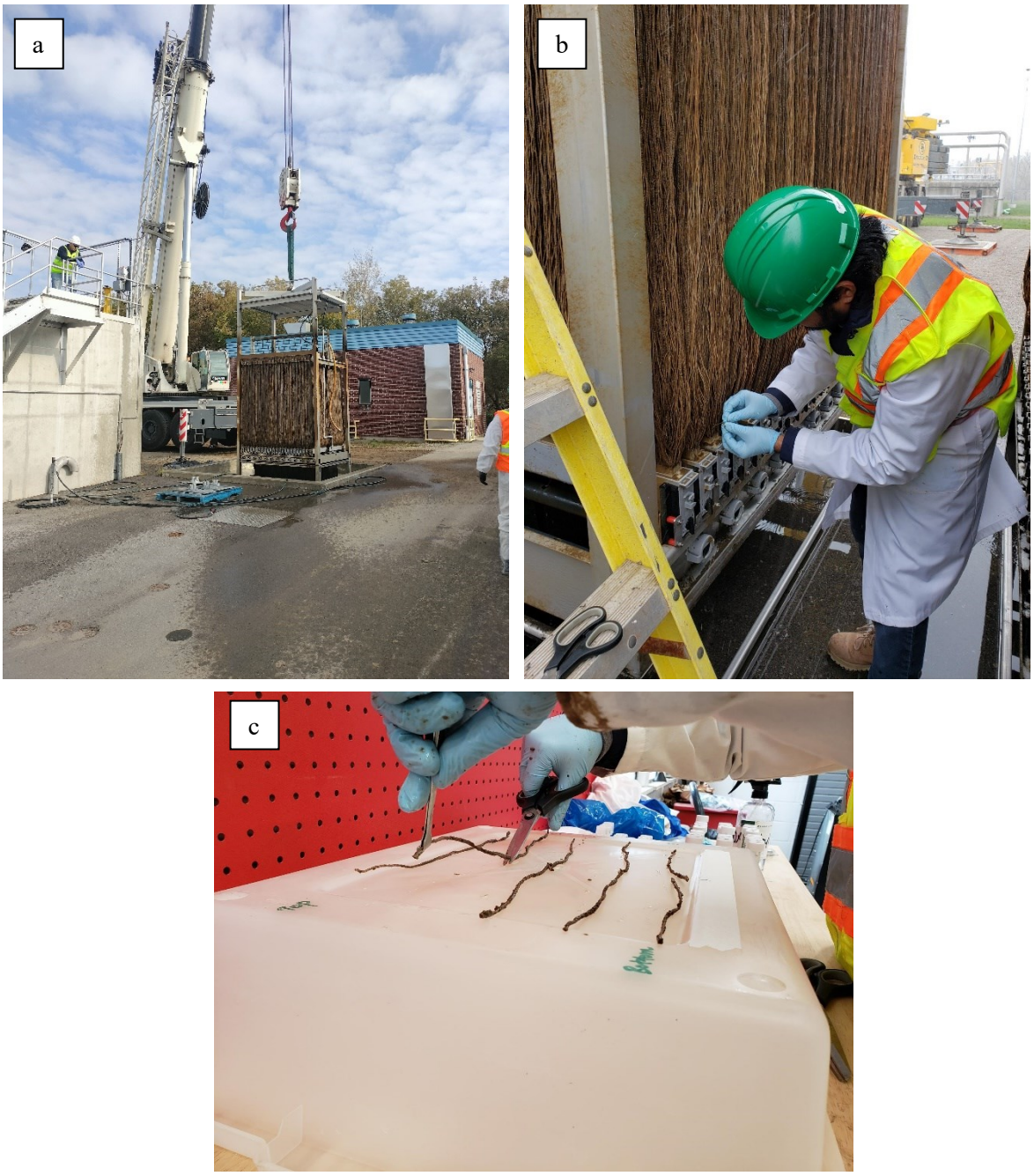

Figure 3.1 – a) Full-scale MABR cassettes lifted from the tanks for membrane harvesting. b) Membrane inspection and harvesting c) Slicing full-length cord into two sets of five sections for biofilm imaging and microbial community analysis.

3.2.2 Optical Coherence Tomography analysis

Biofilm thickness measurements were carried out to gain insights into variations between different cassettes in a tank, paired cassettes in parallel tanks, and operating conditions (phases). The thickness

measurements were obtained from biofilm scans using Optical Coherence Tomography (OCT). OCT analysis is well suited for studying mesoscale biofilm structures as it is fast, can capture images at high resolution, is non-invasive and does not require sample preparation (Wagner & Horn, 2017). Biofilm imaging was conducted using a Ganymede™ Series SD-OCT Systems (Thorlabs, Germany) with a 930 nm wavelength. The biofilm scans were obtained in the two-dimensional longitudinal direction along the membrane fiber with an axial resolution of 4 μm. The biofilm thickness measurements from the OCT scans were obtained using Fiji software (Schindelin et al., 2012). The image processing in Fiji involved adjusting the brightness and contrast using the auto feature to ensure the membrane at the base of the biofilm was distinctly visible. The perpendicular distance between the membrane and the biofilm was measured using the "measure" function within the software manually at 50 locations along the length of the membrane. The average value of the 50 measurements was considered as the representative thickness of the membrane section.

3.2.3 Microbial community analysis

The biofilm microbial community composition and functionality was characterized to gain insight into how spatial and operating conditions impacted their development. Total DNA was extracted from the membrane sections using DNeasy PowerSoil Pro Kits (Qiagen) following a procedure that was modified from the manufacturer's protocol. Instead of the 250 mg soil sample, the modified procedure used a 1 cm section was cut from the sample cord using sterile scalpel blades and transferred to a PowerBead Pro tube containing 800 μL of solution CD1 (Qiagen). The PowerBead Pro tubes were incubated at 65°C for 10 mins and then homogenized for 45 seconds at 5.5 m/s using a FastPrep-24 bead beater (MP Biomedical, Santa Ana, CA). The remainder of the extraction procedure was performed as per the manufacturer's protocol. The quantity of DNA in the sample extracts were quantified using Qubit dsDNA HS Assay Kits (ThermoFisher Scientific). The purity of DNA was also assessed using the NanoDrop 2000 (ThermoFisher Scientific) to ensure there was minimal protein or RNA contamination in the extracts. These QC checks were within the acceptable bounds of the extraction procedure. Sample extracts were stored at -20°C until further analysis.

The microbial community composition was determined by amplifying the V4-V5 regions of the 16S rRNA using universal primers 515F-Y and 926R. Unique six-base barcodes were attached to primers to allow for sample multiplexing and flow cell binding (Bartram et al., 2011). The subsequent amplification and sequencing protocols were previously described (McKnight & Neufeld, 2021) and are briefly summarized herein. All DNA samples were amplified using PCR in 25-μL reaction volumes containing 1X ThermoPol buffer, 15 μg of bovine serum albumin, 200 μM of dNTPs, 0.2 μM of both forward and reverse primers, 0.625 units of Hot Start *Taq* DNA Polymerase (New England Biolabs, MA, USA), and

1-10 ng of template DNA. The cycling conditions for PCR included a 3 min initial denaturation at 95°C, then 35 cycles of denaturation at 95°C for 30 s, annealing at 50°C for 30 s, and extension at 68°C for 1 min, with a final extension time of 7 min at 68°C. Samples that were amplified in triplicate were pooled, quantified, and subsequently combined in equimolar concentrations based on gel quantification to create the amplicon library. Following manufacturer's protocols and guidelines, sequencing of the sample library was done using a MiSeq Reagent Kit v2 (2 x 250 cycles, Illumina, Canada) on a MiSeq System (Illumina, CA, USA) at the University of Waterloo. Paired-end reads were demultiplexed using the MiSeq reporter software (v. 4.0.0.1769). The AXIOME3 pipeline was used to perform quality trimming, primer sequence and chimera removal, paired-end sequence merging, and denoising using DADA2 to generate a final amplicon sequence variant (ASV) table (Callahan et al., 2016; Min et al., 2021). Taxonomic classification of ASVs was done using the SILVA database release 138 (Quast et al., 2013). The raw DNA sequence data is available in the NCBI Sequencing Read archive under the BioProject accession number: PRJNA1104605.

The raw ASV data was used to calculate various diversity indices to serve as quantitative indicators for evaluating the microbial community composition within and between samples. To assess the diversity within a sample, three α diversity indices namely ASV richness (number of ASVs in a sample), evenness (Pielou's J) (how close in numbers the ASVs are), and Shannon index were calculated using the diversity function from the R vegan package (v. 2.6-4), with a rarefaction depth of 10,000. Principal Coordinate Analysis (PCoA) using Bray-Curtis dissimilarity index was performed using AOViz platform (https://github.com/AlexUmbach/AOViz) to study the variability of community composition between different samples collected at a given sampling event and between sampling events. A Bray-Curtis triplot was also created using AOViz platform to understand the relationship between taxonomic abundance, biofilm thickness, and nitrification rate measured during the sampling week. Normalization of data prior to calculation of Bray-Curtis dissimilarity was done using scaling with ranked subsampling (SRS) at a depth of 10000 (Beule & Karlovsky, 2020).

Additionally, the raw ASV data was processed through a Functional Annotation of the Prokaryotic Taxa (FAPROTAX) analysis using FAPROTAX v. 1.2.7 to predict the putative functions of the identified ASVs based on 16S rRNA gene sequences (Louca et al., 2016). The FAPROTAX database employed in this study included modifications to accommodate taxonomic changes to the naming of nitrifying organisms present in SILVA database release 138 that have not been added to the current FAPROTAX database.

3.2.4 Statistical analysis

This study adopted various statistical tests to compare biofilm thickness within and between samples. The variability in the biofilm thickness within a single OCT scan obtained for a membrane section (N=50) was ascertained by the coefficient of variation (COV) (Equation 3.1).

$$COV = \frac{\sigma_s}{\mu_s} * 100\% \quad \text{.....(3.1)}$$

σ_s = Sample standard deviation of 50 measurements within a membrane section (µm)

μ_s = Average of 50 thickness measurements within a membrane section (µm)

When comparing biofilm thickness between samples, each membrane section was considered as an independent sample and the average of the 50 measurements taken within each section was used as its representative thickness (t_i). The thickness values of the five sections were found to be normally distributed in all the cassettes sampled during all the operating conditions based on a Shapiro-Wilk Test ($\alpha = 0.05$). Hence parametric tests were performed to study the variance between two or more samples.

The variability in thickness along a full-length cord was assessed by comparing the average biofilm thickness between the five cut sections in the different cassettes sampled. To do so, the section averages within a cord (N=5) were normalized (Equation 3.2) to a notionally common scale (-1 to +1) for easy visualization of the thicknesses measured over a large range (100-1000 µm).

$$Normalized\ average = \frac{(t_i - t_{average})}{t_{max} - t_{min}} \quad \text{.....(3.2)}$$

t_i = Representative thickness of a membrane section (µm)

$t_{average}$ = Average thickness of the five membrane sections being compared (µm)

t_{max}= Maximum thickness of the five membrane sections being compared (µm)

t_{min} = Minimum thickness of the five membrane sections being compared (µm)

The biofilm thickness at the different locations of a tank (front, middle, and rear cassettes) and between different operating conditions were compared using one-way ANOVA and Tukey's post-hoc tests (P = 0.05). Thicknesses on co-located cassettes in different MABR trains were compared using a Welch's T-test for comparison of samples with unequal variance. The relative percentage difference (RPD) was also estimated to quantify the degree of variability in thickness between the MABR trains.

The three α diversity metrics calculated based on the ASV data were compared between different samples to infer changes in diversity. The variability of the metric between the five sections of a full-length cord was assessed through the COV within the data set (N =5) using equation 3.1. The five membrane sections

of the full-length cord were treated as independent sample replicates of a cassette. The normal distribution of the α diversity metrics of the five sections was confirmed by a Shapiro-Wilk Test (α = 0.05). The variation of the α diversity metrics between the three cassette locations was assessed through a one-way ANOVA test (α = 0.05). The variation between duplicate cassettes co-located in different tanks was assessed though a Welch's T-Test (α = 0.05).

3.3 Results and discussion

The overall objectives of the study were to characterize the biofilm thickness, and microbial community composition and functionality across different spatial scales and operating conditions to obtain further insights into factors impacting on process performance. In line with that, the MABR biofilm characteristics were systematically investigated at different sections of a membrane cord, along the length of the MABR tank, and between different phases. The biofilm thickness and microbial community composition responses are initially discussed individually and then related with the macro-level process performance.

3.3.1 Local spatial variations in biofilm thickness

The dataset on biofilm thickness was initially reviewed to establish the global range of values observed in the study. The entire dataset composited into a bar plot is shown in Figure S3.1 and the thickness measurements in each section are shown in Table S3.1. The thickness measurements spanned across two orders of magnitude from a minimum value of 90 μm to values above the maximum measurable thickness limit (MMT = 1000 μm). The median thickness across all the locations and operating conditions was 742 μm. Over one-third of all the harvested samples had thickness values greater than the MMT and were not included in subsequent statistical comparisons within and between biofilm samples.

The uniformity of biofilm thickness values within each membrane section (N=50) was examined by assessing COV values. A histogram of the COV values for all sections that had thickness in the measurable range is shown in Figure S3.2. The COV values ranged between 7% and 44% with a median value of 16%. A Pareto analysis indicated that 80% of the samples had a COV less than 21%. On the basis of these statistics, it was concluded that there was a relatively low degree of variability in the thickness measurements within the sections. Hence, in subsequent analyses the mean of the 50 readings was employed when evaluating the variability of biofilm thickness between different samples.

The membranes in the MABR cassettes had a length of 1.9 m and were intermittently sparged with air that was released at the base of the cassettes. It was anticipated that the biofilm on the bottom sections would be thinner than the top ones due to their proximity to the initial burst of the sparging gas at the base. To test this hypothesis, the normalized average biofilm thickness (Equation 3.2) of the five sections

of the full-length cords from different sampling times and locations (Figure 3.2) were examined. Membrane cords that reported thickness > MMT were not included in this analysis. From Figure 3.2, it can be seen that there was no discernable trend in the normalized averages for the membrane cords sampled in the middle and rear locations of the tank. The lack of a systematic change in biofilm thickness from the top to the bottom sections suggests that differences in shearing intensity along the length of the cords did not influence the biofilm thickness. Because of this lack of systematic variation, the individual sections from a cord were treated as replicate samples for which average and standard deviation values were calculated for subsequent analyses.

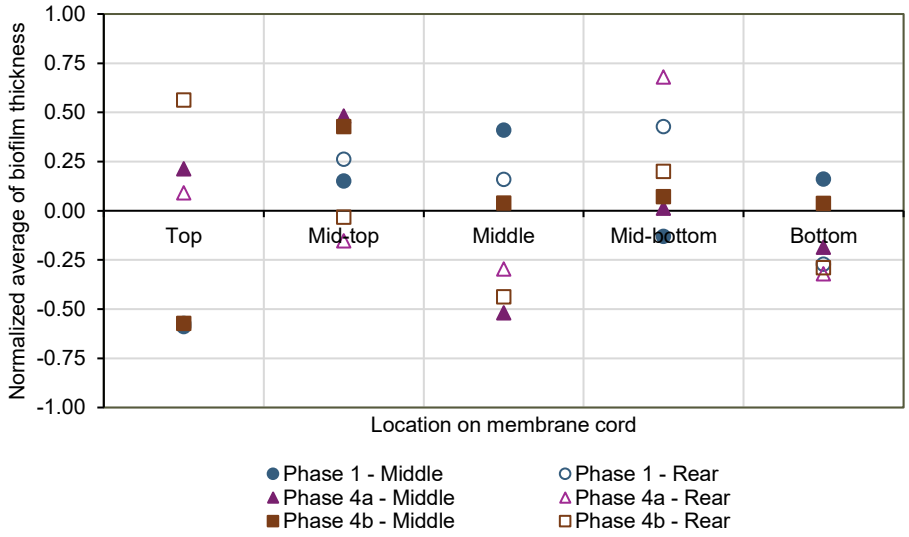

Figure 3.2 – Normalized average biofilm thickness versus cord location for different tank locations and operational conditions.

The MABR process consisted of four tanks operating in parallel and hence the biofilm thicknesses obtained for cassettes that were in the same longitudinal positions in Tanks 3 and 4 during Phase 4b were compared to assess the reproducibility of tanks (Figure 3.3). The biofilm thicknesses in the front cassettes were all greater than the MMT in both the tanks and hence a comparison of these cassettes was not conducted. The thickness values of the middle (C5) and rear (C9) cassettes in the two tanks were found to be different ($P < 0.05$), however, the magnitude of the differences were modest (RPD values of 18% and 21%, respectively). The relatively small difference in biofilm thickness between the parallel operating tanks at the corresponding locations was deemed to likely have little impact on process performance.

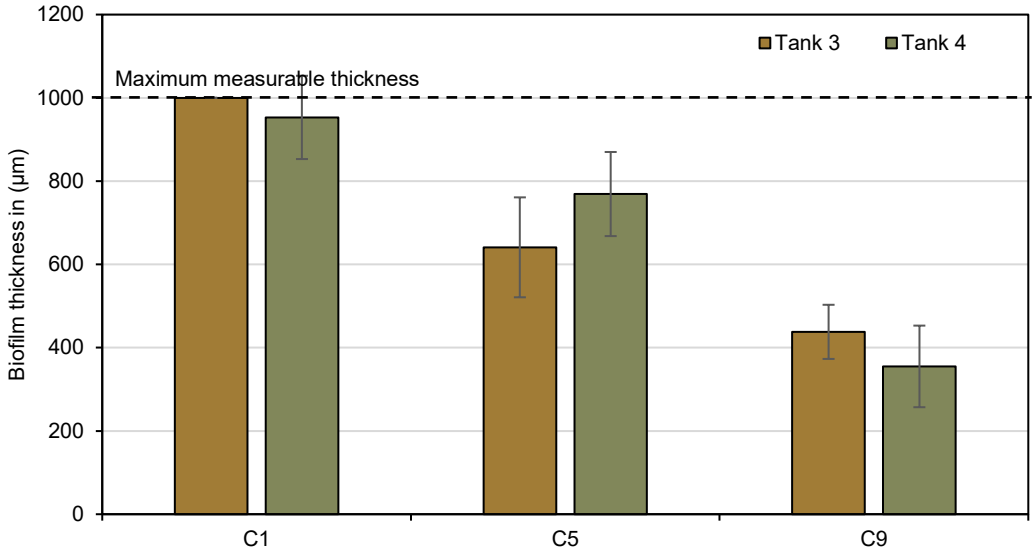

Figure 3.3 – Comparison of biofilm thickness between tank 3 and tank 4 of the full-scale MABR process during Phase 4b. Error bars indicate standard deviation (N=5).

3.3.2 Longitudinal spatial variation in biofilm thickness

The full-scale MABR process had four parallel trains that each had a length to width ratio of 9:1 that is indicative of plug flow mixing conditions (US EPA, 1998). Each of these trains housed nine MABR cassettes arranged in a single row along the tank length. Such a cassette arrangement within a plug flow tank was expected to create a longitudinal substrate gradient and influence biomass growth along the length of tank. Hence the biofilm thicknesses measured at the front, middle, and rear cassettes (Figure 3.4) were compared for each phase of the study to assess whether longitudinal location affected biofilm thickness. In Phase 1, biofilm thickness was found to significantly decrease along the tank ($P < 0.05$) with the average biofilm thickness at the back of the tank (286 ± 30 µm) about 50% of that in the front (595 ± 269 µm). In Phases 4a and 4b, the biofilm thickness was greater than the MMT in the front cassettes and declined to approximately 670 µm in the middle and back cassettes in Phase 4a (Figure 3.4); while in Phase 4b the corresponding values were 698 ± 129 µm and 335 ± 93 µm. The biofilms thicknesses were greater than the MMT for most samples during Phase 3 and hence a longitudinal trend could not be inferred. On the whole, biofilm thickness profiles from three out of the four sampling events displayed a longitudinal thickness gradient that favored thinner biofilms in the rear end of the tank. It was anticipated that such a thickness differential could have significant impacts on microbial community and by extension C and N removal activities along the tank.

Biofilm thicknesses are believed to reflect the net result of the biomass growth rate that is enabled by substrate availability and the rate of biofilm detachment that is controlled by erosional forces (Horn et al., 2003). In the system under study, it was assumed that the shearing was consistent along the length of the MABR tank while substrate loading, and resulting growth rates decreased from the front to the back of the tank due to the plug flow conditions. The thicker biofilms in the front of the tank suggests that the higher growth rates from the higher substrate availability predominated over the erosion rate. On the contrary, at the back of the tank which received a lower substrate loading, the observed thinner biofilms reflected a lower biomass growth rate relative to the erosion rate. Hence, a design change that could be considered in future installations would be to increase the shearing intensities at the front of the tank to maintain thin biofilms along the length of the tank to minimize diffusional resistances.

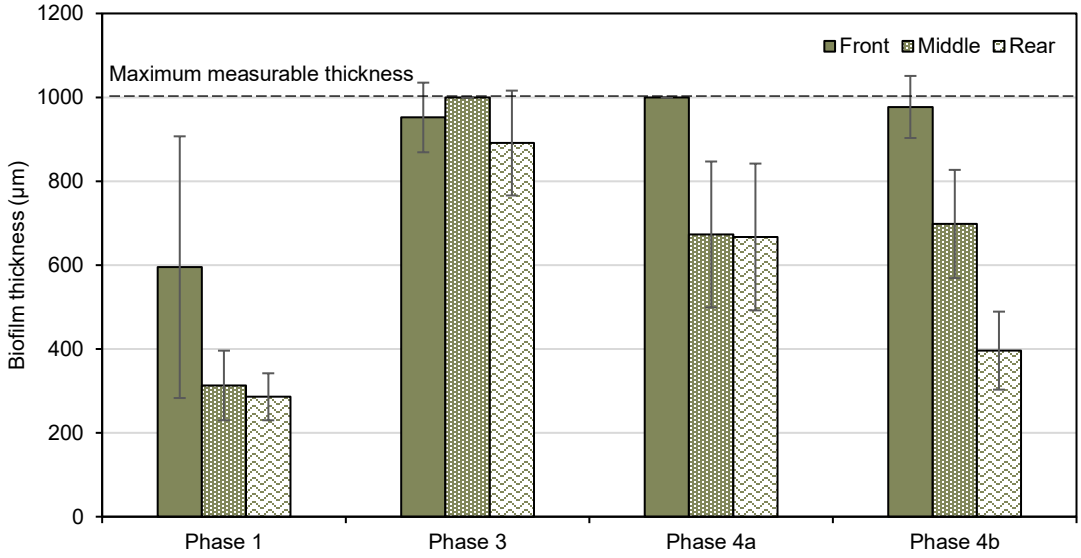

Figure 3.4 – Biofilm thickness along the length of the MABR tank for different operational conditions. Error bars indicate standard deviation (N=5).

3.3.3 Impact of air flow on biofilm thickness

The MABR airflow can influence shearing conditions in the bulk (Peeters et al., 2017) and hence biofilm thickness measurements were compared across the operational phases where air flow was adjusted. For this analysis, biofilm thickness values from cassettes located at the rear end of the tanks were compared as they were mostly within the measurable range during all sampling events. In this regard, biofilms that were established under the lowest and highest air flows employed in phase 3 (4.5 NL m^{-2} hr^{-1}) and phases 1 and 4 (6 NL m^{-2} hr^{-1}), respectively, were compared. Phase 3, with a lower air flow, had a significantly higher average thickness ($P < 0.05$) of at least 819 ± 69 µm (N = 3, two sections had thickness > MML) when compared to the range of values (285-667 µm) observed at the higher air flow employed in Phases 1

and 4. A 25% increase in airflow resulted in a 20-65% reduction in biofilm thickness. Thus, it was confirmed at full scale that the operational airflow has a strong influence on the thickness of biofilms that are established.

Phases 1, 4a and 4b were conducted during warm weather operations at the higher airflow setting (6 NL m^{-2} hr^{-1}) and hence the thickness values obtained in these phases were examined (Figure 3.5) to determine whether thickness was only dependent on temperature and air flow. From Figure 3.5 it can be seen that the biofilm thickness differed between the three operating phases (Figure 3.5). The lowest average thickness (285 ± 30 μm) was observed in phase 1 and this was attributed to the relatively early sampling that was conducted after only two months of MABR comissioning. It is likely that the biofilm was still developing at this time. Further, Phase 4a had a significantly higher average thickness (667 ± 142) when compared to 4b (396 ± 44 μm). The sampling event for Phase 4a was conducted one month after initiation of operation at the high airflow, whereas, the Phase 4b samples were collected after six month of this operation. The decrease in thickness between phase 4a and 4b was attributed to the prolonged exposure to high shearing conditions with the higher flow suggesting that a considerable period of operation is required before biofilm thickness changes. Thus the results indicate that the biofilm is a dyanmic entity and there can be temporal changes in thickness during its initial formation and the operations thereafter.

On the whole, when all the spatial, operational, and temporal trends are considered, the MABR cassette location, process airflow, and the duration of exposure to a given operating condition appear to strongly influence the biofilm thickness. In comparison, the variability within a full-length fiber and between co-located cassettes in different tanks appears to be small.

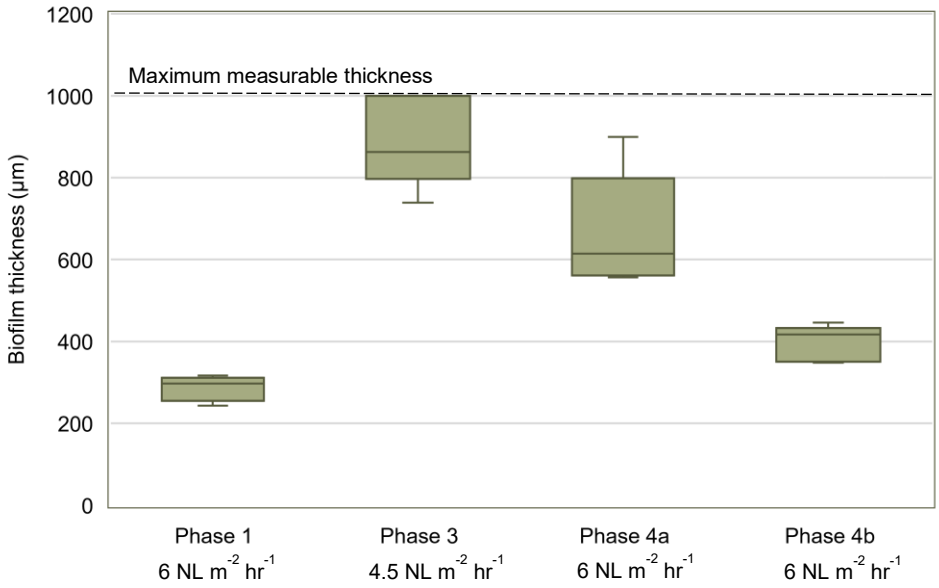

Figure 3.5 – Comparison of biofilm thickness measured in rear cassettes during different phases of operation.

3.3.4 Variations in diversity of the biofilm microbial community

It was hypothesized that biofilm thickness is a key driver of microbial community composition and function which would in turn dictate pollutant removal performance (Suarez et al., 2019). Biofilm thickness was expected to influence the microbial community composition and functionality because of the substrate diffusional limitation and varying redox conditions created by the biofilm. Therefore, the composition and functionality of the MABR microbial community were assessed in a similar manner to that of the biofilm thickness. To support this characterization, alpha and beta diversity indices, FAPROTAX prediction of the community functions, and the raw ASV data were investigated.

Three alpha diversity indices (Figure 3.6) were initially examined as indicators of community complexity. The richness index describes the number of different ASVs in a sample. From figures 3.6 a & d it can be seen that the value of this index ranged between 400 and 1200 over all the membrane sections sampled. However, the richness index simply indicates the presence of a group and does not provide any information on the relative dominance or rarity of the ASVs within the sample. Hence, the evenness index (Figures 3.6 b & e) was examined to evaluate the proportionality of the ASVs relative to each other. The evenness index can range from 0 to 1 with 0 indicating dominance of a single group and 1 indicating all the ASVs are present in equal number. The evenness of ASVs in the current study varied between 0.8-0.9 suggesting a relatively uniform microbial community profile with little dominance by individual ASVs. Lastly, the Shannon index was calculated as a composite metric that reflects both richness and evenness and describes the overall diversity of a sample. The Shannon index values for biofilms in this study

ranged between 5-6. The subsequent discussion addresses the impact of biofilm location on the α diversity of the biofilm samples.

As previously discussed, the full-scale MABR biofilms had similar thicknesses within the full-length cords and between co-located cassettes in different tanks. The alpha diversity metrics were examined to see if the microbial community diversity followed a similar pattern. The variability within the full-length cords was assessed on the basis of the COV of the α-diversity metrics of the five sections of the different full-length cords (Table S3.2). While the COV values for the richness index were as high as 20%, the values for the Shannon index and evenness were modest (< 5%). The relatively small COV values suggest that the α diversity of the biofilm community along the length of cords was similar. Similarly, when the indices were compared between tanks with the Welch T-test, all three α-diversity metrics were found to be similar ($P < 0.05$). Thus, the α-diversity metrics followed similar trends to biofilm thickness when evaluating the local variations in the biofilm characteristics.

The previously discussed longitudinal decrease in biofilm thickness was expected to influence the diversity of the microbial community. Hence, the α-diversity metrics of the front, middle, and rear cassettes were compared for each sampling event by ANOVA test. The results showed that all three α-diversity metrics were similar ($P < 0.05$) along the length of the full-scale tank. This finding was inconsistent with the expectation that the biofilm community diversity will vary with biofilm thickness. It is believed that the lack of effect in this case was due to the limitations of the α-diversity metrics. The similarity in the alpha diversity metrics merely indicates that there are the same number of ASVs and their distributions are even. However, it is possible that two samples can have the same alpha diversity metrics but consist of different microorganisms (Ramette, 2007). Hence, beta diversity metrics were evaluated to further compare the composition of the microbial communities observed in this study.

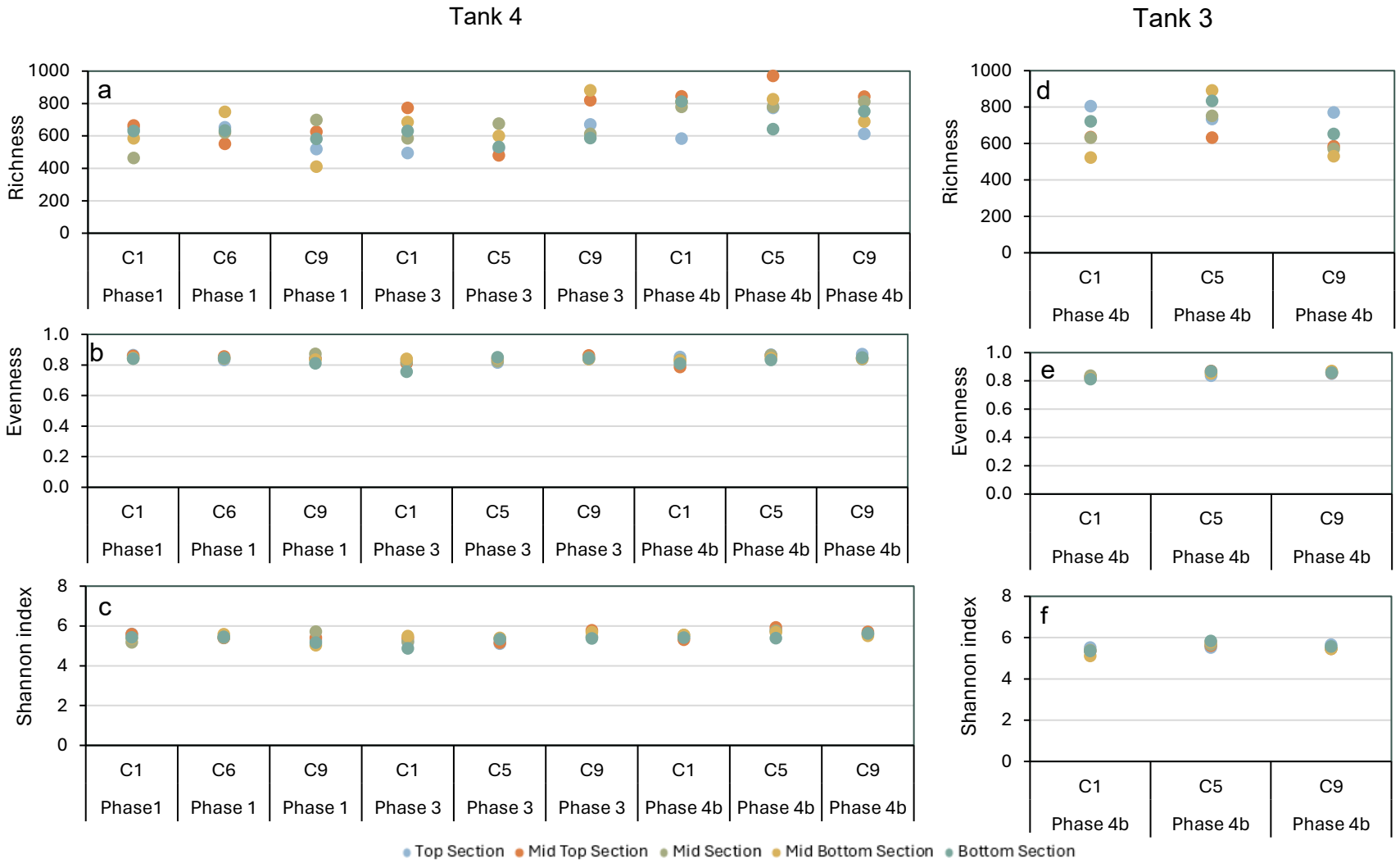

Figure 3.6 – Alpha diversity indices vs location and phase: Richness (a,d), evenness (b,e), Shannon index (c,f)

The Bray-Curtis index is a beta diversity index that quantifies the compositional dissimilarity between two samples by comparing the number of taxa and the relative abundance of the shared taxa (Kers & Saccenti, 2022). It generates a distance metric between two samples where the magnitude of the distance indicates the degree of difference in the community composition. In the current study examination of the Bray-Curtis index between two samples at a time was deemed to be complicated and laborious. Hence, a principal coordinates analysis (PCoA) was carried out to facilitate the comparison of the Bray-Curtis indices between multiple samples. The Bray-Curtis PCoA analysis creates a dissimilarity matrix (or distance matrix) comparing multiple samples and assigns each sample a location in a two-dimensional space based on the matrix values (distance values) (Ramette, 2007). The similarity between different sample communities can be inferred by their position relative to others in the ordination space. Markers that are close to each other in the ordination space are considered to have similar community composition while greater distances between markers indicate dissimilarity.

The similarity of communities between different sections was investigated to study the community composition along the full-length cords. Figure 3.7 a-d presents the Bray-Curtis PCoA plots for biofilms harvested from different cassette locations in Tank 4 during all the sampling events. The samples from the different sections of the full-length cords generally grouped close to each other in distinct clusters in all three sampling events. The proximity of the sample markers in this manner suggests that there was a consistent microbial community composition along the full-length of the membrane cords during the two phases. It should be noted that the PCoA analysis showed some deviations in grouping of samples in some cases. In phase 1, the top two sections of cassette 1 (red markers in figure 3.7a) were distinct from those of the remaining sections. Similarly, cassettes 4 and 5 during phase 3 (blue and cyan markers in figure 3.7b) showed a wider spread in the markers associated with location on the cords. These variabilities could not be attributed to any specific parameter or microbial group as the BC index is a composite index of all the microbial community and their relative abundances. Despite these inconsistencies, when all of the Bray-Curtis dissimilarity index results were considered, it was concluded that the microbial communities along the full-length cord were generally similar.

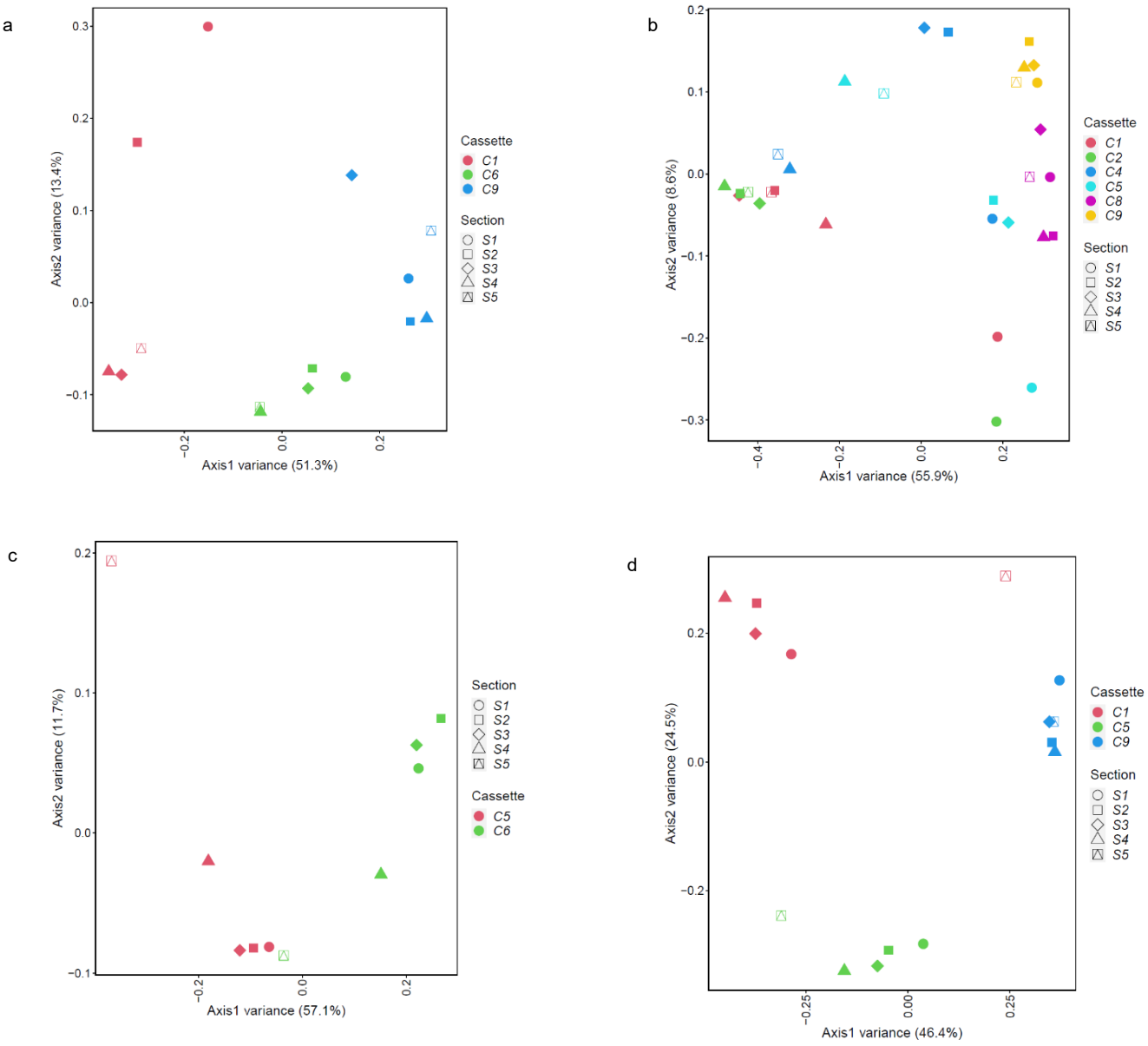

Figure 3.7 – PCoA analysis of Bray-Curtis dissimilarity for biofilm samples collected in tank 4 during phase 1 (a), phase 3 (b), phase 4a (c), and phase 4b (d). The shape of the markers refers to the different sample sections from top (S1) to bottom (S5). The color of the markers refers to the cassette location within tank 4.

The longitudinal variation of the microbial communities in the MABR biofilms was investigated using the Bray-Curtis PCoA plots to explore the relationship with biofilm thickness. Differences in biofilm community due to differences in biofilm thickness would be manifested if the markers from individual cassettes were farther from each other. Examination of figures 3.7 a and d shows the anticipated pattern where the samples representing front, middle, and rear cassettes are separate from each other for samples collected in Phase 1 and Phase 4b. The grouping pattern indicates the microbial community composition was distinctly different between the three locations. In contrast, the PCoA plot for phase 3, that included cassettes that were located immediately next to each other, indicates that there was considerable overlap in the ordination between consecutive cassettes such as C1 and C2 and C4 and C5 (Figure 3.7b). This suggests that while there was a longitudinal change in community profile between different locations in the tank, the shift was gradual with some level of similarity in between adjacent cassettes. However, when comparing front cassettes (C1, C2) with the rear ones (C8, C9) the greater distance between markers suggests that the biofilm communities were substantially different between the two ends of the tank. Overall, the biofilm on a full-length fiber had similar composition throughout while there were differences in communities between cassettes along the length of the MABR. It should be noted that these metrics do not provide information on which specific groups or functionalities were changing. To address this issue the predicted functional profile and ASVs of specific microbes of interest were investigated subsequently.

3.3.5 Functionality of the biofilm microbial community

The biofilm functionality at different spatial and operational scales was investigated using FAPROTAX analysis (Figure 3.8). FAPROTAX is a predictive database that assigns putative functionalities to prokaryotic taxa based on 16s RNA genes that are drawn from literature on cultured strains (Louca et al., 2016). The predicted functionalities include a wide variety of aerobic and anaerobic metabolisms. The key functionalities and their variations are discussed subsequently.

Figure 3.8 –Bubble plot of functionalities predicted using FAPROTAX analysis of MABR biofilm samples along the length of the tank during different phases. The color of the bubble indicates phases. Size of bubbles indicate the magnitude of relative abundance

The front cassettes had the highest biofilm thicknesses in this study and hence it was anticipated that there would be a higher prevalence of organisms with anaerobic metabolic functions due to reduced oxygen penetration (Pellicer-Nàcher et al., 2013). As anticipated, organisms predicted to have fermentative functions were more abundant in C1 (3.9 to 10.7%) than C9 (2.9 to 3.7%) samples during phases 3 and 4b (Figure 3.8). The higher prevalence of fermentative organisms could contribute towards increased denitrification activity in the thicker biofilms due to greater availability of readily biodegradable COD. Similarly, microbes with sulfur reduction functionalities were more abundant in the cassettes with the thick biofilms. The front cassettes had significant sulfur reduction functionality in phase 3 (3 to 6%) and phase 4b (5 to 7%) while this functionality was less prevalent (> 1%) in cassettes with thin biofilms. Phase 1 biofilms did not show any sulfur reduction functionality (Figure 3.8) suggesting that the organisms responsible accumulated in the biofilms during Phases 2 and 3 when the influent loading to the MABR was high and the air flow was reduced (5.5 and 4.5 NL m^{-2} hr^{-1}, respectively). Overall, the longitudinal variation of fermentation and sulfur reduction functionalities suggested that thicker MABR biofilms have higher abundance of organisms with anaerobic functionalities.

Aerobic functionalities were examined to assess if differences in biofilm dissolved oxygen levels across the tank impacted these functions. Aerobic heterotrophy (aerobic_chemoheterotrophy in Figure 3.8) was observed to be prevalent at relative abundances in the range of 3 to 15% when all biofilm were considered. Chapter 2 hypothesized the possibility of oxygen utilization for BOD removal based on the difference between nitrification rates calculated using ammonia removal (NR_{NHX}) and oxygen transfer rate (NR_{OTR}). Thus, the presence of significant aerobic heterotrophic functionality in the biofilms is therefore consistent with this hypothesis. However, organisms performing aerobic heterotrophy were present at a lower relative abundance in the front cassettes in phases 1 and 4b and this was attributed to the thicker biofilms and lower oxygen penetration depth. Similarly, the variation of aerobic autotrophic functions such as nitrification was investigated. Functionalities such as aerobic ammonia oxidation, aerobic nitrite oxidation, and nitrification were more abundant in the thin biofilms that were observed at the rear cassettes than the thick biofilms located at the front (Figure 3.8). The trends in nitrifier ASV abundance are discussed in detail in the next section. Overall, it was concluded that there is a strong relationship between biofilm thickness and aerobic/anaerobic functionalities in the MABR biofilms.

The full-scale performance monitoring results in the previous chapter suggested that there was substantial denitrification occurring in the MABR process. Hence, the denitrification functionalities were examined (figure 2.7) to characterize the presence of this functionality in the MABR. The FAPROTAX analysis predicted that organisms with nitrite denitrification and nitrate denitrification functionalities were present in all the biofilm samples at a similar relative abundance (0.1 to 1%). The prevalence of this functionality

suggests there was a potential for short cut N removal by nitritation and denitritation in the process. Similarly, organisms with nitrous oxide denitrification functionality were present at a relative abundance range of 0.1 to 1% in all the biofilm samples indicating the MABR biofilms were consuming nitrous oxide generated in the nitrification and denitrification processes (Discussed further in Chapter 4). The narrow range of relative abundances of these functionalities over all biofilm samples suggest that there was an interaction between the biomass in the outer portion of the biofilms layer and the suspended biomass in the anoxic bulk phase of the MABR.

3.3.6 Nitrifier composition in MABR biofilms

Enhanced nitrification enabled by the counter-diffusion of substrates is one of the main process advantages of the MABR process. Hence, selected ASVs of ammonia oxidizing bacteria (AOB) and nitrite oxidizing bacteria (NOB) (Figure 3.9) were examined to identify the key nitrifiers (> 0.1 % relative abundance) present in the samples. From Figure 3.9, it can be seen that several species from the *Nitrosomonas* genus were identified as the main ammonia oxidizers in the biofilm samples while species of the *Nitrospira* and *Nitrotoga* genera were identified as the dominant nitrite oxidizers. These organisms are commonly observed nitrifiers in activated sludge (Ahn et al., 2008), MBBRs (Zhao et al., 2022) , and in lab-scale (Bunse et al., 2023; Downing & Nerenberg, 2008a; Mehrabi et al., 2020; Ukaigwe et al., 2023) and full-scale (Uri-Carreño et al., 2023; Zhao et al., 2023) MABR processes. An initial review of Figure 3.8 revealed trends in the relative abundance between cassettes and sampling events which are discussed subsequently.

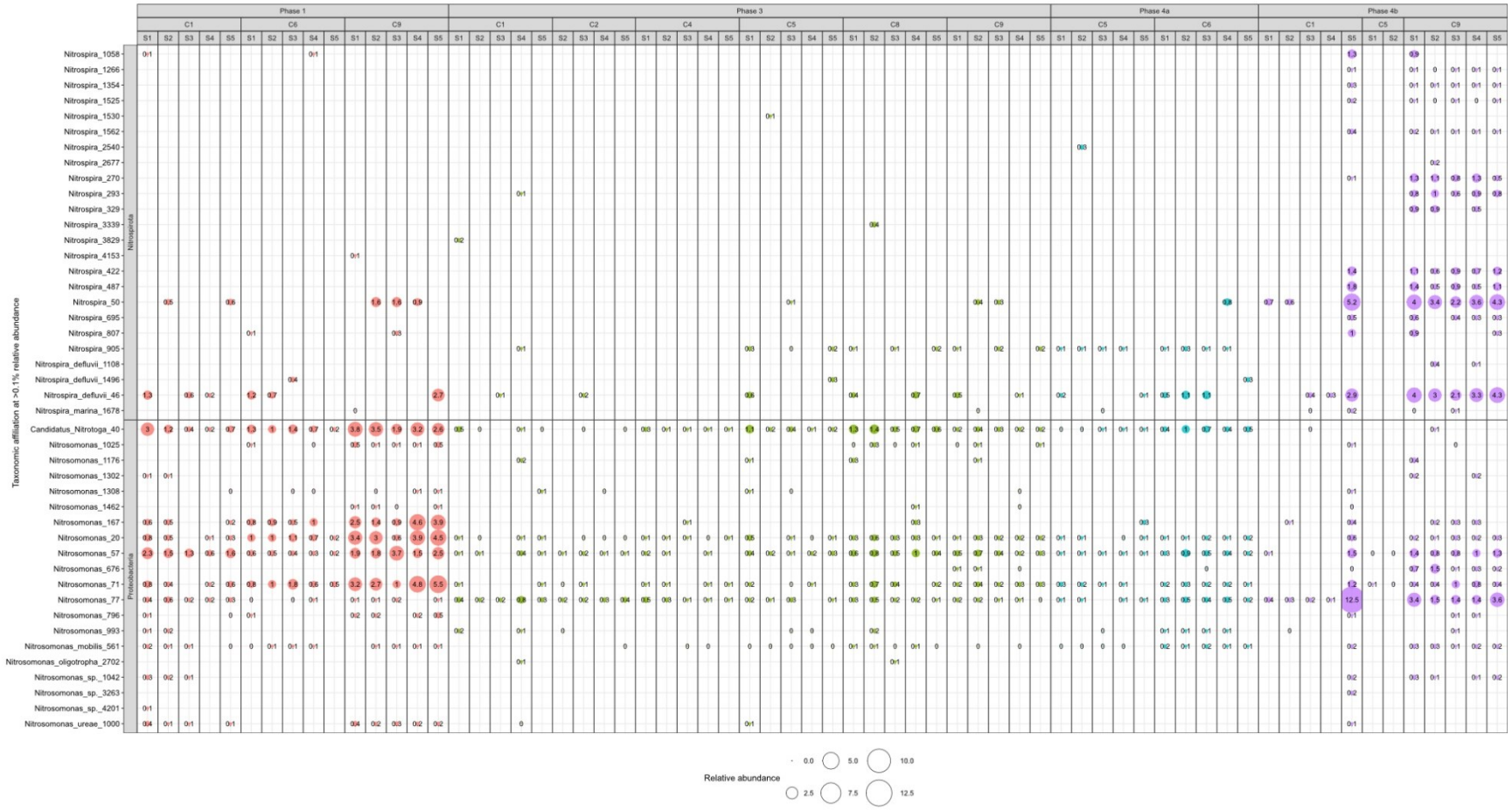

Figure 3.9 – Bubble plot showing relative abundance of nitrifying organisms (> 0.1%) identified in the MABR biofilm samples. The color of the bubble indicates different phases. The size of the bubble indicates the magnitude of relative abundance.

The relative abundance of the AOBs and NOBs were evaluated along the length of the full-scale tank to assess whether there was any correspondence with biofilm thickness. As seen in Figure 3.9, in Phase 1, the relative abundance of several *Nitrosomonas* species increased longitudinally (C1, C5, and C9). Similarly, in Phase 4a, several *Nitrosomonas* and *Nitrospira* species exhibited higher relative abundances in the last cassette. However, such a longitudinal trend was not observed for Phase 3. These trends in nitrifier relative abundance are believed to be due to differences in biofilm thickness that occurred along the tank length and between phases. Thicker biofilms has been found to result from growth of heterotrophs, on the exterior of the biofilm where COD concentrations are higher (Downing & Nerenberg, 2008b). Hence, thicker biofilms can effectively "dilute" observed nitrifier relative abundances by greater contribution of heterotrophs since the sampling and analysis methodologies employed effectively composite biomass across the entire depth of the biofilm. Thinner biofilms with greater oxygen penetration and a relatively smaller heterotrophic fraction, can therefore be expected to have a higher proportion of nitrifier. The lack of a longitudinal trend in Phase 3 was attributed to the thicker biofilm that were present along the entire length of the tank (Figure 3.4). Thus, it was concluded that the biofilm thickness can control the relative proportion of nitrifier abundance in the biofilm with thinner biofilms favoring higher abundance.

The relative abundance of the nitrifiers were compared between the operational phases to assess whether factors other than biofilm thickness affected the presence of these organisms. From figure 3.9, *Candidatus* Nitrotoga was present in relative abundances up to 4.8% in in Phase 1, 1.4 % in Phase 3 and1% in Phase 4a, but was very low (< 0.5 %) in Phase 4b. The observed pattern in relative abundance was inconsistent with the observed biofilm thickness values suggesting that there may be other factors that influence the abundance of *Ca.* Nitrotoga. *Ca.* Nitrotoga is a temperature sensitive nitrite oxidizer which is typically enriched in the temperature range of 10-17℃ (Alawi et al., 2009; Kitzinger et al., 2018). Thus, the cold adaptative nature of *Ca.* Nitrotoga was consistent with their low prevalence in Phase 4b when the operating temperature of 20℃ and the elevated abundances in the remaining phases when the temperature was in the range 14-17 ℃. Conversely, several *Nitrospira* species including *Nitrospira* defluvii were present at higher abundance in Phase 4b when compared to Phase 1 that had a similar airflow but a slightly lower temperature. The variation in temperature sensitivity of nitrite oxidizers has been previously reported (Lantz et al., 2021; Ravishankar et al., 2022; Wegen et al., 2019). However, such trends were not observed in the ammonia oxidizer communities. Overall, the results suggest that while biofilm thickness plays an important role in the abundance of nitrifiers in the MABR biofilms, the selection of nitrite oxidizers can be influenced by other factors such as temperature.

3.3.7 Relating biofilm thickness, microbial community, and nitrification rate

The previously discussed biofilm characterization data indicated a strong interdependence between MABR airflow, biofilm thickness, and biofilm community composition. Hence, the impact of these dynamics at the micro- (microbial community) and meso-scales (biofilm thickness) of the biofilm on the overall process performance (nitrification rate) at the macro scale was investigated. To explore the relationship between these multiple variables, a triplot analysis (Figure 3.10) that correlated the Bray-Curtis dissimilarity of the 16s RNA gene profiles with the influential nitrifier taxa, the biofilm thicknesses and the MABR nitrification rates was conducted. Only tank 4 samples are included in the triplot analysis.

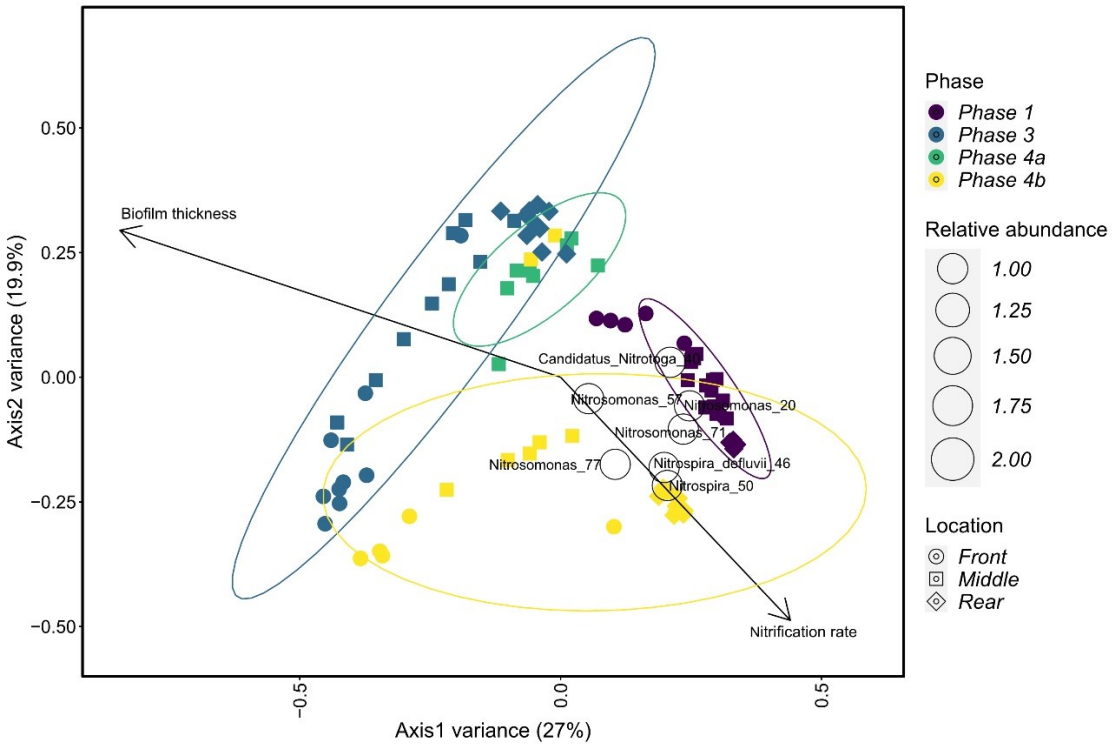

Figure 3.10 – Triplot analysis of 16sRNA gene profiles in the MABR biofilm samples. PCoA of the Bray-Curtis dissimilarity indices marker color indicating phase and shape representing cassette location. ASVs with ammonia oxidation and nitrite oxidation functions present at average relative abundance greater than 0.5% are shown with labelled black circles. Size of circles represents average relative abundance of species across all samples, while location within the ordination space reflects the correlation that specific species have with the different samples. The percent values in the axes labels shows the percentage of overall variation within the samples described by the two principal components.

The correlations between the microbial community composition, the biofilm thickness, and nitrification rates were examined through the orientation of the vectors shown in Figure 3.10. The correlation analysis

revealed that both the biofilm thickness and MABR nitrification rate were significantly correlated ($P < 0.05$) with the 16s RNA gene profiles. Among the two vectors, the biofilm thickness ($R^2 = 0.8$) had a stronger correlation with the overall microbial community profile than MABR nitrification rate ($R^2 = 0.43$). The opposing direction of the two vectors indicates an inverse relation between them where higher nitrification rates were favored by thinner biofilms. Examining the position of the relative abundance bubbles, the dominant nitrifiers such as *Nitrosomonas* and *Nitrospira* species were located close to the Phase 4b samples while *Ca.* Nitrotoga and other *Nitrosomonas* species were located close to Phase 1 samples. This suggests that nitrifiers abundance was favored by the low biofilm thickness under high airflow during phases 1 and 4b. Viewed collectively, biofilm thickness plays a major role in the microbial community composition and function. Thin biofilms favored nitrifier abundance and higher nitrification rates which further emphasizes the importance of optimal biofilm thickness control in full-scale MABR processes.

3.3.8 Implications of the findings

This study generated a sizeable and novel dataset on the characteristics of the biofilms present in a full-scale MABR. The comprehensiveness of this dataset enabled a detailed analysis of spatial and operational variability in the physical and microbial biofilm properties. Based on the findings, two main recommendations for future design and operation of full-scale MABRs have been arrived at

i) The prevalence of longitudinal gradient in biofilm thickness along a plug flow MABR tank observed in this study has important implications for modeling of MABR processes. Prior simulation of full-scale MABR processes has typically assumed a constant biofilm thickness for the full tank volume (Carlson et al., 2021; Elsayed et al., 2021; Flores-Alsina et al., 2023; He & Daigger, 2023; Houweling et al., 2018; Schraa et al., 2019). While this assumption may be valid for MABR installations with only a single cassette, constant biofilm thickness assumptions must be reconsidered when investigating full-scale MABR process with multiple cassettes. When modeling a long row of cassettes within a plug flow tank, simulating the MABR process as multiple reactors with varying biofilm thickness will be a better modeling practice.

ii) The longitudinal variation in biofilm thickness and microbial functionalities is a highly relevant finding for the future design of biofilm thickness control in full-scale MABRs. When the MABR is situated in an upstream position in the secondary treatment process that receives a higher organic loading, employing a more intensive biofilm thickness control at the front end of the MABR process may be beneficial to curb the prevalence of undesirable sulfate reduction which has previously shown to limit nitrite oxidation and increase N_2O

production (Delgado Vela et al., 2021, 2022). Maintaining thinner biofilms at the front of the tank could also improve the overall nitrification rate in the MABR process. Thus, a tapered biofilm thickness control design could be advantageous MABR installations of this nature to maximize nitrification and denitrification in full-scale applications.

3.4 Conclusion

This study characterized the thickness and microbial community composition of full-scale MABR biofilms and evaluated their spatial and operational dynamics. Based on the findings, the following conclusions were drawn.

- The arrangement of MABR cassettes in a single row within a plug flow tank resulted in a longitudinal thickness gradient with biofilms in the front cassette at least twice as thick as the ones in the rear end.
- Biofilm thickness varied with the MABR process airflow that provided thickness control. The rear cassettes at lower airflows (4.5 NL m^{-2} hr^{-1}) had a higher average thickness of 819 ± 69 μm when compared to operation at higher airflow (6 NL m^{-2} hr^{-1}) (285-667 μm).
- α diversity metrics did not vary significantly between samples. In contrast the Bray-Curtis dissimilarity index revealed that community composition and biofilm thickness followed similar trends. The microbial community profile along the length of the membrane cords were similar but varied along the length of the full-scale MABR tank. Community composition also differed between operational phases that had different temperatures and air flows.
- Thicker biofilms had a higher relative abundance of microbes with anaerobic functionalities such as fermentation and sulfur reduction. Biofilm samples collected from all the locations and operating conditions had nitrite denitrification and nitrous oxide denitrification functionality suggesting a widespread potential for short cut N removal and nitrous oxide mitigation in the biofilms.
- *Nitrosomonas* was identified as the primary ammonia oxidizer and *Nitrospira* and *Nitrotoga* were identified as the dominant nitrite oxidizers. Nitrifiers were present at higher relative abundance in thinner biofilms. The prevalence of nitrite oxidizers such as *Ca.* Nitrotoga, *Nitrospira* defluvii, and other *Nitrospira* species appear to be influenced by other factors such as temperature.
- Biofilm thickness and MABR nitrification rate showed a strong and significant correlation with the microbial community composition.
- Phases with thinner biofilm correlated with the higher abundance of the dominant nitrifiers which also resulted in higher nitrification rates. Thus, optimizing the process airflow to provide adequate biofilm thickness control is key to maximizing nitrification rate in full-scale MABR.

3.5 Supplemental information

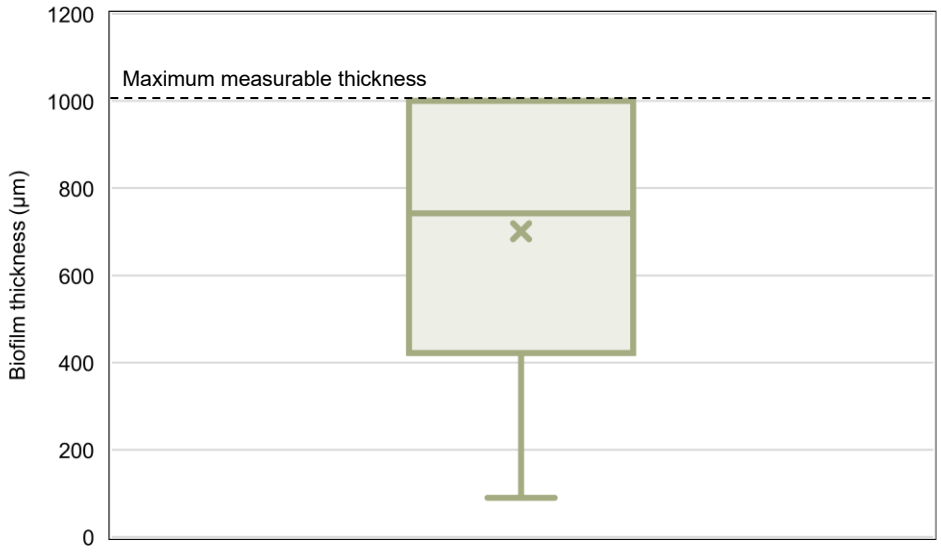

Figure S3.1 – Global analysis of all the biofilm thickness measurements across different locations, operating conditions, and replicates.

Table S3.1 – Thickness measurements obtained from full-scale MABR biofilms sampled at different locations and operational conditions.

Phase	Tank #	Cassette #	Location	Biofilm thickness in different sections of the full-length cord (µm)				
				S1	S2	S3	S4	S5
Phase 1	T4	C1	Front	267 ±118	258 ± 79	762 ± 146	> MMT	689 ± 148
	T4	C5	Middle	202 ± 60	341 ± 46	390 ± 37	288 ± 39	343 ± 72
	T4	C9	Rear	243 ± 44	305 ± 27	297 ± 51	317 ± 50	265 ± 67
Phase 3	T4	C1	Front	> MMT	> MMT	933 ± 65	> MMT	827 ± 89
	T4	C5	Middle	> MMT	> MMT	> MMT	> MMT	> MMT
	T4	C8	Rear	866 ± 117	> MMT	459 ± 98	729 ± 150	> MMT
	T4	C9	Rear	> MMT	855 ± 132	> MMT	862 ± 82	739 ± 72
Phase 4a	T2	C2	Front	> MMT	> MMT	> MMT	> MMT	> MMT
	T4	C5	Middle	551 ± 62	765 ± 142	587 ± 194	591 ± 84	872 ± 77
	T4	C6	Middle	844 ± 173	> MMT	421 ± 167	729 ± 125	614 ± 183
	T3	C8	Rear	698 ± 132	614 ± 89	565 ± 156	900 ± 99	557 ± 120
Phase 4b	T3	C1	Front	766 ± 75	> MMT	> MMT	> MMT	> MMT
	T4	C1	Front	> MMT	> MMT	> MMT	> MMT	> MMT
	T3	C5	Middle	486 ± 118	725 ± 210	628 ± 198	684 ± 97	673 ± 177
	T4	C5	Middle	813 ± 109	787 ± 65	811 ± 83	664 ± 56	> MMT
	T3	C9	Rear	467 ± 64	493 ± 51	442 ± 49	410 ± 35	376 ± 47
	T4	C9	Rear	335 ± 115	253 ± 104	231 ± 62	321 ± 132	282 ± 81
MMT – Maximum measurable thickness (1000 µm)								

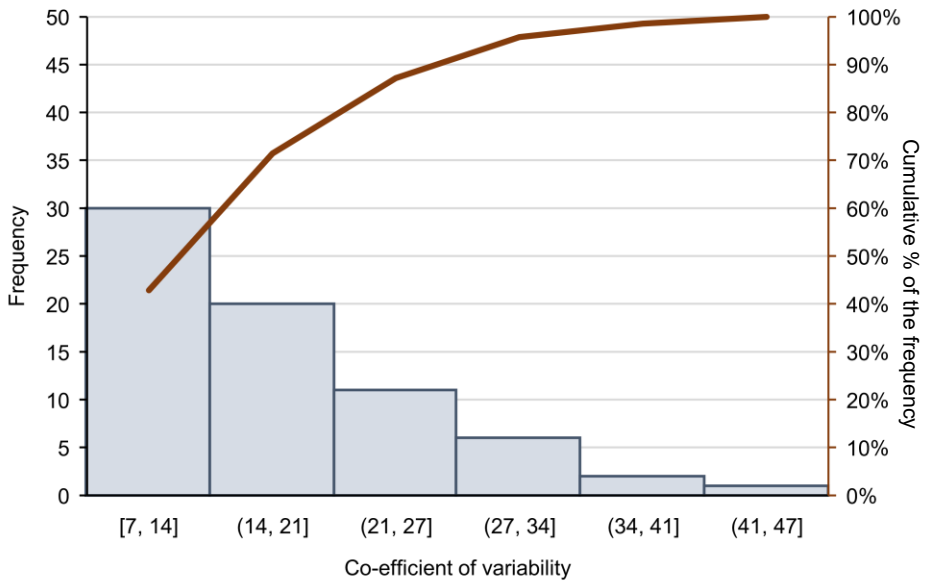

Figure S3.2 – Histogram and Pareto-analysis of the COV of biofilm thickness measurements within the membrane sections.

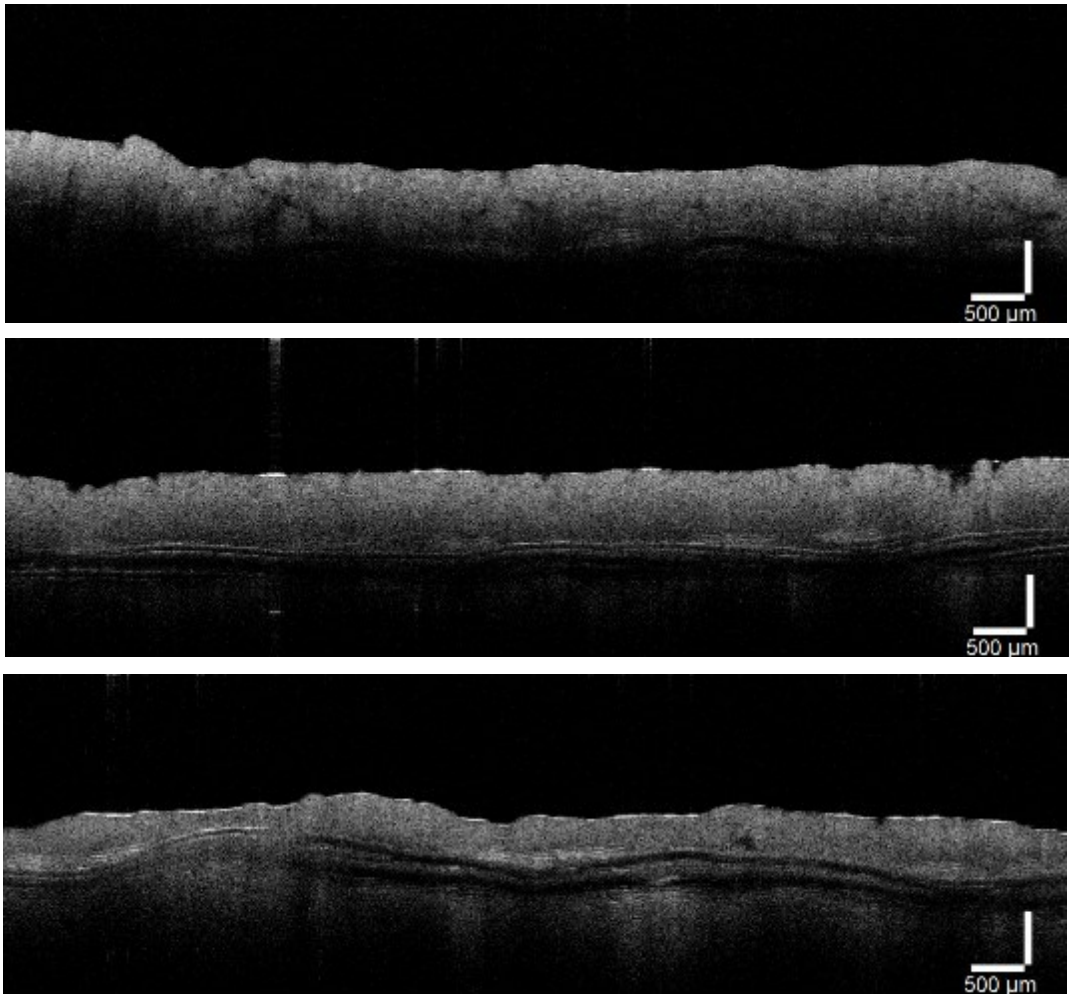

Figure S3.3 – OCT scans of biofilm samples from C1 (top figure), C5 (middle figure), and C9 (bottom figure) during Phase 4b. The average biofilm thickness of these sections were C1 = 766 ± 75 µm, C5 = 684 ± 97 µm, and C9 = 253 ± 104 µm.

Table S3.2 – COV for α diversity metrics between the five sections of full-length cords.

Phase	Cassette number	Co-efficient of variation (%)		
		Richness	Evenness	Shannon index
Phase 1	C1	13	1	3
Phase 1	C6	11	1	1
Phase 1	C9	19	3	5
Phase 3	C1	17	4	5
Phase 3	C5	14	2	3
Phase 3	C9	18	1	3
Phase 4b	C1	14	3	2
Phase 4b	C5	15	2	3
Phase 4b	C9	13	1	1
Phase 4b	C1	16	1	3
Phase 4b	C5	13	2	2
Phase 4b	C9	15	1	2

3.6 References

Ahn, J. H., Yu, R., & Chandran, K. (2008). Distinctive microbial ecology and biokinetics of autotrophic ammonia and nitrite oxidation in a partial nitrification bioreactor. *Biotechnology and Bioengineering*, *100*(6), 1078–1087. https://doi.org/10.1002/bit.21863

Alawi, M., Off, S., Kaya, M., & Spieck, E. (2009). Temperature influences the population structure of nitrite-oxidizing bacteria in activated sludge. *Environmental Microbiology Reports*, *1*(3), 184–190. https://doi.org/10.1111/j.1758-2229.2009.00029.x

Bartram, A. K., Lynch, M. D. J., Stearns, J. C., Moreno-Hagelsieb, G., & Neufeld, J. D. (2011). Generation of Multimillion-Sequence 16S rRNA Gene Libraries from Complex Microbial Communities by Assembling Paired-End Illumina Reads. *Applied and Environmental Microbiology*, *77*(11), 3846–3852. https://doi.org/10.1128/AEM.02772-10

Beule, L., & Karlovsky, P. (2020). Improved normalization of species count data in ecology by scaling with ranked subsampling (SRS): Application to microbial communities. *PeerJ*, *8*, e9593. https://doi.org/10.7717/peerj.9593

Boltz, J. P., Smets, B. F., Rittmann, B. E., van Loosdrecht, M. C. M., Morgenroth, E., & Daigger, G. T. (2017). From biofilm ecology to reactors: A focused review. *Water Science and Technology*, *75*(8), 1753–1760. https://doi.org/10.2166/wst.2017.061

Bunse, P., Orschler, L., Pidde, A. V., & Lackner, S. (2023). Effects of scouring on membrane aerated biofilm reactor performance and microbial community composition. *Bioresource Technology*, *369*, 128441. https://doi.org/10.1016/j.biortech.2022.128441

Callahan, B. J., McMurdie, P. J., Rosen, M. J., Han, A. W., Johnson, A. J. A., & Holmes, S. P. (2016). DADA2: High-resolution sample inference from Illumina amplicon data. *Nature Methods*, *13*(7), 581–583. https://doi.org/10.1038/nmeth.3869

Carlson, A. L., He, H., Yang, C., & Daigger, G. T. (2021). Comparison of hybrid membrane aerated biofilm reactor (MABR)/suspended growth and conventional biological nutrient removal processes. *Water Science and Technology*, *wst2021062*. https://doi.org/10.2166/wst.2021.062

Delgado Vela, J., Bristow, L. A., Marchant, H. K., Love, N. G., & Dick, G. J. (2021). Sulfide alters microbial functional potential in a methane and nitrogen cycling biofilm reactor. *Environmental Microbiology*, *23*(3), 1481–1495. https://doi.org/10.1111/1462-2920.15352

Delgado Vela, J., Gordon, K. J., Klatt, J. M., Dick, G. J., & Love, N. G. (2022). Integrated Modeling and Lab-Scale Investigations Demonstrate the Impact of Sulfide on a Membrane Aerated Biofilm Reactor. *ACS ES&T Water*, *2*(12), 2388–2399. https://doi.org/10.1021/acsestwater.2c00253

Downing, L. S., & Nerenberg, R. (2008a). Effect of oxygen gradients on the activity and microbial community structure of a nitrifying, membrane-aerated biofilm. *Biotechnology and Bioengineering*, *101*(6), 1193–1204. https://doi.org/10.1002/bit.22018

Downing, L. S., & Nerenberg, R. (2008b). Total nitrogen removal in a hybrid, membrane-aerated activated sludge process. *Water Research*, *42*(14), 3697–3708. https://doi.org/10.1016/j.watres.2008.06.006

Elsayed, A., Hurdle, M., & Kim, Y. (2021). Comprehensive model applications for better understanding of pilot-scale membrane-aerated biofilm reactor performance. *Journal of Water Process Engineering*, *40*, 101894. https://doi.org/10.1016/j.jwpe.2020.101894

Flores-Alsina, X., Uri-Carreno, N., Nielsen, P. H., & Gernaey, K. V. (2023). Modelling the impacts of operational conditions on the performance of a full-scale membrane aerated biofilm reactor. *Science of The Total Environment*, *856*, 158980. https://doi.org/10.1016/j.scitotenv.2022.158980

He, H., & Daigger, G. T. (2023). The hybrid MABR process achieves intensified nitrogen removal while N2O emissions remain low. *Water Research*, *244*, 120458. https://doi.org/10.1016/j.watres.2023.120458

Horn, H., Reiff, H., & Morgenroth, E. (2003). Simulation of growth and detachment in biofilm systems under defined hydrodynamic conditions. *Biotechnology and Bioengineering*, *81*(5), 607–617. https://doi.org/10.1002/bit.10503

Houweling, D., Long, Z., Peeters, J., Adams, N., Côté, P., Daigger, G., & Snowling, S. (2018). Nitrifying below the "Washout" SRT: Experimental and Modelling Results for a Hybrid MABR / Activated Sludge Process. 1250–1263. https://www.accesswater.org/publications/proceedings/-299455/nitrifying-below-the--washout--srt--experimental-and-modelling-results-for-a-hybrid-mabr-/-activated-sludge-process

Kers, J. G., & Saccenti, E. (2022). The Power of Microbiome Studies: Some Considerations on Which Alpha and Beta Metrics to Use and How to Report Results. *Frontiers in Microbiology*, *12*, 796025. https://doi.org/10.3389/fmicb.2021.796025

Kitzinger, K., Koch, H., Lücker, S., Sedlacek, C. J., Herbold, C., Schwarz, J., Daebeler, A., Mueller, A. J., Lukumbuzya, M., Romano, S., Leisch, N., Karst, S. M., Kirkegaard, R., Albertsen, M., Nielsen, P. H., Wagner, M., & Daims, H. (2018). Characterization of the First "Candidatus Nitrotoga" Isolate Reveals

Metabolic Versatility and Separate Evolution of Widespread Nitrite-Oxidizing Bacteria. *mBio*, *9*(4), 10.1128/mbio.01186-18. https://doi.org/10.1128/mbio.01186-18

Lantz, M. A., Boddicker, A. M., Kain, M. P., Berg, O. M. C., Wham, C. D., & Mosier, A. C. (2021). Physiology of the Nitrite-Oxidizing Bacterium Candidatus Nitrotoga sp. CP45 Enriched From a Colorado River. *Frontiers in Microbiology*, *12*. https://doi.org/10.3389/fmicb.2021.709371

Liu, H., Yang, F., Shi, S., & Liu, X. (2010). Effect of substrate COD/N ratio on performance and microbial community structure of a membrane aerated biofilm reactor. *Journal of Environmental Sciences*, *22*(4), 540–546. https://doi.org/10.1016/S1001-0742(09)60143-1

Louca, S., Parfrey, L. W., & Doebeli, M. (2016). Decoupling function and taxonomy in the global ocean microbiome. *Science*, *353*(6305), 1272–1277. https://doi.org/10.1126/science.aaf4507

Martin, K. J., & Nerenberg, R. (2012). The membrane biofilm reactor (MBfR) for water and wastewater treatment: Principles, applications, and recent developments. *Bioresource Technology*, *122*, 83–94. https://doi.org/10.1016/j.biortech.2012.02.110

McKnight, M. M., & Neufeld, J. D. (2021). *Microbial community analysis of biofilters reveals a dominance of either comammox Nitrospira or archaea as ammonia oxidizers in freshwater aquaria* (p. 2021.11.24.468873). bioRxiv. https://doi.org/10.1101/2021.11.24.468873

Mehrabi, S., Houweling, D., & Dagnew, M. (2020). Establishing mainstream nitrite shunt process in membrane aerated biofilm reactors: Impact of organic carbon and biofilm scouring intensity. *Journal of Water Process Engineering*, *37*, 101460. https://doi.org/10.1016/j.jwpe.2020.101460

Min, D., Doxey, A. C., & Neufeld, J. D. (2021). AXIOME3: Automation, eXtension, and Integration Of Microbial Ecology. *GigaScience*, *10*(2), giab006. https://doi.org/10.1093/gigascience/giab006

Peeters, J., Adams, N., Long, Z., Côté, P., & Kunetz, T. (2017). Demonstration of innovative MABR low-energy nutrient removal technology at Chicago MWRD. *Water Practice and Technology*, *12*(4), 927–936. https://doi.org/10.2166/wpt.2017.096

Pellicer-Nàcher, C., Domingo-Félez, C., Lackner, S., & Smets, B. F. (2013). Microbial activity catalyzes oxygen transfer in membrane-aerated nitritating biofilm reactors. *Journal of Membrane Science*, *446*, 465–471. https://doi.org/10.1016/j.memsci.2013.06.063

Pellicer-Nàcher, C., Franck, S., Gülay, A., Ruscalleda, M., Terada, A., Al-Soud, W. A., Hansen, M. A., Sørensen, S. J., & Smets, B. F. (2014). Sequentially aerated membrane biofilm reactors for autotrophic

nitrogen removal: Microbial community composition and dynamics. *Microbial Biotechnology*, *7*(1), 32–43. https://doi.org/10.1111/1751-7915.12079

Piculell, M., Welander, P., Jönsson, K., & Welander, T. (2016). Evaluating the effect of biofilm thickness on nitrification in moving bed biofilm reactors. *Environmental Technology*, *37*(6), 732–743. https://doi.org/10.1080/09593330.2015.1080308

Quast, C., Pruesse, E., Yilmaz, P., Gerken, J., Schweer, T., Yarza, P., Peplies, J., & Glöckner, F. O. (2013). The SILVA ribosomal RNA gene database project: Improved data processing and web-based tools. *Nucleic Acids Research*, *41*(D1), D590–D596. https://doi.org/10.1093/nar/gks1219

Qureshi, N., Annous, B. A., Ezeji, T. C., Karcher, P., & Maddox, I. S. (2005). Biofilm reactors for industrial bioconversion processes: Employing potential of enhanced reaction rates. *Microbial Cell Factories*, *4*(1), 24. https://doi.org/10.1186/1475-2859-4-24

Ramette, A. (2007). Multivariate analyses in microbial ecology. *FEMS Microbiology Ecology*, *62*(2), 142–160. https://doi.org/10.1111/j.1574-6941.2007.00375.x

Ravishankar, H., Nemeth, A., Massons, G., Puig, D., Zardoya, D., Carpi, N., Lens, P. N. L., & Heffernan, B. (2022). Factors impacting simultaneous nitrification and denitrification in a membrane aerated biofilm reactor (MABR) system treating municipal wastewater. *Journal of Environmental Chemical Engineering*, *10*(5), 108120. https://doi.org/10.1016/j.jece.2022.108120

Schindelin, J., Arganda-Carreras, I., Frise, E., Kaynig, V., Longair, M., Pietzsch, T., Preibisch, S., Rueden, C., Saalfeld, S., Schmid, B., Tinevez, J.-Y., White, D. J., Hartenstein, V., Eliceiri, K., Tomancak, P., & Cardona, A. (2012). Fiji: An open-source platform for biological-image analysis. *Nature Methods*, *9*(7), Article 7. https://doi.org/10.1038/nmeth.2019

Schraa, O., Alex, J., Rieger, L., & Miletic, I. (2019). *Dynamic modeling of membrane-aerated biofilm reactors*. 1297–1312. Scopus. https://www.scopus.com/inward/record.uri?eid=2-s2.0-85060791213&partnerID=40&md5=f4b85a621265aa07cd2dc9fc9d4e40f0

Semmens, M. J., Dahm, K., Shanahan, J., & Christianson, A. (2003). COD and nitrogen removal by biofilms growing on gas permeable membranes. *Water Research*, *37*(18), 4343–4350. https://doi.org/10.1016/S0043-1354(03)00416-0

Sørensen, K. H., & Morgenroth, E. (2023). *Biofilm reactors*. https://doi.org/10.2166/9781789060362_0813

Stewart, P. S., & Franklin, M. J. (2008). Physiological heterogeneity in biofilms. *Nature Reviews Microbiology*, *6*(3), 199–210. https://doi.org/10.1038/nrmicro1838

Suarez, C., Piculell, M., Modin, O., Langenheder, S., Persson, F., & Hermansson, M. (2019). Thickness determines microbial community structure and function in nitrifying biofilms via deterministic assembly. *Scientific Reports*, *9*(1), Article 1. https://doi.org/10.1038/s41598-019-41542-1

Tian, H.-L., Zhao, J.-Y., Zhang, H.-Y., Chi, C.-Q., Li, B.-A., & Wu, X.-L. (2015). Bacterial community shift along with the changes in operational conditions in a membrane-aerated biofilm reactor. *Applied Microbiology and Biotechnology*, *99*(7), 3279–3290. https://doi.org/10.1007/s00253-014-6204-7

Torresi, E., Fowler, S. J., Polesel, F., Bester, K., Andersen, H. R., Smets, B. F., Plósz, B. Gy., & Christensson, M. (2016). Biofilm Thickness Influences Biodiversity in Nitrifying MBBRs—Implications on Micropollutant Removal. *Environmental Science & Technology*, *50*(17), 9279–9288. https://doi.org/10.1021/acs.est.6b02007

Ukaigwe, S., Zhang, Y., Lee, K., & Liu, Y. (2023). Structural and Microbial Dynamics Analyses of MABR Biofilms. *Journal of Environmental Engineering*, *149*(12), 04023085. https://doi.org/10.1061/JOEEDU.EEENG-7438

Uri-Carreño, N., Nielsen, P. H., Gernaey, K. V., Wang, Q., Nielsen, U. G., Nierychlo, M., Hansen, S. H., Thomsen, L., & Flores-Alsina, X. (2023). The effects of low oxidation-reduction potential on the performance of full-scale hybrid membrane-aerated biofilm reactors. *Chemical Engineering Journal*, *451*, 138917. https://doi.org/10.1016/j.cej.2022.138917

US EPA. (1998). *Technical Support Document for Evaluation of Thoroughly Mixed Biological Treatment Units*. Accessed on: March 18, 2024. Accessed at: https://www3.epa.gov/airtoxics/nsps/socww/guidfn.pdf

Wagner, M., & Horn, H. (2017). Optical coherence tomography in biofilm research: A comprehensive review. *Biotechnology and Bioengineering*, *114*(7), 1386–1402. https://doi.org/10.1002/bit.26283

Wegen, S., Nowka, B., & Spieck, E. (2019). Low Temperature and Neutral pH Define "Candidatus Nitrotoga sp." as a Competitive Nitrite Oxidizer in Coculture with Nitrospira defluvii. *Applied and Environmental Microbiology*, *85*(9), e02569-18. https://doi.org/10.1128/AEM.02569-18

Zhao, J., Ni, G., Piculell, M., Li, J., Hu, Z., Wang, Z., Guo, J., Yuan, Z., Zheng, M., & Hu, S. (2022). Characterizing and comparing microbial community and biofilm structure in three nitrifying moving bed biofilm reactors. *Journal of Environmental Management*, *320*, 115883. https://doi.org/10.1016/j.jenvman.2022.115883

Zhao, X., Xie, Y., Sun, B., Liu, Y., Zhu, S., Li, W., Zhao, M., & Liu, D. (2023). Unraveling microbial characteristics of simultaneous nitrification, denitrification and phosphorus removal in a membrane-aerated biofilm reactor. *Environmental Research*, *239*, 117402. https://doi.org/10.1016/j.envres.2023.117402

Chapter 4 - An improved model to investigate the dynamics of nitrous oxide emissions from a full-scale hybrid MABR facility

Abstract

Current published models for nitrous oxide (N_2O) emissions in membrane aerated biofilm reactors (MABR) have several simplifications that are not representative of full-scale systems. This study developed an improved MABR N_2O model that captured commonly overlooked phenomena such as back diffusion of generated N_2O into MABR lumen gas and the recirculation of the N_2O laden lumen gas for tank mixing and biofilm thickness control. The improved model was validated with measured N_2O concentrations in the lumen gas phase and bulk mixed liquor in a full-scale hybrid MABR facility. The validated model was used to obtain insights into N_2O bioconversion pathways. Model predictions revealed that all N_2O generated in the inner layers of the biofilm was via the ammonium oxidizing organism activity. The N_2O transported to the outer biofilm layers was reduced via the heterotrophic denitrification pathway. The N_2O gas model predicted that up to 70% of the N_2O carried by the recirculated lumen gas was scrubbed into the mixed liquor which was further denitrified. An N_2O emission factor of 0.18 ± 0.01% N_2O-N/N load was estimated for the full-scale MABR process which achieved up to 50% removal of the influent N load, highlighting the potential of this technology to mitigate N_2O emissions when compared to conventional activated sludge.

Keywords: Biofilm, MABR, N_2O emission, membrane diffusion

4.1 Introduction

Wastewater resource recovery facilities (WRRF) have an overall positive impact on the environment by minimizing the release of organic matter and nutrients that can have adverse health effects on receiving waters. However, there is a growing concern about nitrous oxide (N_2O) emission during wastewater treatment as N_2O has a significantly higher global warming potential (298 times) than CO_2 in equivalent mass terms (IPCC, 2007). N_2O is generated as a byproduct during nitrification and denitrification in secondary wastewater treatment processes (Kampschreur et al., 2009). In these processes, N_2O has been reported to be generated through three major biological pathways (Law et al., 2012; Sabba et al., 2018), namely, (i) hydroxylamine oxidation - incomplete oxidation of hydroxylamine formed during ammonia oxidation in an aerobic environment; ii) nitrifier denitrification – autotrophic denitrification of nitrite (NO_2) formed during ammonia oxidation in an aerobic environment; and iii) heterotrophic denitrification – incomplete reduction of NO_3 during denitrification in an anoxic environment. The resulting N_2O emissions could contribute about 78% of the overall plant emissions, which is much higher than the indirect CO_2 emissions estimated for electricity and natural gas consumption (Daelman et al., 2013). Thus, mitigating N_2O emissions is a major challenge in the path towards net-zero and treatment plants may need to be upgraded or optimized to reduce their release.

Membrane aerated biofilm reactors (MABR) are an emerging technology where aeration is achieved through a gas permeable membrane with higher oxygen transfer efficiency than conventional diffused aeration (Soreanu et al., 2010). The membrane also serves as a medium for a counter diffusional biofilm where oxygen and substrates such as ammonia and BOD diffuse from opposite directions (Martin & Nerenberg, 2012). This arrangement enables the growth of nitrifying organisms near the membrane surface where the oxygen concentration is the highest and away from the bulk where the BOD concentration and competition from heterotrophic organisms is higher (Cole et al., 2004; LaPara et al., 2006). While the MABR design offers several process advantages such as energy efficient oxygen delivery (Côté et al., 2015; Uri-Carreño et al., 2021), and simultaneous nitrification and denitrification (Downing & Nerenberg, 2008c), mitigation of N_2O emissions is particularly noteworthy. Bench-scale biofilm reactors treating synthetic wastewater have shown dissolved N_2O concentrations in MABRs about two orders of magnitude lower than conventional co-diffusional biofilms (Kinh et al., 2017a). The lower N_2O in MABR was attributed to the adjacent location of the N_2O production at the membrane-biofilm interface and the N_2O consumption site in the outer anoxic layers of the biofilm that impeded further N_2O diffusion into the bulk (Kinh, et al., 2017a , 2017b). Full-scale monitoring studies have shown that MABRs can achieve intensified TN removal with N_2O emissions lower than the 1.6% N_2O-N per N load emission factor recommended by IPCC for N_2O estimation (Uri-Carreño et al., 2024). In a plant wide modeling study, He & Daigger (2023) showed that N_2O emissions from a hybrid MABR were only 20%

of the emissions from a conventional activated sludge system treating the same wastewater loading. Thus, both experimental and modeling studies suggest that MABRs are a promising alternative to mitigate N_2O emissions.

Process modeling has been employed to understand the N_2O pathways in MABR and investigate the impact of different operational conditions on them. N_2O models describing autotrophic deammonification in an MABR process have been used to investigate the impacts of ammonia and oxygen loading, biofilm properties, aeration strategy, role of anammox activity, and longitudinal substrate gradients on emissions (Chen et al., 2020, 2021; Ni et al., 2013; Ni & Yuan, 2013). Similarly, N_2O models describing conventional nitrification and denitrification reactions have been developed to study the impact of intra-membrane air pressure, biofilm thickness, influent C/N ratio, and hydraulic retention time (Li et al., 2020; Liu et al., 2022). While these studies provide a conceptual framework for N_2O generation in MABR processes, they have several simplifications that are not necessarily representative of full-scale MABR systems. Specifically,

- Prior models ignore back diffusion of N_2O generated in the biofilm into the membrane lumen gas. Uri-Carreño et al. (2020) reported that the majority of N_2O generated in MABR biofilms was present in the membrane exhaust gas and this pathway needs to be included. He & Daigger (2023) included the predicted lumen gas N_2O in their overall emission calculation. However, the N_2O back-diffusion model into MABR lumen is still not validated with measured data.
- Full-scale hybrid MABRs are designed to recycle the exhaust lumen gas for mixing the bulk sludge and control biofilm thickness. The recycled process air laden with N_2O from back diffusion could undergo mass transfer and biotransformation in the bulk anoxic mixed liquor. The exhaust lumen gas-anoxic bulk interaction is not included in any of the published models.

Thus, hybrid MABRs are complex systems with multiple sources and sinks for N_2O and it is critical to capture all these processes accurately. The overall objective of this study is to advance modeling of N_2O in hybrid MABR processes. Specifically, a comprehensive model for predicting liquid and gas phase N_2O in hybrid MABR processes was developed and validated using data from a full-scale hybrid MABR system. The improved model was used to obtain insights into N_2O bioconversions and partitioning occurring in a full-scale hybrid MABR.

4.2 Methodology

4.2.1 Model development

The SIMBA# platform (ifak e.V., Magdeburg, Germany) was employed as a basis for model development. A modified version of the Barker and Dold (1997) activated sludge model called

ASM_inCTRL_V3 (inCTRL Solutions, Toronto, Canada) was used to describe the growth and decay of various microorganisms and removal of chemical oxygen demand (COD) and total nitrogen. The biofilm sub-model for the MABR process has been described by Schraa et al. (2019). The subsequently described biokinetic and gas transfer processes employed for N_2O turnover in this study were added to the ASM_inCTRL_V3 base model.

N_2O Biokinetics Model: The mathematical model described the N_2O biokinetics in both biofilm and suspended sludge biomass through two pathways namely, i) autotrophic denitrification of nitrite by ammonia oxidizing organisms (AOO) and ii) heterotrophic denitrification of nitrite by ordinary heterotrophic organisms (OHO) as shown in Figure 4.1. The stoichiometric coefficients, rate expressions, and parameter values for the selected biokinetic processes and state variables relevant to N_2O emission are presented in Tables S4.1-S4.3 in the Supplemental Information. The description of the two biokinetic pathway is as follows:

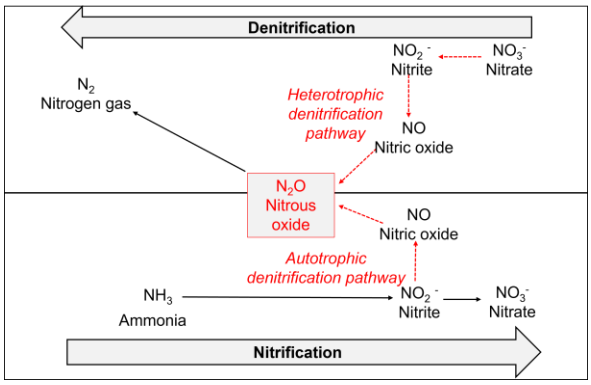

Figure 4.1 – N_2O conversion pathways modelled in this study.

i) Autotrophic denitrification by AOO - This pathway was modelled based on a modified framework from Mampaey et al. (2013) which predicts the sequential formation of nitric oxide (NO) and nitrous oxide (N_2O) from nitrite (NO_2) under two different scenarios using ammonia and biomass as electron donors. The simplified model formulated in this study assumes all N_2O formation is via NO as the precursor and does not consider the formation of intermediates such as hydroxylamine (NH_2OH) and nitrous acid (HNO_2) for a parsimonious approach. This approach has been adopted in other N_2O modeling studies as it involves fewer parameters and easier calibration (Spérandio et al., 2022).

ii) Heterotrophic denitrification by OHO – This pathway was modelled based on a four step denitrification process as described by Hiatt & Grady (2008). The OHO denitrification process involves sequential reduction of NO_2 to N_2 gas with formation of NO and N_2O as intermediates.

The heterotrophic denitrification pathway captures the formation and consumption of N_2O by OHO.

N_2O gas transfer model: The modeling of gas transfer processes in the MABR (Figure 4.2) had two components:

i) Back diffusion of N_2O generated in the biofilm into the lumen gas and the recycling of lumen gas into the anoxic bulk mixed liquor. The back diffusion of N_2O from inner layers of the biofilm into the lumen gas was modeled similar to the forward diffusion of oxygen from the lumen to the biofilm. The rate of N_2O back diffusion is modelled using a differential mass balance on N_2O along the length of the lumen which includes a mass transfer expression for gas diffusion across a membrane (Cussler, 1984).

ii) The lumen gas carrying N_2O was contacted with the anoxic bulk phase using a mass transfer expression involving a mass transfer coefficient multiplied by the concentration difference across the liquid boundary layer on the surface of the gas bubble and employing Henry's law to calculate the liquid phase concentration at the gas-liquid interface.

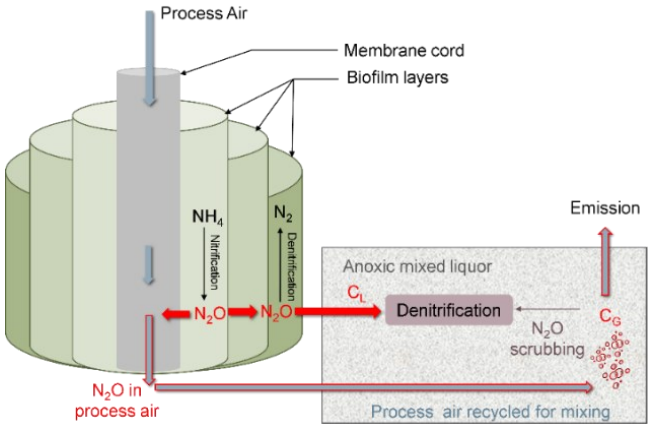

Figure 4.2 - Conceptual diagram for the N_2O gas transfer processes in a hybrid MABR.

4.2.2 Field sampling

The study site was recently upgraded (August 2022) to include an MABR process that is located in an upstream anoxic tank to which return activated sludge is recycled. The MABR tank has 4 parallel treatment trains (21.4 m long x 2.4 m wide x 3.1 m deep) with 9 ZeeLung™ cassettes (Veolia Water Solutions and Technologies) in each train yielding a total membrane surface area of 69,120 m^2. The aeration system for the MABR consists of a dedicated positive displacement blower with a variable frequency drive controller. The lumen air from the membranes is recycled to the integral diffuser at the base of the cassette to provide mixing and sparging to shear off excessive biofilm growth. A slip stream

of the lumen air from each cassette in a train was collected and conveyed into a common gas stream to monitor the O_2 and N_2O concentration in the process air exiting the MABR.

The dissolved and lumen gas N_2O concentrations in the hybrid MABR were measured to provide data for validating the model predictions. The monitoring strategy involved measuring N_2O concentrations in hourly grab samples taken during the morning peak flow conditions (i.e. 8 a.m. to 2 p.m.). Grab samples of the MABR mixed liquor were taken at three locations along the length of one of the MABR trains during three sampling events in June 2023. Gas phase samples of the membrane exhaust from the same MABR train were analyzed for N_2O following the same schedule.

The N_2O concentrations in liquid samples were measured using a Unisense Clarke-type microsensor with a detection limit of 0.1μM N_2O-N (2.4 μg N_2O-N/L). The sensor probe was connected to a Unisense Multimeter and all the data was logged using TracerSuite signal acquisition software (Unisense, Denmark). The sensor was calibrated before each use using a standard two-point calibration following the manufacturer's procedure. The sensor and the data acquisition system were set up in the wet chemistry laboratory at the plant to allow analysis of samples immediately after collection. The gas phase N_2O in the MABR exhaust was measured using a VIASENSOR G200 N_2O Analyzer (QED Environmental Systems, Inc., USA). During start up, the gas phase N_2O meter was run with ambient air for 15 mins. During each sampling the instrument was connected to a slip stream of the MABR exhaust lumen gas. The exhaust air was pumped through the gas meter for 2 minutes and the gas phase N_2O concentration was recorded after the reading stabilized.

The nitrogen removal performance of the MABR was monitored to validate the MABR base model. The monitoring strategy involved collecting 24 hour composite samples of the raw influent, MABR influent, MABR effluent, and plant final effluent thrice a week during the sampling period. The composite samples were collected using refrigerated autosamplers that were maintained at 2°C to minimize biological activity. NH_4-N, TKN, and NO_2^--N and NO_3^--N were measured following Hach Test Method TNT 832, Standard Method 4500, and Ion Chromatography following US EPA Method 300.1, respectively.

4.2.3 Model building and inputs

The SIMBA# model was configured to reflect the full-scale MABR by treating the 4 parallel treatment trains as three CSTRs in series such that the spatial trends in N_2O could be simulated (Figure 4.3). Each MABR block was employed to simulate 12 cassettes (3 cassettes x 4 parallel full-scale tanks). The model included influent characterization, a denitrification zone in front of the three MABRs, and the downstream aeration tank that modeled as three CSTRs in series and the secondary clarifier with recycling and wasting flows.

The values of the biofilm parameters employed in the model are shown in Table 4.1. The MABR blocks were set up with an external controller to maintain a constant biofilm thickness within each MABR and the biofilm thickness decreased along the three MABRs in series. The biofilm thickness values were informed by measurements of harvested fibers using Optical Coherence Tomography (OCT) (discussed in Chapter 3). All biokinetic parameters used in the model were either adopted from published literature or were default values used in the SIMBA# base model. No calibration of the model parameters was performed.

Table 4.1 – Biofilm settings for the MABR model

Parameter		Value	Unit
Liquid diffusion layer thickness		0.5	mm
Fraction of biofilm that is water		0.9	-
Density of particulate fraction of biofilm		1000	kg m^{-3}
Number of biofilm layers		3	-
Ratio of diffusion in biofilm to diffusion in pure water		0.8	-
Biofilm thickness	MABR 1	0.8	mm
	MABR 2	0.7	mm
	MABR 3	0.4	mm

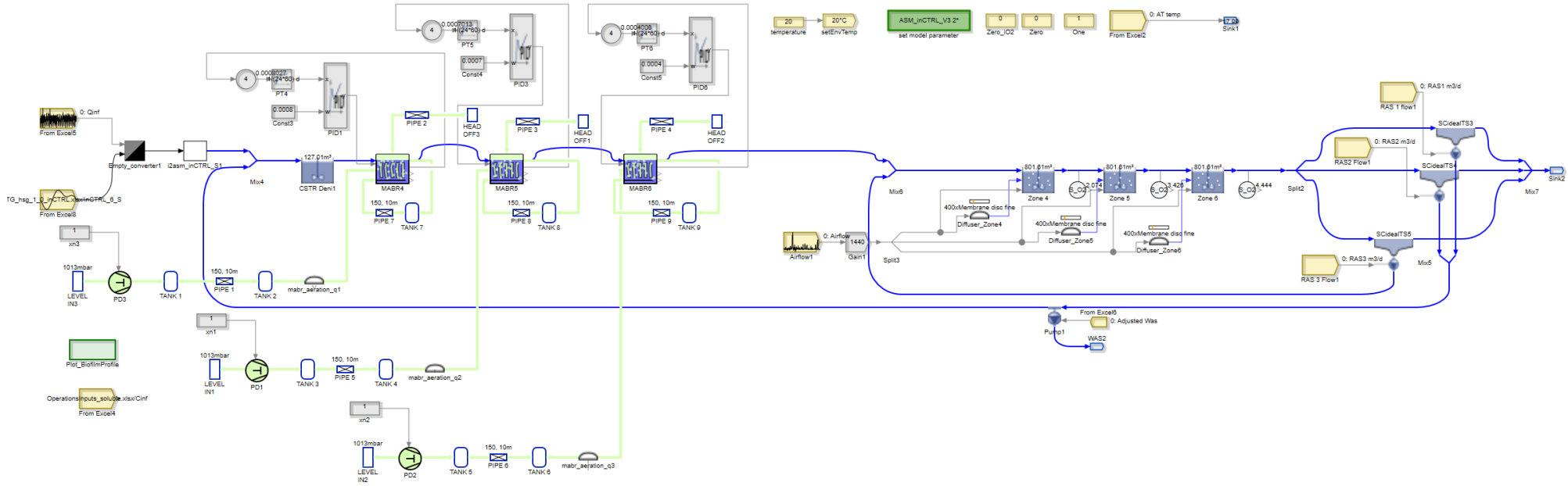

Figure 4.3 – Full-scale model layout assembled in SIMBA#

One of the objectives of the study was to investigate the diurnal patterns in the N_2O emission. Hence, the influent wastewater flow was obtained at 15-minute intervals from the online flow meters in the plant and read into the model. Monthly average values for the raw influent characteristics (Table 4.2) were input into the inCTRL influent generator routine to create influent concentrations that varied diurnally. Other high frequency online measurements such as return and waste activated sludge flows, aeration tank temperature, and process airflows collected by online sensors in the plant were also input into the model.

Table 4.2 – Influent characteristics used for generating diurnal influent concentrations

Parameter	Value
Total COD	650 mg COD L^{-1}
TKN	45 mg N L^{-1}
Alkalinity	500 mg L^{-1} as $CaCO_3$ equivalent
Inert Suspended solids	60 mg L^{-1}
Total Phosphorus	10 mg P L^{-1}

4.2.4 Emission factor calculation

The N_2O-N footprint of wastewater treatment processes is often compared on the basis of emission factors that are calculated as the ratio of the total N_2O-N emission mass flow to the influent N loading. Since the simulations in this study were run dynamically, the MABR emission factor calculation involved the following steps.

- The diurnal N_2O emission rate predicted for the three serial MABR tanks was summed together to obtain a total emission rate curve. The total emission rate was integrated at 24 hour intervals to obtain the daily mass of N_2O emitted for each simulation day.
- The model also simulated an influent N loading curve with a diurnal pattern. The area under the N loading curve was integrated over 24 hours to obtain the daily mass of influent N for each simulation day.
- Finally, the daily N_2O emission factor was calculated as the ratio of daily mass of N_2O emitted to daily mass of influent N.

4.2.5 Model fit assessment

The goodness of model fit between the observed and predicted values were quantified using the following two metrics.

Logarithmic Nash-Sutcliffe coefficient of efficiency (LNSE): The Nash-Sutcliffe coefficient of efficiency (NSE) is a widely used measure of model efficiency for hydrological time series data (Legates & McCabe Jr., 1999). NSE is defined as one minus the ratio of sum of squared errors (SSE) and the variance of the observed data (Nash & Sutcliffe, 1970). NSE values can range from -∞ to 1 with a value of 1 indicating a perfect fit (Krause et al., 2005). In this study, the measured and observed values were log transformed to reduce the effect of high values observed during diurnal peaks and the resulting high SSE term in the numerator (Krause et al., 2005; Oudin et al., 2006). The logarithmic NSE was calculated using equation (4.1).

$$LNSE = 1 - \frac{\sum_{i=1}^{i=N}(logP_i - logM_i)^2}{\sum_{i=1}^{i=N}(logM_i - log\bar{M})^2} \quad \text{.....(4.1)}$$

P – Predicted values

M = Observed values

$\bar{M}$ = Mean of the observed values

N = Total number of observations.

Percentage bias (PBIAS): Percentage bias represents the average tendency of the predicted values to be greater or smaller than the observed values (Gupta et al., 1999) and was calculated using equation (4.2). A value of zero represents optimal prediction with positive and negative magnitudes representing under and over prediction, respectively (Moriasi et al., 2007).

$$PBIAS = \frac{\sum_{i=1}^{i=N}(M_i - P_i)}{\sum_{i=1}^{i=N}(M_i)} * 100\% \quad \text{.....(4.2)}$$

4.3 Results and discussion

4.3.1 Base model validation

Before addressing the N_2O model, it was deemed important to ensure that the base model adequately described the underlying gas transfer and biokinetic processes that impact upon N_2O fate in the MABR. Firstly, the membrane gas transfer model was assessed to verify that gas transfer between the lumen and the biofilm was being described correctly. Figure 4.4 shows the continuously monitored exhaust O_2 concentration in the lumen gas (average of the four parallel full-scale trains) alongside model predictions (average of the three MABRs simulated in series). The measured O_2 fraction in the exhaust lumen gas varied between values of 0.15 to 0.18 and followed a diurnal pattern (Figure 4.4). The highest lumen gas O_2 concentration coincided with low loading conditions that occurred after midnight when the biofilm activity was lowest. As the loading increased with morning peak flow, the lumen gas O_2 dropped steeply to an average daily minimum of 15% around 12 noon because of increased biofilm activity. As seen in Figure 4.4, the exhaust O_2 concentration predicted by the base model aligned well with the measured

trends with a high LNSE (0.9986) and a very small PBIAS (-1%) value. On the basis of the close agreement between measured and predicted lumen gas O_2 levels, it was concluded that the model not only accurately predicted the gas transfer mechanisms between the biofilm and the lumen gas, but also the diurnal variations in biofilm oxygen consumption that resulted from fluctuation in influent wastewater loading. By extension it was concluded that the assumed biofilm thicknesses used in the simulation were appropriate.

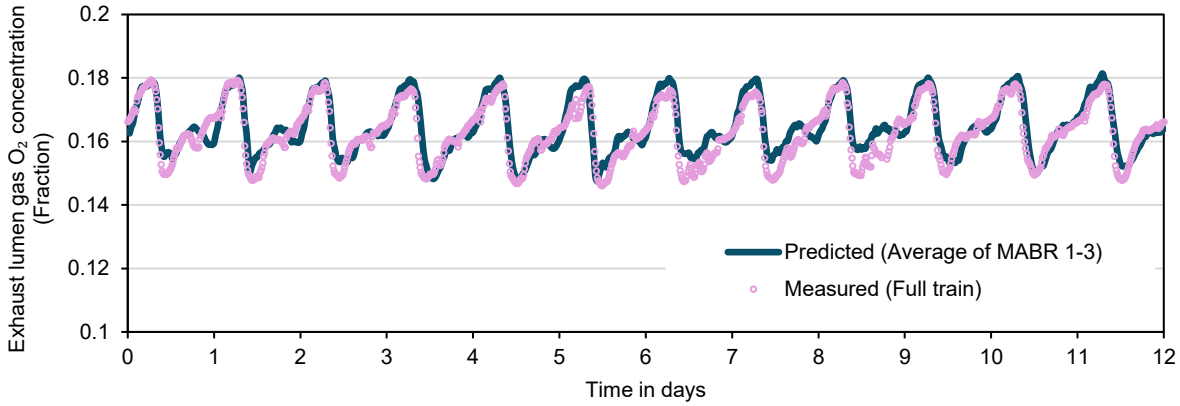

Figure 4.4 – Measured and predicted O_2 concentration in the exhaust MABR lumen gas.

Since N_2O production is associated with biological N removal it was deemed important that the base model accurately describes nitrification and denitrification in the MABR. Hence, the predicted and measured N species concentrations entering and exiting the MABR were compared to assess the model's performance with respect to N conversions. For this comparison, the diurnal simulation was not employed and the MABR model was run with a daily average influent loading to facilitate comparison with the observed data that was based on 24 hour composite samples. Figure 4.5a shows the predicted NH_4-N in the MABR influent and NH_4-N and NO_3-N concentrations in MABR effluent when daily average influent flow and TKN concentration values were employed as model inputs. The measured NH_4-N in the MABR influent and effluent were approximately 20 mg-N/L and 8 mg-N/L, respectively, with very little NO_3-N in the MABR effluent (below 1 mg-N/L) during the monitoring period (Figure 4.5a). The consistent N species concentration in the MABR effluent with time demonstrated that the MABR process was operating at steady state during the monitoring period. The measured data shows that the hybrid MABR process achieved substantial nitrification with over 50% removal of influent NH_4-N and very high denitrification efficiency (> 90%) as evidenced by very low NO_3-N concentrations. The observed simultaneous nitrification and denitrification was well described by the model. As seen in Figure 4.5a, the MABR effluent NH_4-N and NO_3-N concentrations, measured as 24 hour composite samples, compared

well with the model predictions based on average daily average loading with high NSE values of 0.9999 and 0.9998. The model fit assessment also showed satisfactory PBIAS values of 5% and 16% for NH_4-N and NO_3-N concentrations, respectively, with a small degree of underprediction in the MABR effluent. On the basis of the good alignment between measured and predicted N species concentration, it was concluded that the nitrifying and denitrifying processes in the MABR were well described by the SIMBA# model.

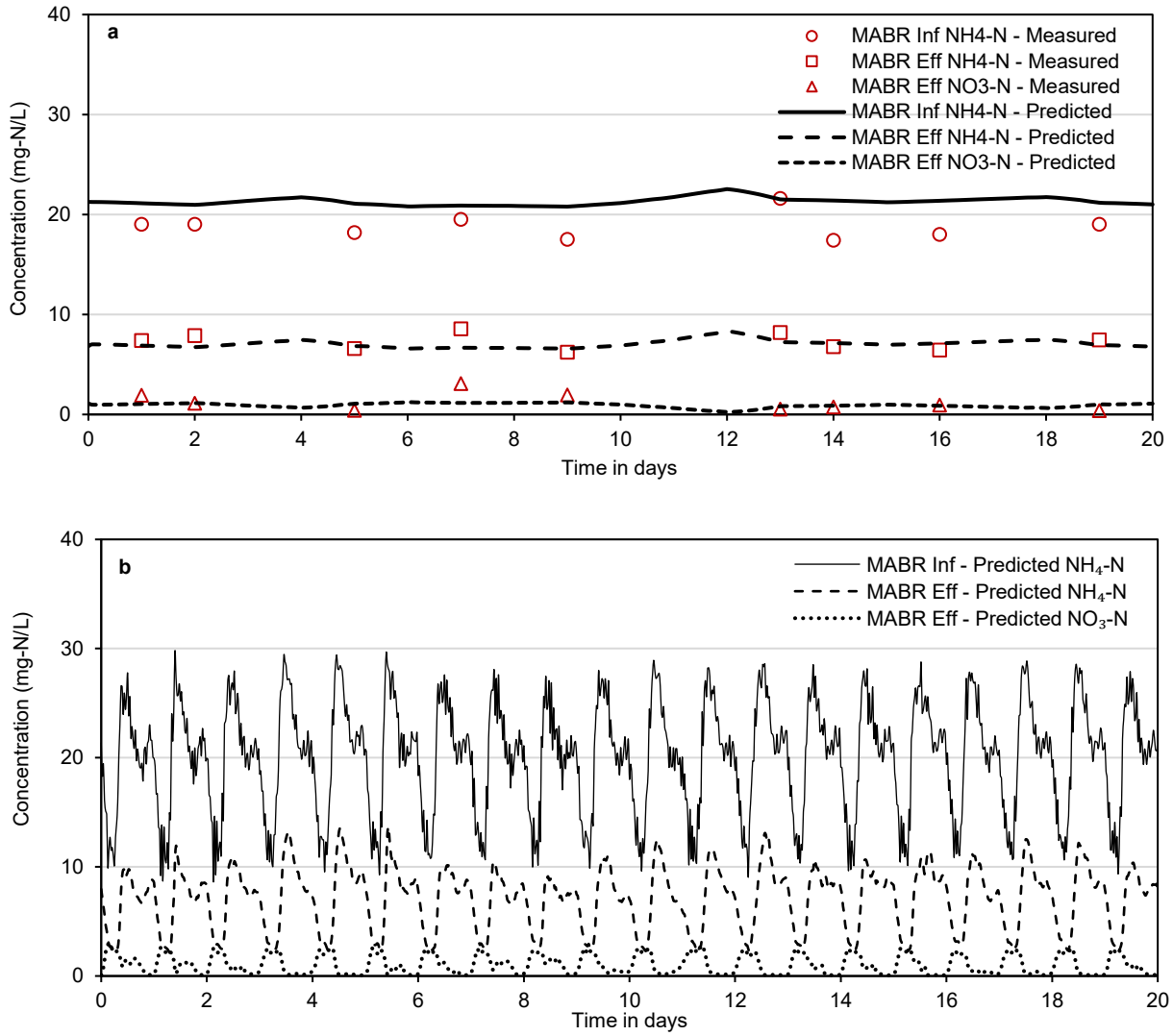

Figure 4.5 –N species concentrations in MABR influent and effluent based on a) daily average influent loading (measured and predicted) b) diurnal influent loading (predicted)

While the MABR effluent concentration showed good prediction based on average loading, it was deemed critical to evaluate its diurnal simulation (Figure 4.5b) to understand the cyclical fluctuations in the SND processes each day. As seen in figure 4.5b, the diurnal pattern of NH_4-N concentration in the

MABR influent and effluent were similar to each other indicating the MABR nitrification swings with the ammonia loading in the tank. On the contrary, the maximum nitrate concentration in the MABR effluent during the diurnal cycle occurred immediately before the start of the peak loading (7 am). Accumulation of nitrate past mid-night through early morning suggests that the denitrification activity in the MABR was limited by carbon availability during this low flow period. Thus, based on the model predictions, we infer that both nitrification and denitrification fluctuate in the MABR as a function of the influent loading and a corresponding effect could be expected with the N_2O emissions as well. Furthermore, it was concluded that the subsequently described N_2O model was built on a representative base model that could satisfactorily describe the underlying processes involved in N_2O conversions and their diurnal variations.

4.3.2 Improved MABR-N_2O model validation

The model predictions of N_2O in the lumen gas and MABR bulk phase were compared against the field-measured values to assess the model validity (Figure 4.6). As seen in Figure 4.6a, the measured N_2O concentrations in the MABR lumen gas increased rapidly in the morning, peaking around 10 am, and decreased in the afternoon on all three sampling days. Spatially, the predicted N_2O concentrations were highest in the first MABR lumen and decreased progressively in subsequent MABRs following the predicted longitudinal decrease in NH_4-N concentrations. The average gas phase concentration measured during the morning peak aligned well withing the range of predicted lumen gas N_2O concentrations in the three MABRs modeled in series. The predictions also spanned the range of the measured maximum and minimum concentrations during the morning peak period (Figure 4.6a). The model fit reported an LNSE of 0.9976 and a very low bias of -2%. On the basis of the strong agreement between predicted and measured gas phase N_2O concentrations it was concluded that: i) N_2O transfer from the biofilm into the membrane lumen gas was described well by the N_2O gas phase model, and ii) the simplified AOO denitrification model structure without intermediates such as hydroxylamine and nitrous acid was sufficient to predict N_2O formation at the membrane-biofilm interface.

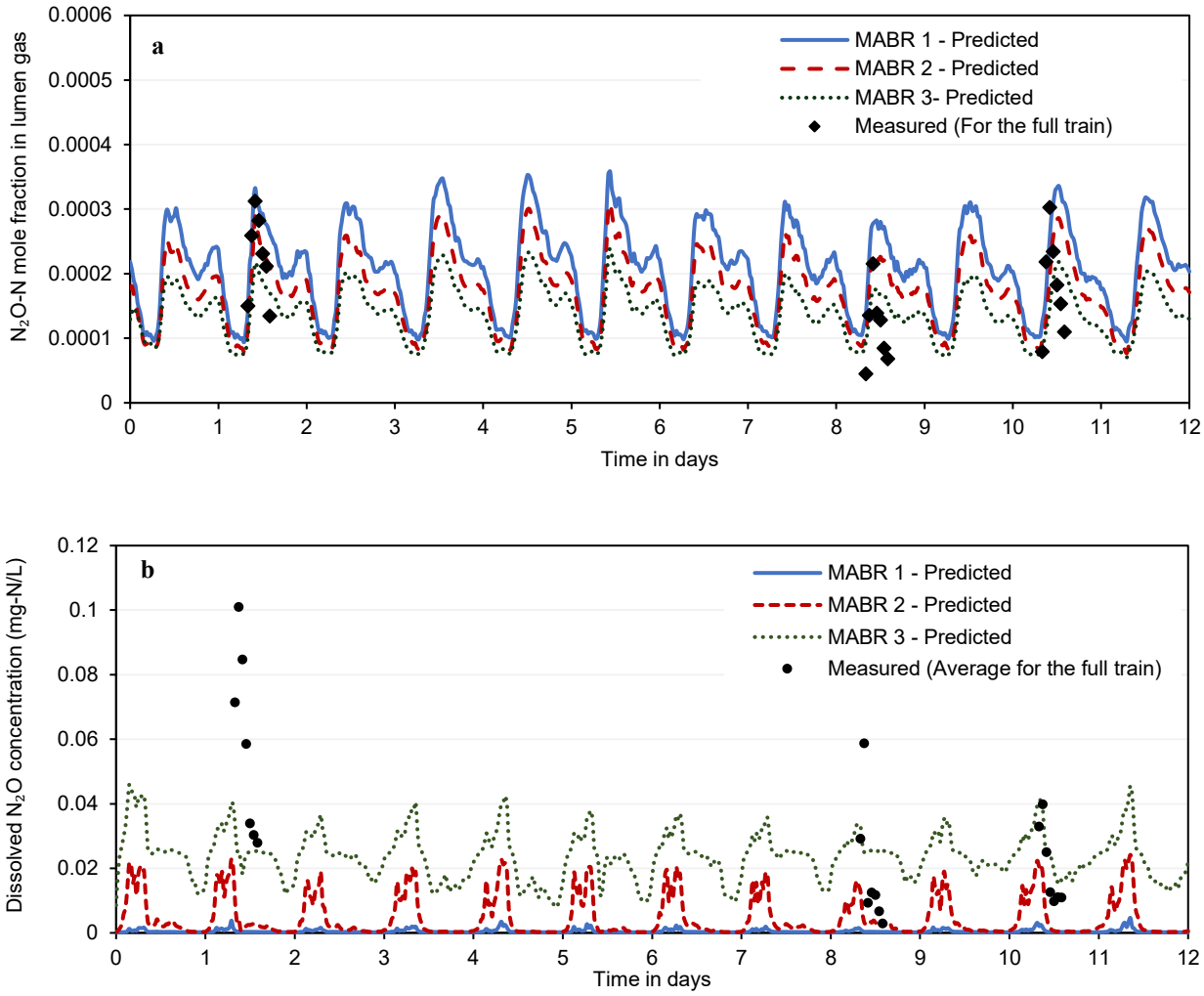

Figure 4.6 – Measured and predicted N_2O concentration in a) exhaust lumen gas and b) mixed liquor.

The diurnal pattern in the measured and modelled N_2O in the MABR mixed liquor was investigated to study its variation over the diurnal cycle. As seen in Figure 4.6b, the observed N_2O concentrations exhibited considerable variability between the sampling days. The concentrations measured on the first sampling day (Day 1) were higher than those of the subsequent two sampling days. While the magnitude varied, the N_2O concentration profiles were generally consistent over the three sampling events. The measured concentrations started off with a maximum value at 8 am and decreased rapidly until midday, after which they stabilized around 2 pm. The predicted dissolved N_2O concentrations showed similar trends during the morning peak flow time; however, the magnitude of the diurnal peaks differed between the three MABRs in series. The N_2O concentrations predicted in the first MABR tank were very low with only a minor peak in concentration in the morning (Figure 4.6b). In MABR 2, the dissolved N_2O peaked

at approximately 0.02 mg-N/L during the morning after which (past 12 noon), the concentration remained very low. Contrarily, MABR 3 had relatively elevated concentrations (0.02 to 0.04 mg-N/L) throughout the day (Figure 4.6b) which was consistent with the diurnal profiles of NH_4-N (Figure 4.5) and lumen gas N_2O (Figure 4.6a). The difference in dissolved N_2O levels between the three tanks in series was attributed to diminishing denitrification in the biofilm and suspended sludge along the tank.

Comparing the measured and predicted dissolved N_2O concentrations, it can be seen that the model underpredicted the dissolved N_2O concentration on day 1. However, on the subsequent two sampling events, the predicted concentrations for the three MABR tanks more closely followed the observed values. The PBIAS for the model fit was moderately high (68%) indicating an underprediction of the dissolved N_2O concentration by the model. However, the LNSE value (0.9137) revealed a good model fit. Based on the LNSE estimate, it was concluded that the improved model described the bulk phase N_2O processes adequately, given the complexity and multitude of bioconversion and gas transfer processes occurring in the MABR mixed liquor. The subsequent discussion explores the roles of AOO and OHO bioconversion processes and gas-transfer processes in the fate of N_2O in hybrid MABRs.

4.3.3 Spatial profiles in substrate and biomass concentrations

The previously described N_2O concentration profiles revealed that the N_2O concentrations in the MABR vary both spatially and diurnally. While the diurnal dynamics could be attributed due to variations in influent loading, interpretation of the spatial trends in N_2O required in-depth analysis of relevant substrates and biomass that drive the bioconversion processes. Hence, selected model state variables were investigated in the biofilm layers and the bulk phase of the three MABRs in series to obtain insights into the spatial variability of active N metabolisms. Figure 4.7 shows the predicted substrate and biomass concentrations in the biofilm and bulk zones. Since the model was run dynamically, the predicted concentrations changed with time. Hence, to simplify presentation, Figure 4.7 presents the concentrations occuring at 12 noon on one of the days that N_2O was monitored (day 10).

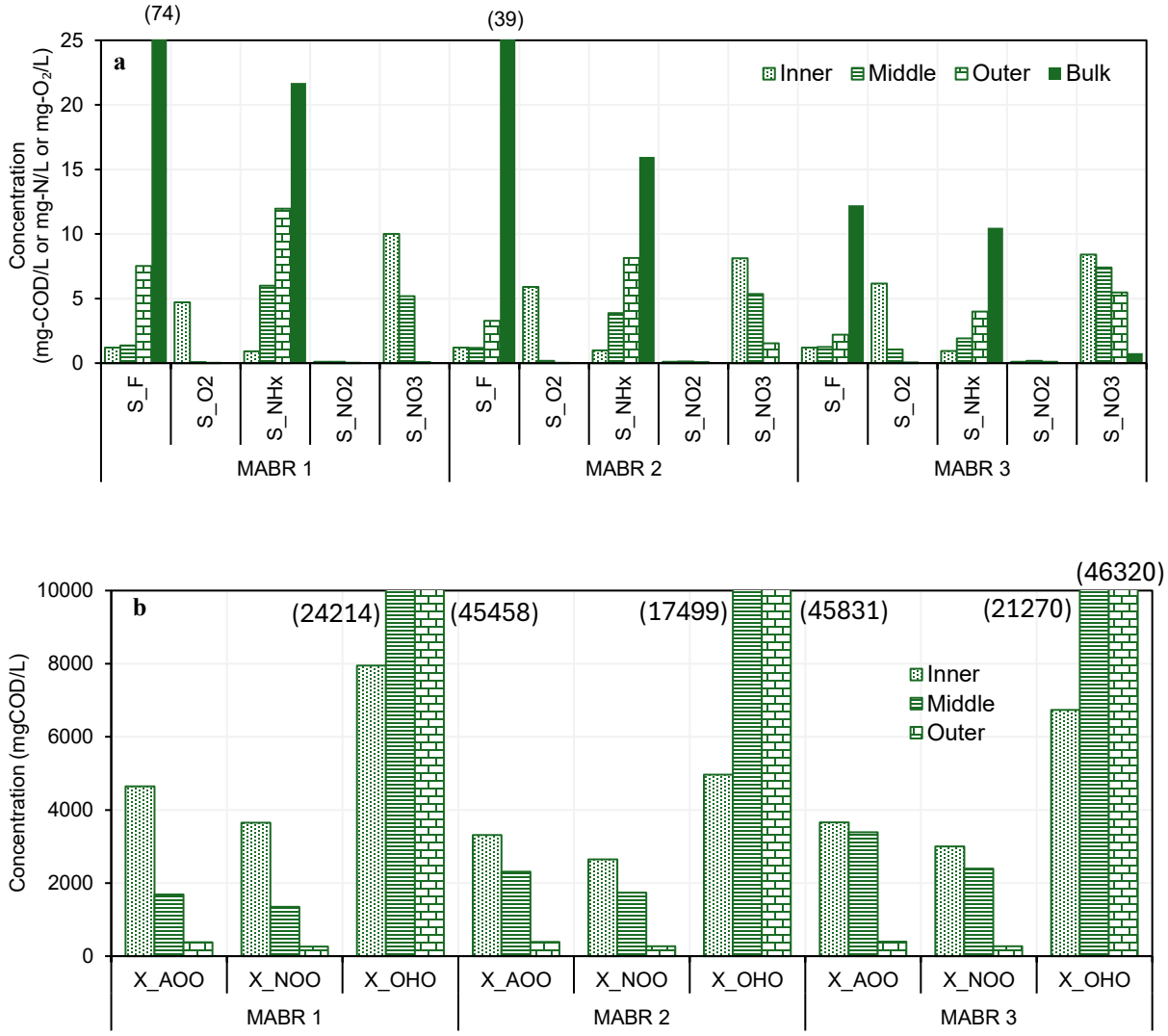

Figure 4.7 – Predicted a) substrate b) biomass concentration in different biofilm layers and bulk zone of the three MABRs modeled in series (snapshot at 12 noon). Values outside the y-axis range are shown in brackets.

The simulated values in Figure 4.7 were investigated to identify the zones contributing to nitrification and denitrification. As seen in Figure 4.7a, the DO concentration was highest near the membrane lumen in the inner biofilm layer in all three MABRs. The DO concentration decreased sharply in the outer layers to yield anoxic environments. As seen in Figure 4.7b, consistent with the DO trends, the highest concentration of AOOs were in the inner layers, resulting in low and high NH_4-N and NO_3-N concentrations, respectively, near the membrane lumen due to nitrification. Very low nitrite concentrations were predicted in all zones and NOOs were active in all three MABRs. The decreasing

nitrate concentration that was accompanied by a dramatic increase in OHO concentrations in the middle and outer layers (at least two order magnitude higher than autotrophs) signifies active denitrification in the outer zones (Figure 4.7b). Thus, each biofilm layer performed different N conversion functions and it was concluded that this stratification of SND activities would influence the relative contributions of the AOO and OHO N_2O bioconversion pathways in the MABR.

The predicted NO_3-N concentrations in the biofilm layers were compared between the three MABRs to gain insight into the longitudinal variations in SND processes. Figure 4.7a indicates a decreasing trend in the NO_3-N concentration in the inner biofilm layer with progression along the MABRs (10 > 8.1 ~ 8.4 mg/L). This suggests that nitrification activity decreased along the longitudinal direction due to a reduction in the NH_4-N concentration gradient between the bulk and biofilm in the three MABRs. The trends in the NO_3-N concentration in the anoxic zones were similarly examined to evaluate denitrification processes. As seen in Figure 4.7a, in MABRs 2 and 3, accumulation of nitrate was predicted in the middle and outer biofilm layers. Additionally, the bulk phase NO_3-N concentration was negligible in the first two MABRs while a value of 0.7 mg-N/L was predicted in MABR 3. The accumulation of nitrate in the later stages of the MABR tank was attributed to a COD limitation. The predicted bulk phase readily biodegradable COD concentration (S_F) decreased from 74 mg COD/L in MABR 1 to 12 mg COD/L in MABR 3 (Figure 4.7a). Hence, the anoxic zones of MABR 3 were carbon limited for denitrification. Overall, the extent of nitrification and denitrification decreased along MABRs 1, 2, 3 and hence it was expected that the longitudinal substrate gradients would impact N_2O fate.

4.3.4 Spatial profiles in N_2O concentration and conversion processes

The spatial trends in N_2O concentration and the underlying N_2O bioconversion pathways were investigated to obtain insights into hotspots of N_2O generation and consumption in the hybrid MABR. Figure 4.8a shows the predicted N_2O concentrations while Figure 4.8b shows the predicted net daily N_2O mass conversions associated with the individual pathways. Figure 4.8c focuses specifically on the daily mass N_2O generated and consumed through OHO denitrification. While dynamic simulations were conducted, for simplicity of presentation Figure 4.8a presents concentrations predicted at 12 noon for one of the N_2O monitoring days (day 10). In Figures 4.8b and 4.8c, the diurnal curves of the individual N_2O rate processes predicted by the model were integrated over a 24 hour period (day 10) to obtain the total N_2O daily mass converted in the different zones.

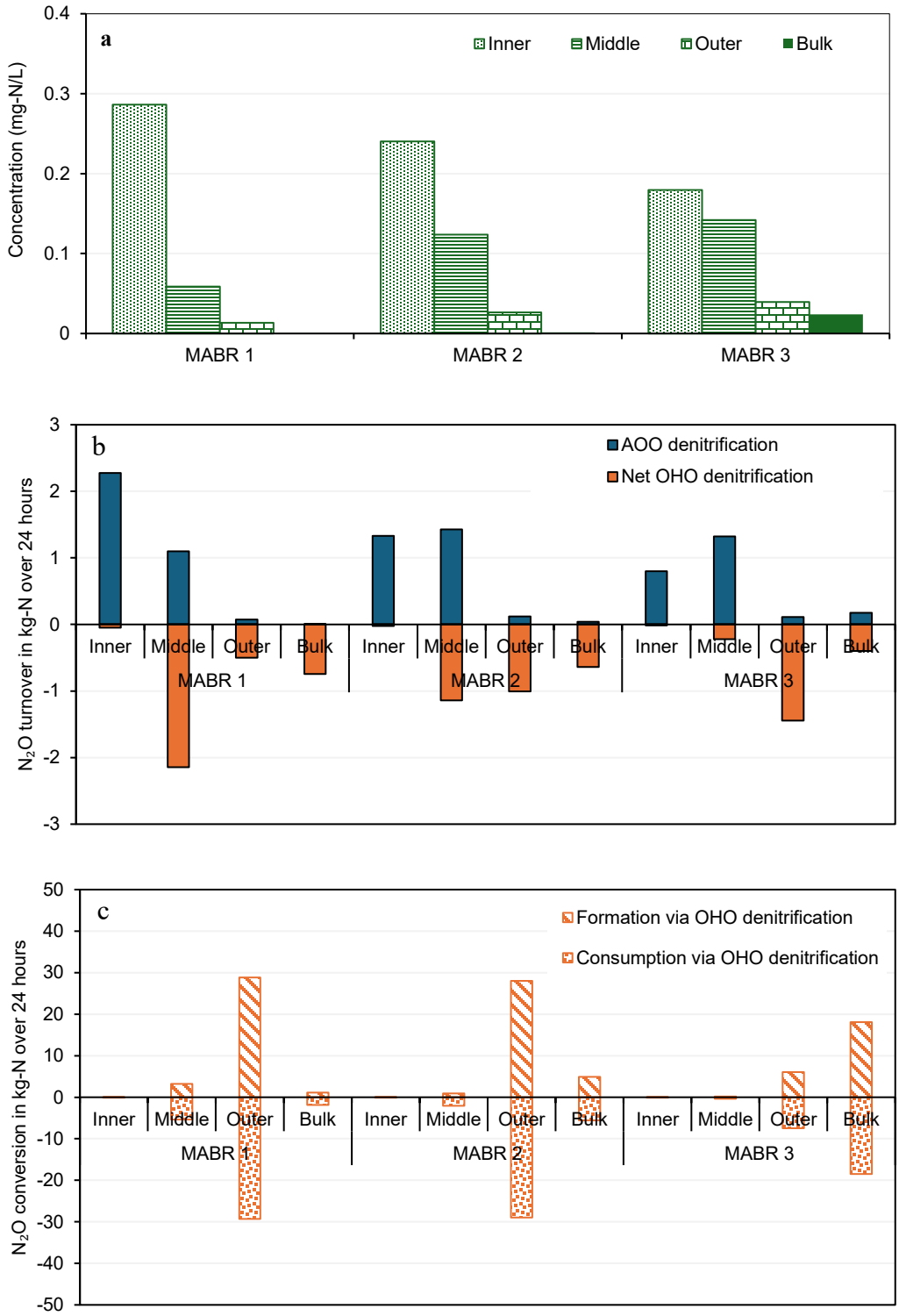

Figure 4.8 – a) Predicted N_2O concentrations (snapshot at 12 noon) b&c) Predicted N_2O conversion (over 24 hours) in biofilm layers and bulk mixed liquor.

The spatial profiles of predicted N_2O concentrations and mass flows via the two bioconversion pathways were compared to obtain insights into hotspots of N_2O generation. As seen in Figure 4.8, the N_2O concentrations were the highest in the inner most biofilm layers where the generation of N_2O through AOO activity was highest. The N_2O concentrations and the daily masses of N_2O generated via this pathway were lower in the outer layers which were consistent with the oxygen, ammonia, and AOO concentration profiles previously discussed (Figure 4.7). Very little generation of N_2O (< 0.2 kg-N) via AOO activity was predicted in the bulk liquor due to lack of DO (Figure 4.7a). Thus, the membrane-biofilm zone, which was previously identified as the hotspot for nitrification, was also a hotspot for N_2O generation. Hence, generation of all the lumen gas N_2O was attributed to the AOO activity.

The spatial profile of the net OHO denitrification pathway was investigated to understand the role of denitrification in N_2O conversions. OHO denitrification acted as both a source and sink for N_2O as seen in Figure 4.8c with extensive formation and consumption activities in the outer biofilm layer that had low DO, high rbCOD, and high OHO concentrations, and active denitrification as discussed earlier. However, the net OHO denitrification conversion was always a negative value indicating net consumption in the biofilm layers. Similarly, net N_2O consumption was predicted in the MABR bulk liquid (Figure 4.8b) and thus, low N_2O concentrations were predicted in the MABR mixed liquor (Figure 4.8a). Thus, the denitrification zones of the biofilm in the outer layers and the MABR bulk serve as hotspots of N_2O consumption.

The predicted AOO denitrification and net OHO denitrification conversion rates were compared between the three MABRs to understand the differences in N_2O bioconversion longitudinally. For this purpose, the conversion rates in all biofilm layers were summed for each pathway. The conversion rates for AOO denitrification descended in magnitude with MABR 1 (3.45 kg-N) > MABR 2 (2.88 kg-N) > MABR 3 (2.23 kg-N) and for OHO denitrification MABR 1 (-2.69 kg-N) > MABR 2 (-2.17 kg-N) > MABR 2 (-1.68 kg-N). Hence, the model predicted similar decreases in N_2O bioconversion of about 35% for AOO denitrification and 37% for OHO denitrification between the front and back of the full-scale MABR tank. The decrease in N_2O bioconversions is attributed to the longitudinal gradient in ammonia loading along the tank. In the MABR bulk phase, the net OHO consumption decreased about 48% from -0.75 to -0.4 kg-N (over 24 hours) (Figure 4.8b) due to a decrease in COD. Overall, the substrate gradients decreased the extent of N_2O production and consumption in both the biofilm and suspended sludge biomasses along the length of the full-scale tank.

4.3.5 N_2O gas-water transfer processes in hybrid MABR

In addition to the activity of the bioconversion processes in the MABR, the recirculation of N_2O laden lumen air to the bulk liquor could also influence N_2O fate in the MABR. The model-predicted N_2O mass flows in the lumen gas entering the mixed liquor and the off-gas leaving the MABR through the headspace were compared to obtain insight into the extent of liquid-gas N_2O transfer in the mixed liquor. Figure 4.9 shows the daily N_2O-N mass in the lumen gas and off-gas of the three MABRs. The model predicted a diurnal N_2O flow rate for the two gas streams and hence, for presentation purposes, the daily mass of N_2O was estimated by integrating the area under the curve over a 24 hour interval. The estimates obtained for one of the simulated days (day 10) are presented in Figure 4.9.

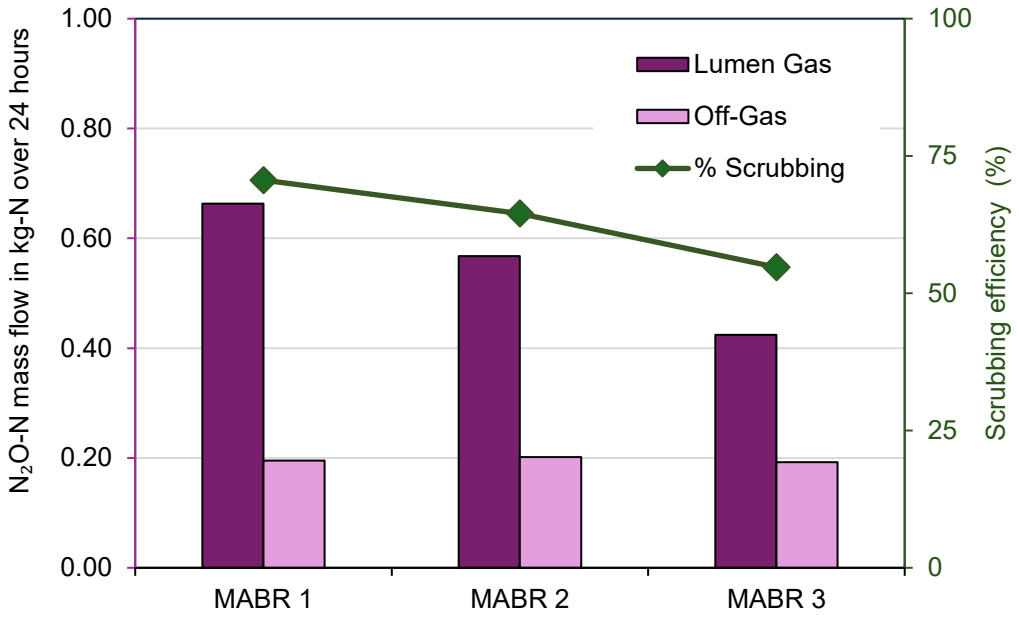

Figure 4.9 – Daily mass of N_2O in the lumen gas entering and off-gas leaving the bulk phase

Figure 4.9 demonstrates that the daily mass of N_2O in the lumen gas varied between 0.6-0.42 kg N_2O-N, whereas the corresponding off-gas mass leaving the MABR was around 0.2 kg N_2O-N. A decrease in N_2O mass from the inlet (lumen gas) to the outlet (off-gas) gas stream indicated scrubbing of N_2O from the gas. Examination of the N_2O concentrations in the two phases revealed that the lumen gas concentrations exceeded Henry's Law-predicted values by 3 to 30 times (depending on time of day) when compared with the dissolved N_2O concentrations (data not shown). Hence, N_2O mass transfer from the gas phase to the liquid phase via scrubbing was highly favored. The scrubbed N_2O was denitrified in the bulk phase as

evidenced by the negative net OHO denitrification rates (Figure 4.8b). Thus, the bulk mixed liquor acts as a sink for destruction of lumen gas N_2O produced in the biofilm.

The scrubbing efficiencies calculated from mass flows of N_2O in the lumen gas and off-gas streams were compared between the three MABRs to understand the variation in the mass transfer process along the length of the full-scale tank. The scrubbing efficiency was highest in the first MABR at 71% followed by MABR 2 at 65% and MABR 3 at 55% (Figure 4.9). The downward trend in scrubbing efficiency resulted from the decreasing N_2O load in the lumen gas that reduced the concentration gradient driving the scrubbing process. However, the estimated daily mass in the off-gas stream for all 3 MABRs were around 0.2 kg N_2O-N. Similar levels of N_2O in the off-gas, despite a substantial concentration differential between the two phases, indicates the scrubbing process was limited by the Henry's law co-efficient for N_2O. The partition constant value for N_2O (1.3×10^{-5}mol m^{-3} Pa^{-1}) is about an order magnitude smaller than oxygen (1.7×10^{-4}mol m^{-3} Pa^{-1}) (Sander, 2015). While there is sufficient mass transfer capacity in the tank to lower the inlet gas phase concentrations, the outlet gas phase concentration appears to be largely controlled by equilibrium as defined by Henry's Law. Overall, the bulk phase mass transfer processes play a major role in the fate of N_2O in the hybrid MABR process and it is important to model the N_2O scrubbing to obtain an accurate estimate of the emissions from MABRs.

4.3.6 Overall N_2O emissions from hybrid MABR

The ultimate goal of the modeling exercise was to estimate gas phase emissions of N_2O leaving the MABR. Hence, the total N_2O-N emission rates calculated as the sum of emissions from the three MABR blocks was investigated (Figure 4.10). The diurnal N_2O-N emission pattern seen in Figure 4.10 is very similar to the patterns in the ammonia loading and the membrane lumen gas concentration. The total N_2O-N emission rate varied between 0.8 kg-N/d during peak morning flow to 0.4 kg-N/d during low flow in the early a.m. The model predictions also described the slight variation in the N_2O-N emission rate that was attributed to daily changes in wastewater loading as seen from the peaks on day 3 and day 6. Overall, it can be seen that the N_2O emission profile was largely driven by lumen gas processes.

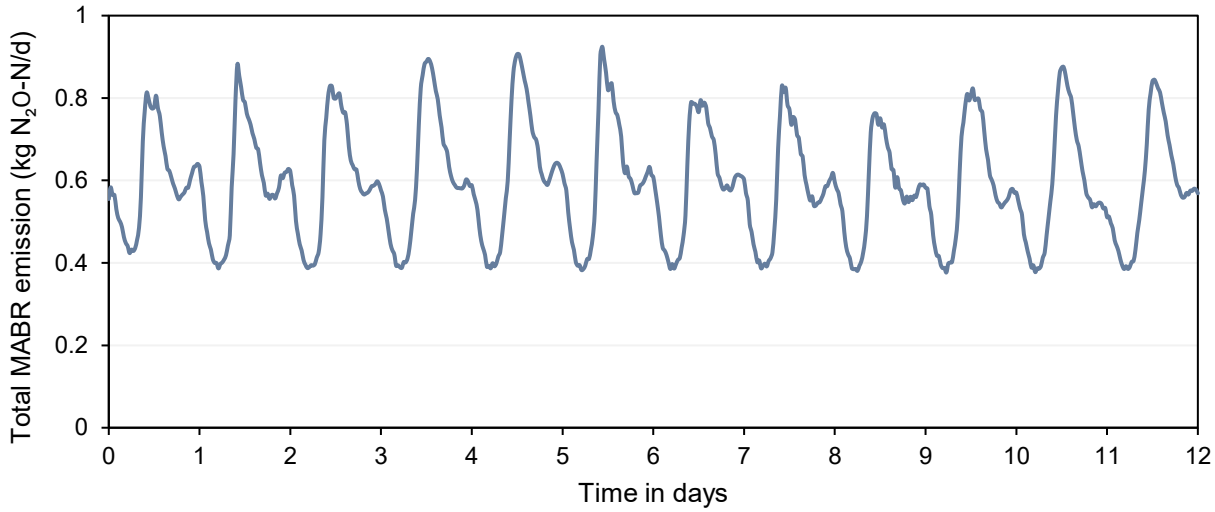

Figure 4.10 – Total N_2O-N emissions from overall MABR

N_2O emission factors that were calculated from the modeling results were subsequently compared with literature values. The average N_2O emission factor predicted for the full-scale hybrid MABR process was 0.18 ± 0.01% kg N_2O-N/kg N over the simulation period. The low N_2O emission factor signifies that MABRs can achieve high levels of SND in a reduced carbon footprint. On comparison with other MABR studies, the predicted emission factor was more than 4 times lower than the 0.8% measured by Uri-Carreno et al. (2023) in two full-scale MABRs. The mismatch may be because the emission calculation in Uri-Carreno et al. (2023) considered that all the lumen gas was vented into the atmosphere directly, as there was no recirculation into the bulk mixed liquor. Other bench-scale studies have reported emission factors for MABR as low as 0.00058% (Kinh et al., 2017b). However, the bench-scale set up was a biofilm-only MABR without any bulk phase biomass and back diffusion of N_2O into the lumen gas was not considered. This is the first study to report an N_2O emission factor for a representative full-scale MABR process including all the relevant N_2O transformation and transport processes. However, the estimated emission factor was only for the MABR process which achieved up to 50% removal of the influent N loading and did not consider emissions from nitrification in the downstream aeration process. The overall plantwide emission factor will be higher than the estimated value.

4.3.7 Limitations of this study

The model presented in this paper is a significant advancement in describing the multiple N_2O sources and sinks related to bioprocesses and gas transfers in MABRs. The improved model was validated with gas phase and liquid phase N_2O measurements. The following considerations could further improve model validation.

- The measured N_2O data used for validating the model only captured the morning peak flow between 8 am to 2 pm on three monitoring days. Continuous monitoring of the gas and liquid phase N_2O for multiple days would be helpful in validating the full diurnal cycle in the plant.
- This study monitored and modeled N_2O emissions during summer weather conditions (June 2023). A recent modeling study (Seshan et al., 2024) suggests that different N_2O bioconversion pathways may dominate under different seasonal conditions. Hence, it would be beneficial to validate the model over multiple seasons.
- The model simulated the lumen gas recirculation as a continuous gas stream. In practice, the lumen gas is collected in a gas accumulator at the bottom of the cassette and released periodically. Future improvements of the current model could include the intermittent sparging feature to obtain a more accurate diurnal N_2O emission curve.

4.4 Conclusions

Mitigation of N_2O emissions from biological nitrogen removal is a critical step in minimizing the wastewater treatment process carbon footprint. The MABR is an emerging intensification technology that has also been demonstrated to curb N_2O emissions. Prior modeling studies had several simplifications and did not include all mass transfer processes among process air, biofilm, and suspended sludge. This study developed and validated an improved model that accounts for relevant N_2O bioconversion and gas-liquid mass transfer processes in a hybrid MABR process. The base model was validated with lumen gas exhaust oxygen concentration and the MABR effluent ammonia and nitrate concentrations. The N_2O gas transfer models added to the base model predicted the lumen gas N_2O concentration extremely well. The predicted dissolved N_2O concentrations aligned with the range of measured concentrations for two out of the three sampling days. Application of the improved model to the full-scale hybrid MABR revealed that:

- AOO activity in the innermost layer of the biofilm was a significant source of N_2O which then diffused to both the lumen gas and the outer biofilm layers.
- The middle and outer layers of the biofilm and the bulk mixed liquor where denitrification was active resulted in a net consumption of N_2O through the heterotrophic denitrification pathway.
- The decreasing longitudinal substrate concentrations along the MABR tank decreased the N_2O bioconversions in both the biofilm and suspended sludge.
- Comparing the predicted N_2O mass flows in the gas streams entering and leaving the MABR bulk showed that there was substantial N_2O scrubbing (55-70%) into the MABR mixed liquor.
- The model predicted a low N_2O emission factor of $0.18 \pm 0.01\%$ while achieving up to 50% removal of the influent N load demonstrating that hybrid MABRs are a low emission alternative for intensification of wastewater treatment processes.

4.5 Supplemental information

Table S4.1 - Stoichiometric matrix for selected state variables related to biological N_2O conversion processes.

Processes \ State Variables	S_S	S_{O_2}	S_{NH_x}	$S_{NO_2^-}$	S_{NO}	S_{N_2O}	S_{N_2}	X_{AOO}	X_{OHO}
Autotrophic N_2O processes (A – NH_x as electron donor; B – Biomass as electron donor)									
A: $NO_2^- \rightarrow NO$	0	$\frac{-1(2.28 - Y_{AOO})}{Y_{AOO}}$	$\frac{-1}{Y_{AOO}} - 1\ i_{N,Bio}$	$\frac{-1}{Y_{AOO}}$	$\frac{2}{Y_{AOO}}$	0	0	1	0
B: $NO_2^- \rightarrow NO$	0	0	$i_{N,Bio}$	-1.75	1.75	0	0	-1	0
A: $NO \rightarrow N_2O$	0	$\frac{-1(2.28 - Y_{AOO})}{Y_{AOO}}$	$\frac{-1}{Y_{AOO}} - 1\ i_{N,Bio}$	$\frac{1}{Y_{AOO}}$	$\frac{-2}{Y_{AOO}}$	$\frac{2}{Y_{AOO}}$	0	1	0
B: $NO \rightarrow N_2O$	0	0	$i_{N,Bio}$	0	-1.75	1.75	0	-1	0
Heterotrophic N_2O processes									
$NO \rightarrow N_2O$	$\frac{-1}{Y_{OHO,S,NO_x}}$	0	$-1\ i_{N,Bio}$	0	$\frac{-1(1 - Y_{OHO,S,NO_x})}{EEQ_{NO,N_2O} . Y_{OHO,S,NO_x}}$	$\frac{(1 - Y_{OHO,S,NO_x})}{EEQ_{\ N_2O,NO} . Y_{OHO,S,NO_x}}$	0	0	1
$N_2O \rightarrow N_2$	$\frac{-1}{Y_{OHO,S,NO_x}}$	0	$-1\ i_{N,Bio}$	0	0	$\frac{-1(1 - Y_{OHO,S,NO_x})}{EEQ_{\ N_2,N_2O} . Y_{OHO,S,NO_x}}$	$\frac{(1 - Y_{OHO,S,NO_x})}{EEQ_{\ N_2O,NO} . Y_{OHO,S,NO_x}}$	0	1

Table S4.2 - N_2O biokinetics reaction rate expressions

Autotrophic N_2O processes (A – NH_x as electron donor; B – Biomass as electron donor)	
A: $NO_2^- \rightarrow NO$	$f_{DNT,A} \cdot \mu_{AOO} \cdot \frac{S_{NH_x}}{K_{NH_x,AOO} + S_{NH_x}} \cdot \frac{S_{O_2}}{K_{O_2,AOO} + S_{O_2}} \cdot \frac{S_{NO_2}}{K_{NO_2,NOB} + S_{NO_2}} \cdot X_{AOO}$
B: $NO_2^- \rightarrow NO$	$f_{DNT,A} \cdot f_B \cdot \mu_{AOO} \cdot \frac{S_{NO_2}}{K_{NO_2,NOB} + S_{NO_2}} \cdot X_{AOO}$
A: $NO \rightarrow N_2O$	$\mu_{AOO} \cdot \frac{S_{O_2}}{K_{O_2,AOO} + S_{O_2}} \cdot \frac{S_{NH_x}}{K_{NH_x,AOO} + S_{NH_x}} \cdot \frac{S_{NO}}{K_{NO,AOO} + S_{NO}} \cdot X_{AOO}$
B: $NO \rightarrow N_2O$	$f_B \cdot \mu_{AOO} \cdot \frac{S_{NO}}{K_{NO,AOO} + S_{NO}} \cdot X_{AOO}$
Heterotrophic N_2O processes	
$NO \rightarrow N_2O$	$\mu_{OHO} \cdot \eta_{anox,4} \frac{S_{S_S}}{K_{S_S,OHO} + S_{S_S}} \cdot \frac{K_{O_2,OHO,NO}}{K_{O_2,OHO,NO} + S_{O_2}} \cdot \frac{S_{NO}}{K_{NO,OHO} + S_{NO} + S_{NO}^2/K_{I4,NO,OHO}} \cdot X_{OHO}$
$N_2O \rightarrow N_2$	$\mu_{OHO} \cdot \eta_{anox,5} \frac{S_{S_S}}{K_{S_S,OHO} + S_{S_S}} \cdot \frac{S_{N_2O}}{K_{N_2O,OHO} + S_{N_2O}} \cdot \frac{K_{O_2,OHO,N_2O}}{K_{O_2,OHO,N_2O} + S_{O_2}} \cdot \frac{K_{I5,NO,OHO}}{K_{I5,NO,OHO} + S_{NO}} X_{OHO}$

Table S4.3 - Parameter values

Parameter	Description	Value	Unit	Reference
Autotrophic N_2O processes				
Y_{AOO}	AOO yield	0.15	g COD gN^{-1}	Wiesmann (1994)
μ_{AOO}	Maximum specific growth rate of AOOs	0.9	d^{-1}	SIMBA# default
$i_{N,Bio}$	N content of biomass	0.07	gN $gCOD^{-1}$	Henze et al. (2000)
$f_{DNT,A}$	Fraction of NH_x oxidized with NO_2^- as partial electron acceptor	0.028	-	Mampaey et al. (2013)
f_B	Ratio of maximum NO formation rate in scenario B vs scenario A	2.4	-	Mampaey et al. (2013)
$K_{NH_x,AOO}$	Ammonia half saturation for AOOs	0.7	gN m^{-3}	SIMBA# default
$K_{O_2,AOO}$	Oxygen half saturation for AOOs	0.25	gO_2 m^{-3}	SIMBA# default
$K_{NO,AOO}$	Nitric oxide half saturation for AOO	1	gN m^{-3}	Mampaey et al. (2013)
$K_{NO_2,NOO}$	Nitrite half saturation for NOO	0.1	gN m^{-3}	SIMBA# default
Heterotrophic N_2O processes				
Y_{OHO,S,NO_x}	Anoxic yield of OHOs on substrate	0.54	gCOD $gCOD^{-1}$	SIMBA# default
$EEQ_{N_2O,NO}$	Electron equivalence of N_2O to NO	0.57	gO_2 gN^{-1}	Hiatt & Grady (2008)
EEQ_{N_2,N_2O}	Electron equivalence of N_2 to N_2O	0.57	gO_2 gN^{-1}	Hiatt & Grady (2008)
μ_{OHO}	Maximum specific growth rate of OHOs	3.2	d^{-1}	SIMBA# default
$\eta_{anox,4}$	Anoxic factor for NO to N_2O via OHOs	0.35	-	Hiatt & Grady (2008)
$\eta_{anox,5}$	Anoxic factor for N_2O to N_2 via OHOs	0.35	-	Hiatt & Grady (2008)

$K_{S_S,OHO}$	Substrate half saturation for OHOs	5	gCOD m^{-3}	SIMBA# default
$K_{O_2,OHO,NO}$	Oxygen half saturation for NO to N_2O via OHOs	0.05	gO_2 m^{-3}	Hiatt & Grady (2008)
K_{O_2,OHO,N_2O}	Oxygen half saturation for NO to N_2O via OHOs	0.05	gO_2 m^{-3}	Hiatt & Grady (2008)
$K_{N_2O,OHO}$	Nitrous oxide half saturation for OHOs	0.05	gN m^{-3}	Hiatt & Grady (2008)
$K_{NO,OHO}$	Nitric oxide half saturation for OHOs	0.05	gN m^{-3}	Hiatt & Grady (2008)
$K_{I4,NO,OHO}$	NO inhibition coefficient for NO to N_2O via OHOs	0.3	gN m^{-3}	Hiatt & Grady (2008)
$K_{I5,NO,OHO}$	NO inhibition coefficient for N_2O to N_2 via OHOs	0.075	gN m^{-3}	Hiatt & Grady (2008)

4.6 References

Barker, P.S. and Dold, P.L. (1997). General model for biological nutrient removal activated-sludge systems: model presentation. *Water Environment Research*, 69(5), 969-984.

Chen, X., Huo, P., Liu, J., Li, F., Yang, L., Li, X., Wei, W., Liu, Y., & Ni, B.-J. (2021). Model predicted N2O production from membrane-aerated biofilm reactor is greatly affected by biofilm property settings. *Chemosphere*, *281*, 130861. https://doi.org/10.1016/j.chemosphere.2021.130861

Chen, X., Yang, L., Sun, J., Wei, W., Liu, Y., & Ni, B.-J. (2020). Influences of Longitudinal Heterogeneity on Nitrous Oxide Production from Membrane-Aerated Biofilm Reactor: A Modeling Perspective. *Environmental Science & Technology*, *54*(17), 10964–10973. https://doi.org/10.1021/acs.est.0c04067

Cole, A. C., Semmens, M. J., & LaPara, T. M. (2004). Stratification of Activity and Bacterial Community Structure in Biofilms Grown on Membranes Transferring Oxygen. *Applied and Environmental Microbiology*, *70*(4), 1982–1989. https://doi.org/10.1128/AEM.70.4.1982-1989.2004

Côté, P., Peeters, J., Adams, N., Hong, Y., Long, Z., & Ireland, J. (2015). A New Membrane-Aerated Biofilm Reactor for Low Energy Wastewater Treatment: Pilot Results. WEFTEC 2015. https://www.accesswater.org/publications/proceedings/-277906/a-new-membrane-aerated-biofilm-reactor-for-low-energy-wastewater-treatment--pilot-results

Daelman, M. R. J., van Voorthuizen, E. M., van Dongen, L. G. J. M., Volcke, E. I. P., & van Loosdrecht, M. C. M. (2013). Methane and nitrous oxide emissions from municipal wastewater treatment – results from a long-term study. *Water Science and Technology*, *67*(10), 2350–2355. https://doi.org/10.2166/wst.2013.109

Downing, L. S., & Nerenberg, R. (2008). Total nitrogen removal in a hybrid, membrane-aerated activated sludge process. *Water Research*, *42*(14), 3697–3708. https://doi.org/10.1016/j.watres.2008.06.006

Gupta, H. V., Sorooshian, S., & Yapo, P. O. (1999). Status of Automatic Calibration for Hydrologic Models: Comparison with Multilevel Expert Calibration. *Journal of Hydrologic Engineering*, *4*(2), 135–143. https://doi.org/10.1061/(ASCE)1084-0699(1999)4:2(135)

He, H., & Daigger, G. T. (2023). The hybrid MABR process achieves intensified nitrogen removal while N2O emissions remain low. *Water Research*, *244*, 120458. https://doi.org/10.1016/j.watres.2023.120458

Hiatt, W. C., & Grady, C. P. L. (2008). An Updated Process Model for Carbon Oxidation, Nitrification, and Denitrification. *Water Environment Research*, *80*(11), 2145–2156. https://doi.org/10.2175/106143008X304776

Kampschreur, M. J., Temmink, H., Kleerebezem, R., Jetten, M. S. M., & van Loosdrecht, M. C. M. (2009). Nitrous oxide emission during wastewater treatment. *Water Research*, *43*(17), 4093–4103. https://doi.org/10.1016/j.watres.2009.03.001

Kinh, C. T., Riya, S., Hosomi, M., & Terada, A. (2017). Identification of hotspots for NO and N2O production and consumption in counter- and co-diffusion biofilms for simultaneous nitrification and denitrification. *Bioresource Technology*, *245*, 318–324. https://doi.org/10.1016/j.biortech.2017.08.051

Kinh, C. T., Suenaga, T., Hori, T., Riya, S., Hosomi, M., Smets, B. F., & Terada, A. (2017). Counter-diffusion biofilms have lower N2O emissions than co-diffusion biofilms during simultaneous nitrification and denitrification: Insights from depth-profile analysis. *Water Research*, *124*, 363–371. https://doi.org/10.1016/j.watres.2017.07.058

Krause, P., Boyle, D. P., & Bäse, F. (2005). Comparison of different efficiency criteria for hydrological model assessment. *Advances in Geosciences*, *5*, 89–97. https://doi.org/10.5194/adgeo-5-89-2005

LaPara, T. M., Cole, A. C., Shanahan, J. W., & Semmens, M. J. (2006). The effects of organic carbon, ammoniacal-nitrogen, and oxygen partial pressure on the stratification of membrane-aerated biofilms. *Journal of Industrial Microbiology and Biotechnology*, *33*(4), 315–323. https://doi.org/10.1007/s10295-005-0052-5

Law, Y., Ye, L., Pan, Y., & Yuan, Z. (2012). Nitrous oxide emissions from wastewater treatment processes. *Philosophical Transactions: Biological Sciences*, *367*(1593), 1265–1277.

Legates, D. R., & McCabe Jr., G. J. (1999). Evaluating the use of "goodness-of-fit" Measures in hydrologic and hydroclimatic model validation. *Water Resources Research*, *35*(1), 233–241. https://doi.org/10.1029/1998WR900018

Li, M., Du, C., Lan, M., Sun, Z., Liu, R., & Li, B. (2020). Nitrogen removal and nitrogenous intermediate production of the heterotrophic membrane-aerated biofilm: A mathematical modeling investigation. *Korean Journal of Chemical Engineering*, *37*(3), 525–535. https://doi.org/10.1007/s11814-019-0454-0

Liu, Y., Zhu, T., Ren, S., Zhao, T., Chai, H., Xu, Y., Peng, L., & Liu, Y. (2022). Contribution of nitrification and denitrification to nitrous oxide turnovers in membrane-aerated biofilm reactors (MABR):

A model-based evaluation. *Science of The Total Environment*, *806*, 151321. https://doi.org/10.1016/j.scitotenv.2021.151321

Mampaey, K. E., Beuckels, B., Kampschreur, M. J., Kleerebezem, R., van Loosdrecht, M. C. M., & Volcke, E. I. P. (2013). Modelling nitrous and nitric oxide emissions by autotrophic ammonia-oxidizing bacteria. *Environmental Technology*, *34*(12), 1555–1566. https://doi.org/10.1080/09593330.2012.758666

Martin, K. J., & Nerenberg, R. (2012). The membrane biofilm reactor (MBfR) for water and wastewater treatment: Principles, applications, and recent developments. *Bioresource Technology*, *122*, 83–94. https://doi.org/10.1016/j.biortech.2012.02.110

Moriasi, D., N., Arnold, J. G., Van Liew, M. W., Bingner, R. L., Harmel, R. D., & Veith, T. L. (2007). Model Evaluation Guidelines for Systematic Quantification of Accuracy in Watershed Simulations. *Transactions of the American Society of Agricultural and Biological Engineers*, *50*(3), 885–900.

Nash, J. E., & Sutcliffe, J. V. (1970). River flow forecasting through conceptual models part I — A discussion of principles. *Journal of Hydrology*, *10*(3), 282–290. https://doi.org/10.1016/0022-1694(70)90255-6

Ni, B.-J., Smets, B. F., Yuan, Z., & Pellicer-Nàcher, C. (2013). Model-based evaluation of the role of Anammox on nitric oxide and nitrous oxide productions in membrane aerated biofilm reactor. *Journal of Membrane Science*, *446*, 332–340. https://doi.org/10.1016/j.memsci.2013.06.047

Ni, B.-J., & Yuan, Z. (2013). A model-based assessment of nitric oxide and nitrous oxide production in membrane-aerated autotrophic nitrogen removal biofilm systems. *Journal of Membrane Science*, *428*, 163–171. https://doi.org/10.1016/j.memsci.2012.10.049

Oudin, L., Andréassian, V., Mathevet, T., Perrin, C., & Michel, C. (2006). Dynamic averaging of rainfall-runoff model simulations from complementary model parameterizations. *Water Resources Research*, *42*(7). https://doi.org/10.1029/2005WR004636

Sabba, F., Terada, A., Wells, G., Smets, B. F., & Nerenberg, R. (2018). Nitrous oxide emissions from biofilm processes for wastewater treatment. *Applied Microbiology and Biotechnology*, *102*(22), 9815–9829. https://doi.org/10.1007/s00253-018-9332-7

Seshan, S., Poinapen, J., Zandvoort, M. H., van Lier, J. B., & Kapelan, Z. (2024). Limitations of a biokinetic model to predict the seasonal variations of nitrous oxide emissions from a full-scale wastewater treatment plant. *Science of The Total Environment*, *917*, 170370. https://doi.org/10.1016/j.scitotenv.2024.170370

Soreanu, G., Lishman, L., Dunlop, S., Behmann, H., & Seto, P. (2010). An assessment of oxygen transfer efficiency in a gas permeable hollow fibre membrane biological reactor. *Water Science and Technology*, *61*(5), 1165–1171. https://doi.org/10.2166/wst.2010.877

Spérandio, M., Lang, L., Sabba, F., Nerenberg, R., Vanrolleghem, P., Domingo-Félez, C., Smets, B. F., Duan, H., Ni, B.-J., & Yuan, Z. (2022). Modelling N2O production and emissions. In L. Ye, J. Porro, & I. Nopens (Eds.), Quantification and Modelling of Fugitive Greenhouse Gas Emissions from Urban Water Systems (pp. 167–196). IWA Publishing. https://doi.org/10.2166/9781789060461_0167

Uri-Carreño, N., Nielsen, P. H., Gernaey, K. V., Domingo-Félez, C., & Flores-Alsina, X. (2024). Nitrous oxide emissions from two full-scale membrane-aerated biofilm reactors. *Science of The Total Environment*, *908*, 168030. https://doi.org/10.1016/j.scitotenv.2023.168030

Uri-Carreño, N., Nielsen, P. H., Gernaey, K. V., & Flores-Alsina, X. (2021). Long-term operation assessment of a full-scale membrane-aerated biofilm reactor under Nordic conditions. *Science of The Total Environment*, *779*, 146366. https://doi.org/10.1016/j.scitotenv.2021.146366

Chapter 5 - Do full-scale hybrid membrane aerated biofilm reactors enhance the removal of organic micropollutants?

Abstract

The design features in a hybrid membrane aerated biofilm reactor (MABR) such as varying redox conditions and increased biomass residence time in the biofilms can be advantageous for the removal of various organic micropollutants (OMP). However, the OMP removal performance of MABRs remains unexplored. This study monitored the removal of 16 OMPs over multiple seasons in a full-scale conventional activated sludge treatment process (CAS) before and after an upgrade with a hybrid membrane aerated biofilm reactor (MABR) process. A comparison of OMP concentrations in the plant effluent showed that 12 out of 16 target compounds were present at lower concentrations after the upgrade. An examination of plantwide removal efficiencies revealed that highly removable compounds (> 75%) such as acetaminophen, ibuprofen, naproxen, triclosan, triclocarban, and norfluoxetine and the recalcitrant carbamazepine were not impacted by the addition of the MABR process. However, six compounds namely gemfibrozil, sulfamethoxazole, trimethoprim, atorvastatin and its ortho- and para-hydroxy metabolites, that were poorly removed (< 25%) by the CAS configuration had moderate removals (25 to 75%) with the hybrid MABR/CAS configuration. After the MABR upgrade it was found that six OMPs showed higher removal under warm weather conditions (19.3 ± 1.6°C) when compared to cold weather conditions (13 ± 1.2°C). Mass balance analyses on the MABR tank revealed a broad range of compound specific responses such as complete biotransformation (acetaminophen), partial removal (naproxen), and compound formation from unmeasured precursors (sulfamethoxazole, carbamazepine). Overall, long-term monitoring of the full-scale facility before and after the upgrade revealed that upgrading of CAS to a hybrid MABR configuration can enhance the removal of some OMPs that are poorly removed by the CAS process alone.

Keywords: Organic micropollutants, pharmaceuticals and personal care product ingredients, membrane aerated biofilm reactor (MABR), seasonality, biotransformation, sorption.

5.1 Introduction

Organic micropollutants (OMPs) are a broad class of anthropogenic contaminants that occur at ng/L to µg/L concentrations in natural waters due to their everyday use as pharmaceuticals, personal care product ingredients, surfactants, and biocides (Alvarino et al., 2018). Although their concentrations are typically low, the presence of OMPs is concerning because they are often biologically active with persistent, bioaccumulative, toxic, and endocrine disrupting characteristics (Boxall et al., 2012; Schwarzenbach et al., 2006; Shao et al., 2019; Stamm et al., 2016). Water resource recovery facilities (WRRFs) are not normally designed to treat OMPs and hence they discharge some of these contaminants into the environment (Petrie et al., 2015; Ternes, 1998). However, commonly adopted treatment technologies such as conventional activated sludge (CAS) have been found to only remove some OMPs with the extent of removal dependent on their chemical structure and treatment operating conditions (Oulton et al., 2010). Toxicological surveys in wastewater effluent impacted streams have shown that WRRF upgrades to improve nitrification can also reduce the presence of some OMPs and decrease the incidence of reproductive ill-effects in fish (Hicks et al., 2017; Nikel et al., 2023). Hence, there is an interest in assessing whether emerging nutrient removal technologies can further reduce the discharge of OMPs to watersheds and protect aquatic ecosystems.

Prior studies have shown that advanced biological wastewater treatment processes can enhance OMP removal when compared to the CAS configuration. Biological nutrient removal (BNR) configurations that include multiple redox zones have been found to enhance the biotransformation of some OMPs in the anoxic and anaerobic zones (Inyang et al., 2016; Lakshminarasimman et al., 2018; Suarez et al., 2010) and also reduce effluent toxicity when compared to CAS (Parker et al., 2014). This is because of the recirculation of activated sludge between different redox zones that enables facultative heterotrophic organisms and their diverse enzymes pools with broad specificity to metabolize OMPs even under low dissolved oxygen (DO) conditions (Ogunlaja & Parker, 2015; Phan et al., 2016). Other treatment designs such as membrane bioreactors (MBR) characterized by high mixed liquor suspended solids (MLSS) concentration and longer solids retention time (SRT) have also shown higher removal of OMPs due to the growth of slow growing organisms (Maeng et al., 2013; Radjenović et al., 2009). Similarly, biofilm based processes such as the moving bed biofilm reactor (MBBR) and integrated fixed film activated sludge system (IFAS) have been reported to achieve higher removals and more rapid biotransformation of OMPs when compared to suspended growth systems (Falås et al., 2012; Falås et al., 2013; Mazioti et al., 2015; Murray et al., 2017). The longer biomass retention time in the biofilms and the stratified microbial communities along with substrate and redox gradients have been identified as possible reasons for improved removal of OMPs in biofilm-based treatment processes (Falås et al., 2012). Overall, advanced

biological treatments designs create favor the growth of a more diverse microbial community that eventually improve the removal of a broader class of OMPs when compared to CAS systems.

The membrane aerated biofilm reactor (MABR) process integrates the beneficial features of several advanced secondary treatment technologies. MABRs support biofilm growth on an oxygen permeable membrane that can result in a stratification of redox zones associated with the establishment of an oxygen gradient in the biofilm. The presence of biofilms can also increase the overall SRT to support the growth of diverse, slow growing microorganisms. The potential for enhanced OMP degradation in a stratified biofilm could be further enhanced by immersing the biofilm in an anoxic suspended growth basin (hybrid design) that would further support the removal of pollutants through metabolic pathways associated with the presence of multiple redox conditions (Li et al., 2008). Mei et al. (2020) observed a stepwise degradation of nitroaniline in a stratified MABR where the parent compound was reduced to form phenylenediamine in the anaerobic layer of the biofilm that was further oxidized in the aerobic layer. The nitrate that was formed as a secondary pollutant was denitrified in the anoxic layer (Mei et al., 2020). Thus, hybrid MABR systems could potentially be advantageous in enhancing the removal of a wide array of OMPs through a combination of oxidizing and reducing conditions.

Several bench-scale studies have investigated the impact of MABR operational conditions on the fate and removal of OMPs. Celik et al. (2018) and Taskan et al. (2019) investigated the removal of oxytetracycline and tetracycline, respectively, and found that their flux into the biofilm increased with hydraulic retention time (HRT) (7.5 to 18 hours) and O_2 pressure in the membrane (0.14 to 0.41 bar). In addition, increased biofilm thickness (0.33 to 1.02 mm) in a lab-scale biofilm-only MABR system improved the removal of multiple OMPs (Sanchez-Huerta et al., 2022). The enhanced removal with thicker biofilms was attributed to the combined activity of both nitrifiers and heterotrophs (Sanchez-Huerta et al., 2023). Overall, the literature indicates that MABR operational conditions and biofilm thickness could impact OMP removal.

While these smaller-scale studies provide a basic understanding of the role of operating conditions on OMP removal they were often conducted with a synthetic wastewater that did not contain additional sources of carbon (Elad et al., 2023), and had high OMP concentrations (Çelik et al., 2018; Taşkan et al., 2019). It is anticipated that these conditions may lead to responses that are not representative of real wastewater systems where OMP concentrations are dilute, and alternative more-readily biodegradable substrate are available to support biomass growth. It is considered critical to evaluate OMP removal in real wastewater with a complex substrate profile and representative concentrations to understand the true performance of MABRs. In addition, prior studies have focused on biofilm-only systems that did not have a bulk phase suspended sludge and had small membrane surface areas (10^{-3} to 10^{-1} m^2). No study has so far evaluated the fate of OMP in full scale hybrid MABRs that have an anoxic suspended growth phase.

Further, OMP removal in MABRs has also not been investigated over the range of conditions (i.e. temperature and flow) that can change with season. Hence, the objective of this study was to evaluate the performance of a full-scale hybrid MABR system in removing an array of OMPs over a range of seasonal conditions that are typical of North America. This was achieved by monitoring OMP removal in a full scale WRRF before and after an MABR upgrade over a period of three years. The data obtained from the multi-year sampling campaign was used to construct contaminant mass balances to elucidate the fate mechanisms and individual treatment processes responsible for OMP removal.

5.2 Methodology

5.2.1 Sampling plan

A detailed description of the study site is presented in Chapter 2. The process flowsheets for the facility before and after the MABR upgrade are shown in Figure 5.1. Before the upgrade, time composite samples (24 equally weighted hourly samples) of the plant influent and the plant effluent (Figure 5.1a) were collected using refrigerated autosamplers (Hach, London, ON, Canada) maintained at 2°C to reduce biological activity during sample collection. Samples were collected on three consecutive days during select months of 2020 (Sep to Dec), 2021 (Jan), 2022 (Feb to Aug). Sampling days were designated as warm and cold conditions if the aeration tank temperatures were > 15°C and < 15°C, respectively. After the upgrade, an additional sampling point was included for the MABR effluent (mixed liquor sample as shown in Figure 5.1b) to facilitate quantification of OMP removal in the MABR and aeration tank separately. Post-upgrade samples were collected on three consecutive days each month between Sept 2022 to Sept 2023. The samples were transported in coolers containing ice packs (< 2°C) to the university lab within a few hours of collection. As soon as the samples were received in the lab, they were preserved with 1 g/L sodium azide and 50 mg/L ascorbic acid and filtered using a 1 μm pore size glass fiber filters (Pall Corporation, Missisauga, Canada). The filtered and preserved samples were extracted within 72 hours.

The sampling campaign included monitoring of the plant operations to support the subsequent assembly of contaminant mass balances. Data on wastewater and solids stream flows and aeration tank temperature were obtained from online sensors at the plant. The total suspended solids (TSS) concentration in the composite samples of the raw influent and MABR effluent, and grab samples of the aeration tank mixed liquor suspended solids (MLSS) and the wasting stream were measured during every sampling event following standard methods 2540 D.

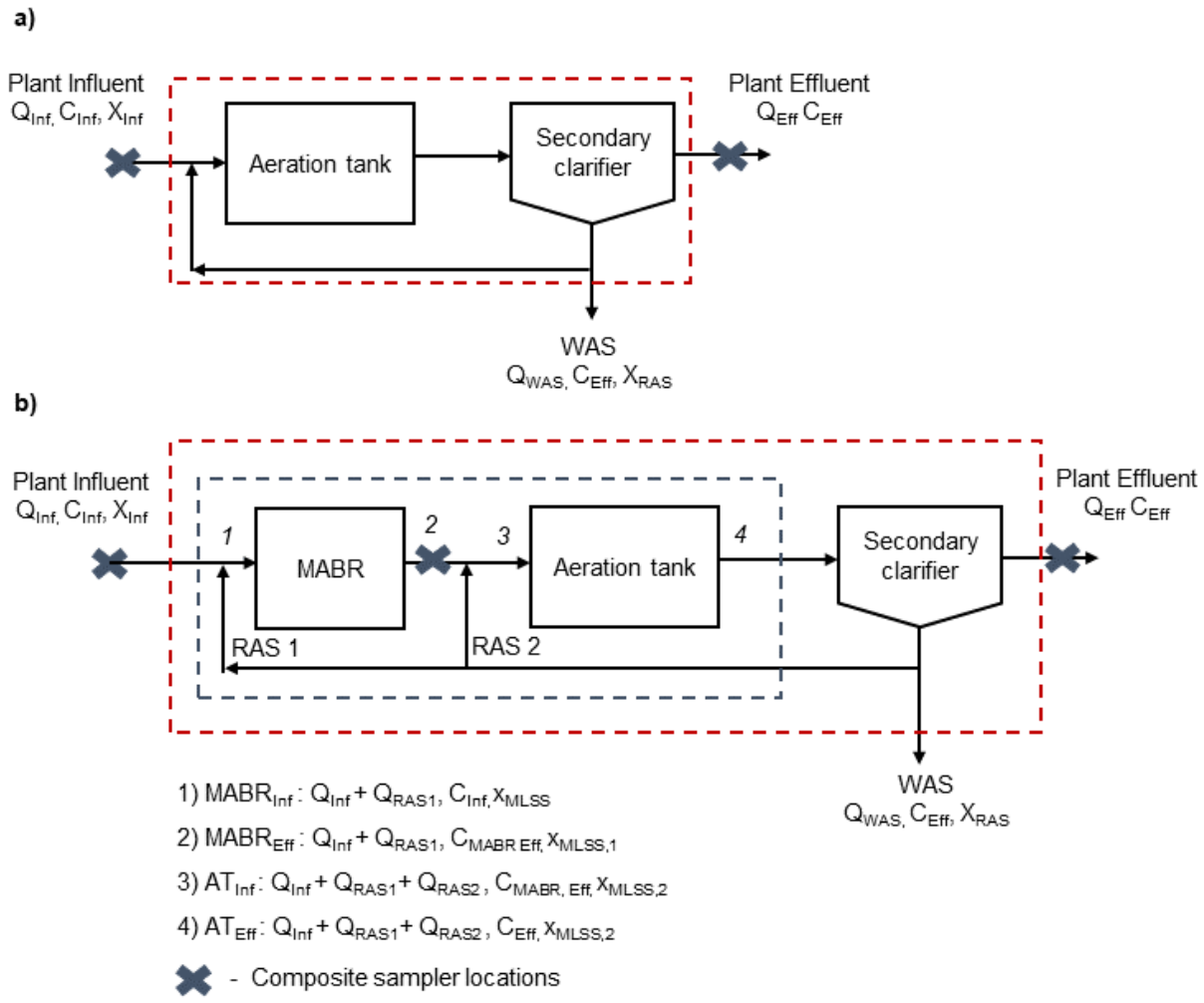

Figure 5.1 - Layout of the study site in its a) CAS configuration before upgrade and b) hybrid MABR/CAS configuration after upgrade.

5.2.2 Reagents and chemicals

The target list of 16 OMPs and their physico-chemical properties are shown in Table 5.1. These chemicals were selected because: i) they are known to occur in a variety of watersheds (Arlos et al., 2015; Ternes, 1998; Verlicchi et al., 2012); ii) some of them are known to elicit effects in aquatic life (Cizmas et al., 2015; Ebele et al., 2017; Patel et al., 2019); and iii) they represent a wide range of usage and chemical functionalities. All chemicals employed to prepare stock solutions and establish standard curves were purchased from Sigma-Aldrich, USA. The deuterated standards used for the quantitation of each of the target chemicals were purchased from TRC Chemicals, Canada and CDN Isotopes, Canada. Both the regular and deuterated standards were dissolved in methanol to prepare a 1 g/L stock solution which was stored in amber glass vials in a -20°C freezer. All the solvents used in the extraction and instrumental

analysis were of HPLC grade and were purchased from Fischer Scientific, Canada, while ultrapure water was from a lab-scale MilliQ water purification system (MilliporeSigma, Oakville, Canada).

Table 5.1 – Target OMPs and their physico-chemical properties.

No.	Organic micropollutant	Category	Chemical formula	pK_a*	Sorption distribution coefficient K_d# in L/kg Average (Range)
1.	Trimethoprim (TMP)	Antibiotic	$C_{14}H_{18}N_4O_3$	7.12	192 (25-330)
2.	Sulfamethoxazole (SULF)		$C_{10}H_{11}N_3O_3S$	1.6, 5.7	120 (11-269)
3.	Fluoxetine (FLX)	Antidepressant	$C_{17}H_{18}F_3NO$	10.1	2694 (880-6000)
4.	Norfluoxetine (NFLX)		$C_{16}H_{16}F_3NO$	NA	
5.	Ibuprofen (IBU)	Nonsteroidal anti-inflammatory drugs	$C_{13}H_{18}O_2$	4.9	90 (6-453)
6.	Naproxen (NPX)		$C_{14}H_{14}O_3$	4.15	64 (10-217)
7.	Diclofenac (DCF)		$C_{14}H_{11}Cl_2NO_2$	4.15	46 (2-151)
8.	Acetaminophen (ACE)	Analgesic	$C_8H_9NO_2$	9.38	84
9.	Gemfibrozil (GFZ)	Lipid regulators	$C_{15}H_{22}O_3$	4.5	63 (19-129)
10.	Atorvastatin (ATOR)		$C_{33}H_{35}FN_2O_5$	4.3, 14.9	93
11.	o-hydroxy atorvastatin (o-ATOR)	Human metabolites of ATOR	$C_{33}H_{35}FN_2O_6$	NA	
12.	p-hydroxy atorvastatin (p-ATOR)		$C_{33}H_{35}FN_2O_6$	NA	
13.	Carbamazepine (CBZ)	Anticonvulsant	$C_{15}H_{12}N_2O$	13.9	38 (1-135)
14.	Triclosan (TCS)	Antimicrobial	$C_{12}H_7Cl_3O_2$	7.9	3890
15.	Triclocarban (TCCB)		$C_{13}H_9Cl_3N_2O$	12.7	25703
16.	Caffeine (CAFF)	Stimulant	$C_8H_{10}N_4O_2$	14	190 (30-350)

*pK_a values adopted from https://pubchem.ncbi.nlm.nih.gov/

#K_d values are adopted from Pomiès et al. (2013) and the references therein.

5.2.3 OMP analysis

The analytical procedure for measuring the OMPs concentration followed an isotope dilution method as described in (Mehdi et al., 2018). All the samples were extracted and analyzed in triplicates. The analysis started with pH adjusting 100 mL sample aliquots to 2 ± 0.1 using 10 N concentrated sulfuric acid. The acidified samples were spiked with 100 µL of deuterated standard mix after which the target compounds were extracted and concentrated through a solid phase extraction procedure. Target compound extraction was done using Bond Elut Plexa Cartridges (6 cc, 500 mg, Agilent Technologies, Santa Clara, United

States) preconditioned with 5 mL of methanol and MilliQ water manually in a manifold extraction set up. After sample loading, the cartridges were rinsed with MilliQ water and 5% methanol solution in water and eluted with 6 mL of methanol. The extracted samples were evaporated to dryness under a gentle nitrogen gas stream. The residual analytes in the vials were reconstituted in 500 µL of methanol. The reconstitution solution also had 75 µg/L of lorazapem and chloramphenicol as instrument controls to ensure the samples were injected properly. Extracted samples were store in a -20°C freezer until instrumental analysis. Analysis of OMPs was performed in an Agilent 1260 HPLC and an Agilent 6460 triple quadrupole (QQQ) mass spectrometer with electrospray ionization. The chromatographic separation of the analytes was accomplished using an Agilent ZORBAX Eclipse Plus C18 column at 40°C and a binary gradient of 5mM ammonium acetate in water and methanol. The method detection limits can be found in Supplemental Information Table S5.1.

5.2.4 Quality control and quality assurance

The quality control/quality assurance procedure included employing a procedural blank as a negative control to identify any extraneous contamination in each sample extraction batch. The procedural blanks consisted of a 100 mL MilliQ water sample spiked with 100 µL of 100 µg/L deuterated standard mix. The procedural blanks almost always reported concentrations less than the detection limit. The QA/QC procedure also included duplicate matrix spike samples, per batch, to adjust for target compound recovery. The matrix spike samples consisted of 100 mL MilliQ water with 100 µL of 100 µg/L regular and deuterated standards. A summary of the QA/QC results is provided in Table S5.3 in Supplementary Information.

5.2.5 Contaminant mass balance and removal efficiency calculations

The measured OMP concentrations were used to assemble OMP mass balances to evaluate the overall plantwide removal and elucidate the contribution of biotransformation in the MABR and aeration tanks and sorption to the mixed liquor to OMP removal. The average of three replicates analyzed was considered as the representative concentration for each sample in a sampling day. The removal and mass balance calculations were performed for each sampling day and then composited during data analysis. Since, the analytical method measured only the soluble fraction of the OMPs in the samples, the OMPs associated with the solids fraction in plant influent and MABR effluent samples were estimated based on sorption-distribution co-efficients (K_d) that were obtained from the literature (Table 5.1). For two target OMPs which were human metabolites of atorvastatin, K_d values were not available in the literature. Hence the values of the parent compounds were adopted to approximate the metabolite values. This was deemed to be a conservative assumption that predicts the upper bound of sorption as the two metabolites are hydroxylated and could be expected to have lower sorption potential than the parent compound. In the

subsequently discussed mass balances, the mass flow of OMPs associated with the solids in the final plant effluent were assumed to be negligible due to the relatively low tendency of the target OMPs to partition to solids and the very low suspended solids in this stream (<25 mg TSS/L). The equations developed for plant wide mass balance (Figure 5.1) are described by Equations 5.1-5.5.

$$M_{Inf} = Q_{Inf}.C_{Inf}.(1 + K_d X_{Inf}) \quad \text{....(5.1)}$$

$$M_{WAS} = Q_{WAS}.C_{Eff}.K_d.X_{WAS} \quad \text{.....(5.2)}$$

$$M_{Eff} = Q_{Eff.}C_{Eff} \quad \text{.....(5.3)}$$

$$M_{bio} = M_{Inf} - M_{Eff} - M_{WAS} \quad \text{.....(5.4)}$$

$$Plantwide\ overall\ OMP\ removal\ efficiency = \frac{M_{Inf} - M_{Eff}}{M_{Inf}} * 100\% \quad \text{.....(5.5)}$$

M_{Inf} = OMP mass flow in the influent (g/d)

M_{WAS}= OMP mass flow in the wasting stream (g/d)

M_{Eff} = OMP mass flow in the plant effluent (g/d)

M_{bio} = OMP mass flow biotransformed (g/d)

Q_{Inf} = Daily average influent flow (m^3/d)

C_{Inf} = OMP concentration in the plant influent (ng/L)

X_{Inf} = TSS concentration in the plant influent (mg/L)

Q_{WAS}= Daily average WAS flow (m^3/d)

C_{Eff}= OMP concentration in the WAS stream (ng/L)

X_{WAS} = TSS concentration in the WAS stream (mg/L)

In the pre-upgrade configuration, all biotransformation (M_{bio}) in the plant was attributed to the activity of the organisms in the aeration tank. However, post MABR upgrade, M_{bio} included biotransformations in both the MABR and aeration tanks. In order to divide the biotransformation into the individual tanks, additional mass balances were assembled for the post-upgrade plant configuration (Figure 5.1b). As seen in Figure 5.1b, the MABR effluent included both the plant influent and RAS flows. A new system boundary was drawn to calculate the mass flows in the blended flow as shown in Equations (5.6) to (5.9). Biotransformations in the MABR and aeration tank (AT) were estimated separately using equations (5.10) and (5.11). The mass balance calculations assumed that the sorption process was instantaneous and that K_d values were the same for all streams.

$$MABR_{in} = Q_{Inf}C_{Inf}\left(1 + K_d X_{Inf}\right) + Q_{RAS,1}.C_{Eff}.K_d.X_{RAS} \quad \text{.....(5.6)}$$

$$MABR_{out} = (Q_{Inf} + Q_{RAS,1}) * C_{MABR,Eff} * \left(1 + K_d X_{MLSS,1}\right) \quad \text{.....(5.7)}$$

$$AT_{in} = MABR_{out} + (Q_{RAS,2} * C_{,Eff} * (1 + K_d X_{RAS})) \quad \text{.....(5.8)}$$

$$AT_{out} = (Q_{Inf} + Q_{RAS,1} + Q_{RAS,2}) * C_{Eff} * \left(1 + K_d X_{MLSS,2}\right) \quad \text{…..(5.9)}$$

$$R_{MABR} = \frac{MABR_{in} - MABR_{out}}{MABR_{in}} * 100\% \quad \text{…..(5.10)}$$

$$R_{AT} = \frac{AT_{in} - AT_{out}}{MABR_{in}} * 100\% \quad \text{…..(5.11)}$$

$MABR_{in}$ = OMP mass flow in MABR influent (g/d)

$MABR_{out}$ = OMP mass flow in MABR effluent (g/d)

AT_{in} = OMP mass flow in aeration tank influent (g/d)

AT_{out} = OMP mass flow in aeration tank effluent (g/d)

$Q_{RAS,1}$ = Flow of RAS stream 1 (m^3/d)

$Q_{RAS,2}$ = Flow of RAS stream 2 (m^3/d)

$C_{MABR,Eff}$ = OMP concentration in the MABR effluent (ng/L)

$X_{MLSS,1}$ = MLSS concentration in the MABR tank (mg/L)

$X_{MLSS,2}$ = MLSS concentration in the aeration tank (mg/L)

X_{RAS} = TSS concentration in the RAS stream (mg/L)

R_{MABR} = Removal through biotransformation in MABR (%)

R_{AT} = Removal through biotransformation in aeration tank (%)

5.2.6 Statistical analysis

The measured OMP concentrations and calculated removal efficiencies for different sampling days were categorized into four groups on the basis of upgrade (before and after) and seasonality (cold and warm) to analyze the plant performance as a function of the two test variables. An initial Shapiro-Wilk test (α = 0.05) indicated that the concentration and percentage removal data were not normally distributed. Hence, the non-parametric Kruskal-Wallis Test was used to ascertain whether the upgrade and seasonality impacted the concentration and removal values. A Dunn's post-hoc test was used for multiple comparisons of the concentration and removal datasets between different upgrade and seasonality scenarios. The P value was adjusted using a Bonferroni correction (α/number of comparisons (2x2)) from the standard 0.05 value to P* = 0.0084 (adjusted P-value) to minimize the risk of Type I error when making multiple comparisons (Armstrong, 2014). In cases where there was a statistically significant difference in the concentration or the removal values, the magnitude of the difference between the averages was determined using relative percentage difference (Equation 5.12).

$$RPD\ (\%) = \frac{|X_1 - X_2|}{\frac{X_1 + X_2}{2}} * 100\% \quad \text{…..(5.12)}$$

X_1 and X_2 are the average concentration or removal values being compared.

5.3 Results and discussion

The overall objective of the study was to evaluate the full-scale OMP removal performance as a function of MABR upgrade and seasonality. Hence, the larger dataset collected over three years was clustered into four categories namely, before upgrade warm conditions (21 sampling days), before upgrade cold conditions (15 sampling days), after upgrade warm conditions (24 sampling days), and after upgrade cold conditions (15 sampling days) to facilitate multiple comparisons between the various scenarios. The impact of MABR addition was examined by comparing the before upgrade warm and after upgrade warm scenarios. Warm condition was chosen because the MABR operational conditions were stable, and the plant showed steady N removal rates as seen in Phase 1 and Phase 4 results in Chapter 2. The impact of seasonality was assessed for both the pre and post upgrade scenarios by comparing the warm weather and cold weather data under the two plant configurations. The comparisons were made using the effluent OMP concentration first, followed by analyses of removal efficiencies.

5.3.1 Impact of upgrade and seasonality on OMP concentrations

The OMP concentrations in the plant effluent is a toxicologically relevant indicator for the overall quality of the treated wastewater discharging into the receiving water bodies. Hence, the OMP concentrations in the plant effluent before and after the upgrade (Figure 5.2) were compared to assess the impact of MABR addition on the effluent quality. After the MABR upgrade, the plant effluent concentration decreased significantly ($P^* < 0.008$) for 12 of the 16 compounds (Figure 5.2). The magnitude of change in concentration varied depending on the OMPs. Compounds such as ibuprofen ($P^* = 0.004$), naproxen ($P^* < 0.001$), caffeine ($P^* < 0.001$) and triclosan ($P^* < 0.001$) had an RPD more than 110% indicating a wide difference in the plant effluent concentration after upgrade. Whereas other compounds such as atorvastatin, ortho- and para- hydroxy atorvastatin, sulfamethoxazole, trimethoprim, carbamazepine, and gemfibrozil had a moderate difference with slightly lower RPD values ranging between 15% to 68%. The average concentrations of diclofenac, fluoxetine, and norfluoxetine were found to be statistically similar indicating no impact of upgrade. Overall, after the addition of MABR, the average OMP concentrations showed an overall reduction in occurrence levels of majority of the targeted OMPs.

The average plant effluent OMP concentrations were compared between summer and winter conditions under the two plant configurations to study the impact of seasonality on the plant effluent quality. The average wastewater temperatures were 13.1 ± 1.2 ℃ and 19.3 ± 1.5 ℃ during the cold and warm weather sampling months, revealing an average temperature differential of 6 ℃ between the two scenarios. Comparison of the average concentrations before upgrade showed that only norfluoxetine was significantly different ($P^* = 0.002$) between the warm and cold weather conditions. For all the other compounds the difference was not statistically significant ($P^* > 0.008$). However, after upgrade, about

half of the target OMPs (8 compounds) reported a significant difference between the summer and winter weather concentrations (Figure 5.2). Triclosan was the only compound that reported a very small (RPD = 10%) but statistically significant increase (P* = 0.007) in the average plant effluent concentration from 31 to 35 ng/L. Remaining seven compounds showed significantly lower concentrations during warm weather conditions. Naproxen reported the highest RPD of 82% with a significant decrease (P* = 0.002) in average plant effluent concentration from 1060 ng/L to 441 ng/L. Similarly, compounds such as ibuprofen, atorvastatin, o-hydroxy atorvastatin, p-hydroxy atorvastatin, trimethoprim, norfluoxetine, and gemfibrozil reported a significantly lower concentration during warm weather conditions with RPD ranging between 65-45%. Overall, the seasonal comparisons after MABR addition shows that there is a significant impact of wastewater temperature on the occurrence levels of a subset of monitored OMPs in the plant effluent after the upgrade.

Viewed collectively, the two levels of comparisons indicate that addition of MABR resulted in a general improvement in the overall effluent quality of the plant with respect to the measured target compounds and the extend of the impact was influenced by the seasonality of wastewater temperature. However, the observed impacts could also be due to any variations in the influent OMP concentration over time and due to seasonal spikes in the usage of some of the pharmaceuticals (Vieno et al., 2005). Hence, plantwide OMP removal efficiencies calculated based on contaminant mass flows were assessed to study plant performance as a function of the upgrade and seasonality.

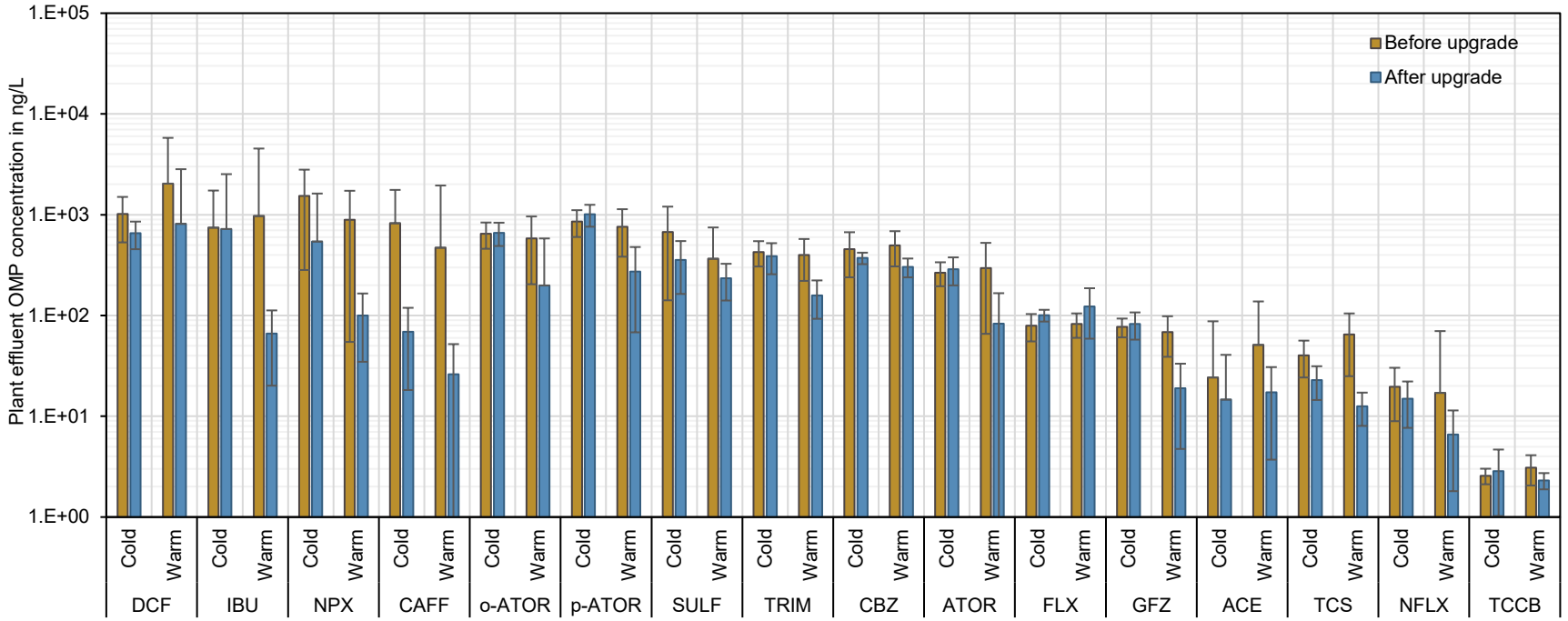

Figure 5.2 – OMP concentration in the plant effluent measured before and after upgrade during cold and warm weather conditions. Error bars indicate standard deviation between different sampling days.

5.3.2 Plantwide OMP removal before MABR upgrade

The plantwide removal efficiency of OMPs for the CAS-only configuration to establish a baseline against which the upgraded plant performance was compared. An initial review of the removal efficiencies revealed that the target OMPs exhibited a wide range of removal. Hence, to facilitate a structured discussion, the target compounds were clustered into three groups based on the magnitudes of removal efficiency. Figure 5.3 (a-c) shows the plantwide removal efficiencies and the contributions of the different fate pathways relative to the influent contaminant mass load during warm and cold weather conditions.

Group 1 – High removal (> 75%): Group 1 consisted of six compounds namely, acetaminophen, caffeine, ibuprofen, naproxen, triclosan, triclocarban, and norfluoxetine that had average removals over 85% during both warm and cold weather conditions (Figure 5.3a). On average, less than 10% of the influent mass load of the Group 1 compounds left the plant through the effluent indicating very good treatment. For compounds with lower K_d values (< 1000 L/kg) such as acetaminophen, caffeine, ibuprofen, and naproxen almost all the removal was due to biotransformation and removal through wasting was negligible. In contrast, triclosan and triclocarban, that had higher K_d values (3890 L/kg and 25703 L/kg, respectively), reported 10-15% and 20-25% of the influent contaminant load removed through sorption with the remaining fraction of influent mass loading (75%) removed by biotransformation. Thus, biotransformation was likely the predominant removal mechanism for group 1 compounds that represented OMPs with a broad range of sorption affinities.

Group 2 – Moderate removal (75 to 25%): Compounds that had moderate plantwide removals from 25 to 75% were categorized in group 2. Before the MABR upgrade, three compounds namely sulfamethoxazole, gemfibrozil, and fluoxetine were in this group (Figure 5.3b). Among the biotransformation played a greater role in the removal sulfamethoxazole (60-70%) followed by gemfibrozil. Removal through sorption was negligible for both the compounds because of their relatively low sorption affinities (Table 5.1). However, fluoxetine with a higher sorption affinity reported almost all of its removal through adsorption with a relatively smaller contribution from biotransformation (Figure 5.3b). Thus, compounds that reported moderate removals were primarily removed through biotransformation and adsorption depending on their sorption affinity.

Group 3 – Poor removal (< 25%): About half of the measured compounds were poorly removed (<25%) by the plant when it was in the CAS configuration. As seen in Figure 5.3c, OMPs such as trimethoprim, atorvastatin and its two hydroxy metabolites, and diclofenac had average removals between 10-25%, whereas carbamazepine reported the lowest average removal of less than 5%. Less than 25% of the influent contaminant load of the group 3 compounds was biotransformed. The poor removals of these

targeted compounds over a range of temperatures reflects a significant limitation of the CAS configuration in this regard.

The contribution of adsorption pathway to the overall removal of highly sorptive compounds ($K_d < 1000$) was investigated to understand its significance relative to biotransformation. For fluoxetine, a compound with a moderately high K_d value (2694 L/kg) about half of the influent mass load was removed by sorption. The fraction of fluoxetine removed through sorption was much higher than triclosan and triclosan (Figure 5.3a) that had higher K_d values. This was due to the differences in biodegradability of the compounds. For triclosan and triclocarban, the aqueous phase concentrations were maintained low by biodegradation, and this reduced the corresponding sorbed concentrations. On the contrary, fluoxetine was less amenable to biotransformation and higher aqueous concentrations led to greater partitioning to solids. Thus, the extent of removal by sorption was influenced by sorption affinity and the degree of biotransformation of the compounds.

The study site in its CAS configuration was capable of seasonal nitrification with very low ammonia removal during cold weather conditions (Chapter 2). Hence, the plantwide removal efficiencies calculated before upgrade were compared between cold and warm weather conditions to assess if the variations in nitrification impacted the OMP removal before upgrade. Analysis of variance between the two datasets revealed that there was no statistical significance ($P^* > 0.008$) in the difference between the average cold and warm weather removal efficiencies of all 16 OMPs. Similar overall removal efficiencies suggest that the autotrophic microorganisms involved in nitrification may not be solely responsible for OMP transformation. Heterotrophic microbes are capable of co-metabolic transformation of OMPs through reactions such as hydroxylation, hydrolysis, and demethylation catalyzed by commonly available non-specific enzymes (Kennes-Veiga et al., 2021). Transformation of OMPs such as sulfamethoxazole, trimethoprim, ibuprofen, naproxen, diclofenac, and triclosan have been observed in aerobic heterotrophic reactors (Falås et al., 2012; Fernandez-Fontaina et al., 2016; Khunjar et al., 2011; Tran et al., 2009). Thus, the similar removals of OMPs during both the seasonal conditions underpins the significant role played by heterotrophs in the CAS process.

Looking collectively, more than half of the targeted OMPs were removed poorly by the CAS system. Assessment of the individual fate processes showed that biotransformation was the major removal mechanism for all of the compounds and removal through sorption was minimal for most compounds. Moreover, there was no significant difference in OMP removal between cold and warm weather conditions before the upgrade.

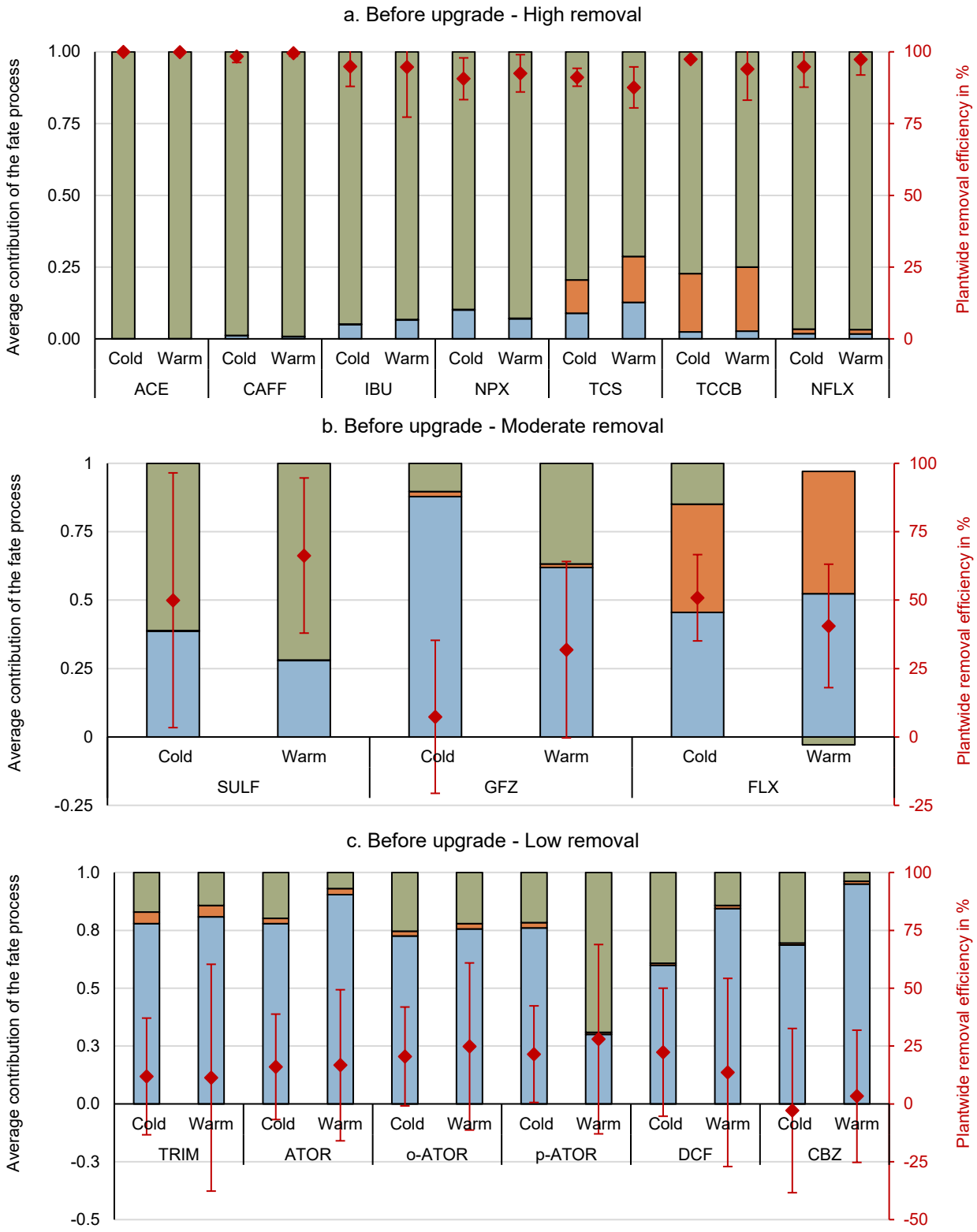

Figure 5.3 - Plantwide OMP removal efficiency before (a-c) and after (d-f) MABR upgrade during cold and warm operational conditions. Compounds are categorized into high, moderate, and low removal based on the magnitude of the overall removal efficiency.

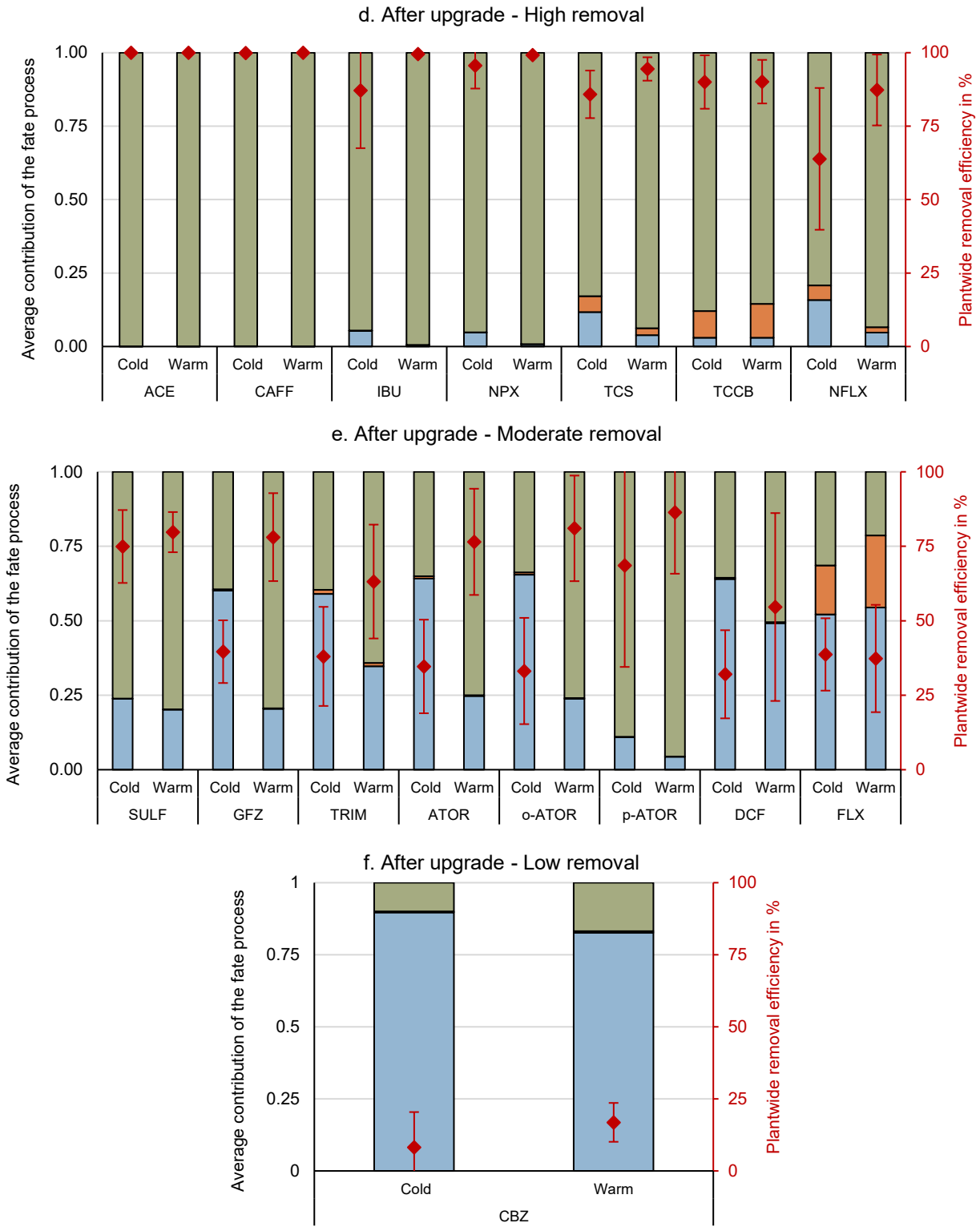

Figure 5.3 (Continued) - Plantwide OMP removal efficiency before (a-c) and after (d-f) MABR upgrade during cold and warm operational conditions. Compounds are categorized into high, moderate, and low removal based on the magnitude of the overall removal efficiency.

5.3.3 Plantwide OMP removal after MABR upgrade

The plantwide removal efficiencies from before and after the upgrade were compared to assess the impact of MABR addition during warm conditions. Warm condition was selected because the post-upgrade plant operational conditions were maintained steady and the MABR showed optimal performance during this time period as seen in Chapter 2. The post-upgrade removal efficiencies are shown in Figure 5.3 (d-f) for the previously defined groups based on the magnitude of removal efficiencies. The OMPs may be listed in a corresponding different group if the removal efficiency changed after the upgrade. The observed trends within each removal group are discussed subsequently.

Group 1 – High removal (> 75%): The compounds that had high removal efficiencies (> 75%) associated with group 1 remained the same as before the upgrade (Figure 5.3d). However, three compounds namely, caffeine, naproxen, and triclosan reported a small but statistically significant higher removal (<10% increment) post upgrade. One exception to this trend was norfluoxetine that reported a statistically significant reduction in average removal from 96% to 86% after the upgrade. Overall, while there were some small differences between some compounds, the addition of the MABR maintained the high removal performance of group 1 compounds as the CAS-alone configuration.

The relative roles of biotransformation and sorption of group 1 compounds were compared before and after the upgrade to assess if there were any changes in the contribution of the two fate mechanisms. Biotransformation dominated the overall removal for all the six compounds identified in the group similar to the pre upgrade trends (Figure 5.3d). However, for triclosan and triclocarban, there were subtle changes in the relative contribution of sorption vs biotransformation after the upgrade. As discussed previously, triclosan and triclocarban exhibited the 10-25% removals through sorption before the upgrade (Figure 5.3a). However, after the upgrade less than 10% of the triclosan and triclocarban were removed through sorption. Correspondingly, the contribution of biotransformation increased after the upgrade for these compounds. Thus, inclusion of MABR decreased the overall contaminant load in both the wastewater effluent and solids wasting stream for highly sorptive and biodegradable compounds.

Examining the seasonal differences in removal after upgrade, the removal efficiency of ibuprofen, naproxen, triclosan under warm weather conditions were significantly higher ($P < 0.008$) than cold weather months (Figure 5.3d). However, the RPD between the averages less than 15% for all three compounds suggesting a very small change. Viewed collectively, the MABR upgrade did not change the overall removal of group 1 compounds drastically. However, the upgrade had an impact on removal through biotransformation of some compounds.

Group 2 – Moderate removal (25 to 75%): The number of compounds in group 2 (25-75% removal) increased from two to eight with the upgrading of the plant. Compounds that previously reported poor removal (< 25%) such as trimethoprim, atorvastatin, o-hydroxy atorvastatin, p-hydroxy atorvastatin, and diclofenac showed increased average removals of 63%, 77%, 81%, 87%, and 55%, respectively, after upgrading and during warm weather conditions (Figure 5.3e). Except for sulfamethoxazole and fluoxetine, the increase in average removal was statistically significant for all the other compounds. Thus, inclusion of the MABR process improved the overall removal efficiency of a number of OMPs that were poorly removed by the CAS configuration.

Examining the biotransformation contribution towards the overall removal, p-hydroxy atorvastatin reported the highest fraction of biotransformation among the group 2 compounds with over 90% of the removal during warm months post upgrade (Figure 5.3e). This was followed by the contribution of biotransformation to the removal of sulfamethoxazole, gemfibrozil, atorvastatin, and o-hydroxy atorvastatin that was approximately 70%. Thus, the enhanced removal seen in group 2 compounds post MABR upgrade were mostly due to improvement in biotransformation.

The compounds in group 2 after the upgrade had a range of K_d values. Hence, they were assessed further to elucidate the roles of sorption and biotransformation in their overall removal. Except fluoxetine, all the compounds had very little removal through sorption (Figure 5.3e). The highly sorptive behavior of fluoxetine was consistent with the trend seen in pre-upgrade scenario. However, the average contribution of biotransformation to the removal of fluoxetine increased from almost nil to nearly 20%. Thus, improvement in biotransformation post MABR upgrade decreases the removal through adsorption for OMPs with high sorption affinity.

The warm and cold weather overall removals were compared to assess if there was a seasonality effect. In group 2, gemfibrozil, atorvastatin, and p-hydroxy atorvastatin reported a significantly ($P^* < 0.008$) higher removal during warm weather conditions with a considerable improvement with RPD values of 65%, 75%, and 23%, respectively (Figure 5.3f). However, these compounds did not exhibit significant seasonal difference before the upgrade when they were poorly removed. A higher sensitivity of select OMPs to seasonality post removal could be due to the varying MABR operational conditions in terms of organic loading, process airflow and the resulting biofilm thickness during the winter 2023 period (Phases 2 and 3 in Chapter 2). Viewed collectively, inclusion of the MABR process resulted in marked improvement of several compounds that were poorly removed by the CAS process. The enhancement of the removal was due to improvement in the extent of OMP biotransformation in the plant.

Group 3 – Poor removal (< 25%): Carbamazepine remained recalcitrant after the MABR upgrade (Figure 5.3f). The extent of biotransformation and sorption remained similar to the patterns observed before upgrade as well. Carbamazepine is a notoriously recalcitrant compound and is regarded as an anthropogenic tracer because of its persistence (Clara et al., 2004). The poor biodegradability of carbamazepine could be due to its highly stable, three ring fused structure that is difficult to access biologically. Full-scale studies in CAS and MBR systems have shown that removal of carbamazepine was independent of SRT, even at retention times as long as 100 days (Clara et al., 2005; Joss et al., 2005; Zhang et al., 2008). Other studies have shown that carbamazepine was recalcitrant in biotransformation experiments using anoxic and anerobic activated sludge (Inyang et al., 2016; Lakshminarasimman et al., 2018). Overall, the recalcitrance of carbamazepine observed in the current study with the MABR upgrade was consistent with that reported elsewhere for advanced process configurations.

The trends in improved OMP removal after MABR upgrade were compared with other advanced treatment configurations to explore if the responses observed in this study are typical of other configurations with similar design features. For OMPs such as diclofenac and gemfibrozil, the average overall removal increased by 2.5 times (31 to 78%) and 4.5 times (13% to 54%), respectively, after the MABR upgrade (Figure 5.3 c and e). Similar increases have also been observed in MBBR biofilms with higher biotransformation rates for diclofenac and gemfibrozil when compared to suspended sludge biomass (Falås et al., 2012). MBRs operating at longer SRTs have shown a higher removal of diclofenac and gemfibrozil, from 50% to 87% and 39% to 90%, respectively between MBR and CAS systems (Radjenovic et al., 2007). Diclofenac has also been shown to transform to a greater degree in biofilm reactors with anoxic redox conditions when compared with aerobic removal (Zwiener & Frimmel, 2003). Thus, from the overall literature evidence, the enhanced removal of some OMPs post MABR addition could be due to the differing redox conditions and increased biomass residence time in the biofilm.

5.3.4 Biotransformation in MABR and aeration tanks

The previously discussed removal efficiencies were based on a plantwide boundary and the observed removals after upgrade included biotransformation in both the MABR and the aeration tank. Hence, mass balance analyses were performed to quantify the removal through biotransformation in MABR and aeration tanks individually (Equations 5.6-5.12). An initial analysis of the mass balance results revealed that the OMPs exhibited a variety of removal patterns in the MABR. Hence select compounds were chosen (Figure 5.4) to represent the different removal groups and capture the varied removal behavior observed in MABR and discussed subsequently. The results for the remaining compounds are shown in supplemental information (Figure S5.1).

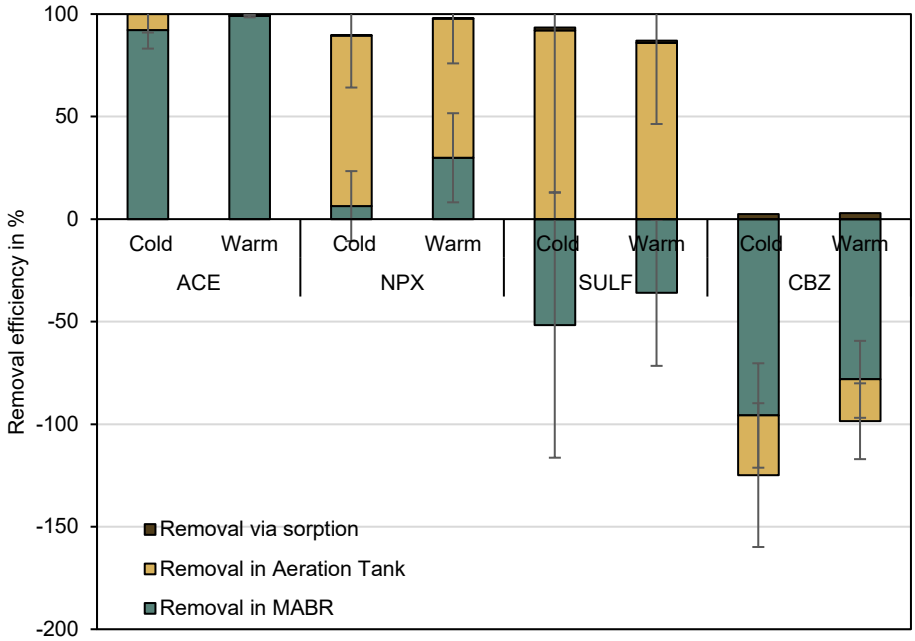

Figure 5.4 – Percentage removal through biotransformation in MABR and aeration tank to overall removal of selected OMPs post upgrade.

It was hypothesized that readily degraded group 1 compounds such as acetaminophen and naproxen would biodegrade in the hybrid MABR because of its upstream location that receives the wastewater before aeration tank. Biotransformation in the MABR tank removed almost all of the acetaminophen under warm temperatures (Figure 5.4). With cold temperatures, the combined contribution of the MABR biofilm and the suspended sludge to the overall removal remained high (average = 93%) while the aeration tank contribution increased relative to its contribution under warm conditions. On the contrary, the aeration tank contributed a greater fraction of the removal of naproxen when compared to the hybrid MABR and, as with acetaminophen, its contribution was greater under warm conditions. The MABR tank contributed only 30% of the overall removal in the warm conditions and 7% in the cold conditions (Figure 5.4). Overall, biotransformation in the MABR tank contributed either wholly or partially towards the removal of readily biodegradable compounds but its contribution was highly compound-specific.

The fate of sulfamethoxazole was examined to assess the contribution of the hybrid MABR to removal of a moderately degradable compound (group 2). The mass balance analysis indicated that sulfamethoxazole demonstrated opposing responses in the MABR and aeration tanks. In the hybrid MABR apparent negative removals were observed indicating that the detectable concentrations were increased while the aeration tank resulted in its removal (Figure 5.4). The apparent formation of sulfamethoxazole may have resulted from the deconjugation of unmeasured sulfamethoxazole human metabolites that were present in

the raw wastewater. Conjugated products of sulfamethoxazole such as N-acetyl sulfamethoxazole and sulfamethoxazole glucuronide have been reported to occur at comparable or even higher concentrations than the parent compound in wastewater influent (Brown & Wong, 2018; Göbel et al., 2005). In the biological treatment process, the conjugated groups are cleaved releasing the parent compound leading to an apparent negative removal (Achermann et al., 2018; Brown et al., 2020). The upstream location of the MABR with its anoxic bulk phase environment appeared to result in a condition where formation from deconjugation exceeded biodegradation of sulfamethoxazole that has been reported to degrade in aerobic, anoxic, and anaerobic environments (Alvarino et al., 2016; Hai et al., 2011). Thus, the hybrid MABR process resulted in a net formation of sulfamethoxazole although the subsequent aeration tank was able to remove a large fraction of the sulfamethoxazole leaving the MABR.

Examining the seasonality of sulfamethoxazole transformations in the individual tanks, the average percentage apparent formation in MABR was relatively higher during cold weather (-51%) when compared to warm weather (-37%) conditions (Figure 5.4a). Lower apparent formation during warm conditions could be because of potential increase in competition from sulfamethoxazole degradation reactions occurring simultaneously in the process. Enhanced removal of sulfamethoxazole could also be seen when comparing the percentage removal in aeration tank. Converse to MABR, the average percentage removal of sulfamethoxazole was slightly higher in the warm weather conditions (92%) compared to cold weather (86%). Overall, even though sulfamethoxazole shows an apparent overall negative removal in hybrid MABR, seasonal variations in the extent of apparent formation suggests that there could be competing transformation reactions occurring in the process.

The behavior of carbamazepine was examined as a compound that was representative of the poorly degradable (group 3) category. Carbamazepine had apparent negative removals in both tanks (Figure 5.4). The MABR tank, that was located ahead of the aeration tank, reported greater concentrations of dissolved carbamazepine. Carbamazepine is known to transform in the human body to form a range of excreted metabolites including hydroxylated products, N-glucuronide conjugates, and oxidation products such as carbamazepine epoxides which have been detected in wastewaters (Kaiser et al., 2014; Miao et al., 2005; Puranik et al., 2013). The human metabolites such as the glucuronide conjugates could be deconjugated through enzymatic reactions and transform into the parent compound during wastewater treatment resulting in apparent negative removals of carbamazepine (Vieno et al., 2007; Zhang et al., 2008). Thus, the apparent negative removals for carbamazepine seen in the hybrid MABR were likely due to extensive release of the target compound from the unmeasured conjugated human metabolites.

The cold conditions had a greater extent of carbamazepine apparent formation with an overall average of 124% when compared to 98% in warm weather conditions (Figure 5.4). The difference in magnitude of

apparent formation indicates that there was a seasonal dependence in the degradation of parent compound removal as seen previously for sulfamethoxazole. The lower magnitude of apparent formation could be because of a relatively higher degree of carbamazepine removal occurring in parallel during warm weather conditions. Although carbamazepine is widely known to be resistant to biotransformation, some studies have shown 20-60% removal in MBRs operating at very long SRTs (88 days) and alternating oxic-anoxic redox conditions (Hai et al., 2011; Wijekoon et al., 2013). Overall, the seasonal comparison revealed that carbamazepine could undergo some level of biodegradation in both MABR and aeration tank. However, the decrease in mass was overshadowed by extensive release from precursors.

Viewed collectively, the mass balance analyses on the individual treatment tanks showed that the MABR could significantly impact on OMPs but its contribution to overall removals was highly compound specific. Of particular interest was that, as the first process in the biological treatment sequence, its contribution to either positive or apparent negative removals was frequently greater than that of the downstream aeration tanks. Further, in cases where removal in the MABR performance was reduced (low temperatures or apparent formation from precursors) the aeration tank was often able to polish the MABR effluent.

While the mass balance provided some insights into the contaminant biotransformation in the individual tanks, the approach also has some limitations. Since this study only measured the aqueous phase OMP concentration, the total concentration was estimated using K_d values adapted from literature. The uncertainty with using the same K_d value for both influent and mixed liquor solids, and the values themselves could be potential sources of error that could influence the contaminant mass loads in the mixed liquor streams in and out of the bioreactors. A potential solution for this problem is to measure the total OMP concentration in the mixed liquor samples for removal calculations in the individual tanks.

5.4 Conclusion

The hybrid MABR process has design features such as alternative redox conditions and longer biomass retention time through establishment of a biofilm, which could be beneficial for the treatment of OMPs such as pharmaceuticals and personal care product ingredients in municipal wastewater. This study monitored the removal of a wide range of commonly occurring OMPs in a full-scale WRRF in its CAS and hybrid MABR/CAS configuration over three years during warm and cold weather conditions. The results of the study showed that:

- Of the 16 target compounds, 12 OMPs showed a decreased concentration after the MABR upgrade demonstrating its presence can improve effluent quality.
- A comparison of removal efficiency before and after the upgrade under warm weather conditions, showed that highly removable compounds such as acetaminophen, ibuprofen, and naproxen, and recalcitrant compounds such as carbamazepine were not impacted by MABR addition.
- Six OMPs were moved from the poorly removed group to the moderately removed group with the upgrade.
- The enhanced removal after MABR upgrade was influenced by seasonality, with compounds such as atorvastatin, p-hydroxy atorvastatin, and gemfibrozil showing a significantly higher removal during warm weather conditions.
- The role of the hybrid MABR process in overall removal was highly variable and compound specific with a wide range of responses such as complete biotransformation, partial biotransformation to apparent formation of target compounds from unmeasured precursors.
- Overall, the full-scale monitoring results show that upgrading CAS facilities with a hybrid MABR could result in enhanced treatment and removal of organic micropollutants.

5.5 Supplemental information

Table S5.1 – Method detection limit and matrix spike recovery for the target compounds

OMP	MDL of target OMPs in ng/L	Recovery of matrix spike in % (Average ± standard deviation)
NPX	1.22	100 ± 12
DCF	9.02	99 ± 7
IBU	2.4	99 ± 12
GFZ	0.43	100 ± 5
TCCB	0.44	100 ± 5
TCS	1.75	100 ± 7
ACE	NA	104 ± 42
SULF	8.3	104 ± 27
CAFF	5.07	106 ± 67
TRIM	4.05	103 ± 31
CBZ	4.38	104 ± 28
p-ATOR	7.63	102 ± 22
NFLX	0.67	97 ± 37
FLX	1.08	98 ± 20
o-ATOR	4.96	101 ± 24
ATOR	3.08	101 ± 26

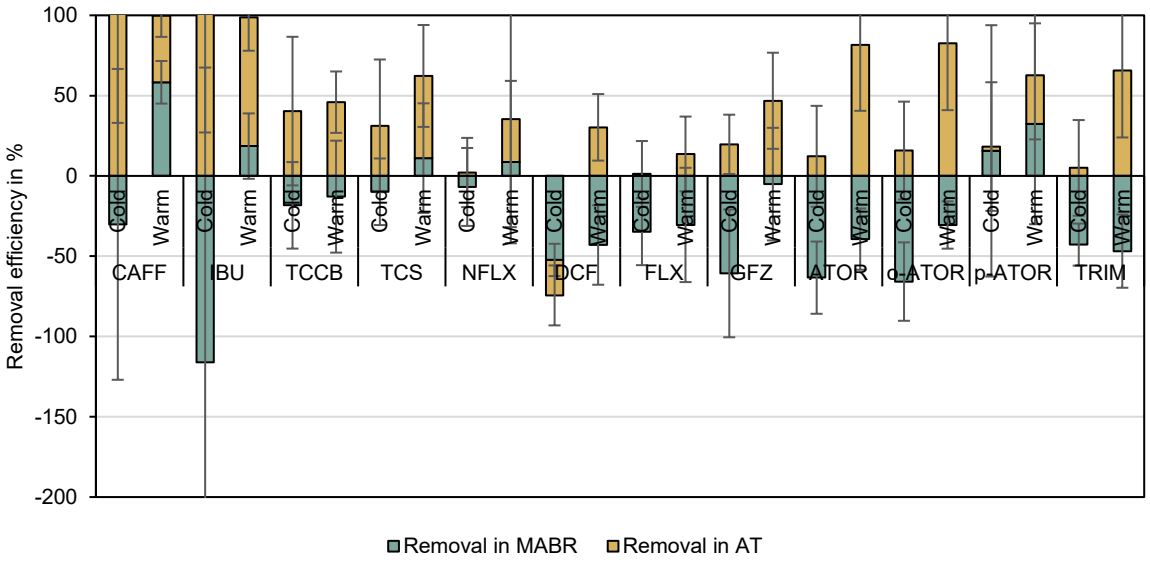

Figure S5.1 - Removal through biotransformation in MABR and aeration tank

5.6 References

Achermann, S., Bianco, V., Mansfeldt, C. B., Vogler, B., Kolvenbach, B. A., Corvini, P. F. X., & Fenner, K. (2018). Biotransformation of Sulfonamide Antibiotics in Activated Sludge: The Formation of Pterin-Conjugates Leads to Sustained Risk. *Environmental Science & Technology*, *52*(11), 6265–6274. https://doi.org/10.1021/acs.est.7b06716

Alvarino, T., Lema, J., Omil, F., & Suárez, S. (2018). Trends in organic micropollutants removal in secondary treatment of sewage. *Reviews in Environmental Science and Bio/Technology*, *17*(3), 447–469. https://doi.org/10.1007/s11157-018-9472-3

Alvarino, T., Nastold, P., Suarez, S., Omil, F., Corvini, P. F. X., & Bouju, H. (2016). Role of biotransformation, sorption and mineralization of 14C-labelled sulfamethoxazole under different redox conditions. *Science of The Total Environment*, *542*, 706–715. https://doi.org/10.1016/j.scitotenv.2015.10.140

Arlos, M. J., Bragg, L. M., Parker, W. J., & Servos, M. R. (2015). Distribution of selected antiandrogens and pharmaceuticals in a highly impacted watershed. *Water Research*, *72*, 40–50. https://doi.org/10.1016/j.watres.2014.11.008

Armstrong, R. A. (2014). When to use the Bonferroni correction. *Ophthalmic & Physiological Optics: The Journal of the British College of Ophthalmic Opticians (Optometrists)*, *34*(5), 502–508. https://doi.org/10.1111/opo.12131

Boxall, A. B. A., Rudd, M. A., Brooks, B. W., Caldwell, D. J., Choi, K., Hickmann, S., Innes, E., Ostapyk, K., Staveley, J. P., Verslycke, T., Ankley, G. T., Beazley, K. F., Belanger, S. E., Berninger, J. P., Carriquiriborde, P., Coors, A., DeLeo, P. C., Dyer, S. D., Ericson, J. F., … Van Der Kraak, G. (2012). Pharmaceuticals and Personal Care Products in the Environment: What Are the Big Questions? *Environmental Health Perspectives*, *120*(9), 1221–1229. https://doi.org/10.1289/ehp.1104477

Brown, A. K., Ackerman, J., Cicek, N., & Wong, C. S. (2020). *In situ* kinetics of human pharmaceutical conjugates and the impact of transformation, deconjugation, and sorption on persistence in wastewater batch bioreactors. *Environmental Pollution*, *265*, 114852. https://doi.org/10.1016/j.envpol.2020.114852

Brown, A. K., & Wong, C. S. (2018). Distribution and fate of pharmaceuticals and their metabolite conjugates in a municipal wastewater treatment plant. *Water Research*, *144*, 774–783. https://doi.org/10.1016/j.watres.2018.08.034

Çelik, A., Casey, E., & Hasar, H. (2018). Degradation of oxytetracycline under autotrophic nitrifying conditions in a membrane aerated biofilm reactor and community fingerprinting. *Journal of Hazardous Materials*, *356*, 26–33. https://doi.org/10.1016/j.jhazmat.2018.05.040

Cizmas, L., Sharma, V. K., Gray, C. M., & McDonald, T. J. (2015). Pharmaceuticals and personal care products in waters: Occurrence, toxicity, and risk. *Environmental Chemistry Letters*, *13*(4), 381–394. https://doi.org/10.1007/s10311-015-0524-4

Clara, M., Strenn, B., Gans, O., Martinez, E., Kreuzinger, N., & Kroiss, H. (2005). Removal of selected pharmaceuticals, fragrances and endocrine disrupting compounds in a membrane bioreactor and conventional wastewater treatment plants. *Water Research*, *39*(19), 4797–4807. https://doi.org/10.1016/j.watres.2005.09.015

Clara, M., Strenn, B., & Kreuzinger, N. (2004). Carbamazepine as a possible anthropogenic marker in the aquatic environment: Investigations on the behaviour of Carbamazepine in wastewater treatment and during groundwater infiltration. *Water Research*, *38*(4), 947–954. https://doi.org/10.1016/j.watres.2003.10.058

Ebele, A. J., Abou-Elwafa Abdallah, M., & Harrad, S. (2017). Pharmaceuticals and personal care products (PPCPs) in the freshwater aquatic environment. *Emerging Contaminants*, *3*(1), 1–16. https://doi.org/10.1016/j.emcon.2016.12.004

Elad, T., Hally, M. P., Domingo-Félez, C., Knoop, O., Drewes, J. E., Valverde-Pérez, B., & Smets, B. F. (2023). Exploring the effects of intermittent aeration on the performance of nitrifying membrane-aerated biofilm reactors. *Science of The Total Environment*, *891*, 164329. https://doi.org/10.1016/j.scitotenv.2023.164329

Falås, P., Andersen, H. R., Ledin, A., & Jansen, J. la C. (2012). Impact of solid retention time and nitrification capacity on the ability of activated sludge to remove pharmaceuticals. *Environmental Technology*, *33*(8), 865–872. https://doi.org/10.1080/09593330.2011.601764

Falås, P., Baillon-Dhumez, A., Andersen, H. R., Ledin, A., & la Cour Jansen, J. (2012). Suspended biofilm carrier and activated sludge removal of acidic pharmaceuticals. *Water Research*, *46*(4), 1167–1175. https://doi.org/10.1016/j.watres.2011.12.003

Falås, P., Longrée, P., la Cour Jansen, J., Siegrist, H., Hollender, J., & Joss, A. (2013). Micropollutant removal by attached and suspended growth in a hybrid biofilm-activated sludge process. *Water Research*, *47*(13), 4498–4506. https://doi.org/10.1016/j.watres.2013.05.010

Fernandez-Fontaina, E., Gomes, I. B., Aga, D. S., Omil, F., Lema, J. M., & Carballa, M. (2016). Biotransformation of pharmaceuticals under nitrification, nitratation and heterotrophic conditions. *Science of The Total Environment*, *541*, 1439–1447. https://doi.org/10.1016/j.scitotenv.2015.10.010

Göbel, A., Thomsen, A., McArdell, C. S., Joss, A., & Giger, W. (2005). Occurrence and Sorption Behavior of Sulfonamides, Macrolides, and Trimethoprim in Activated Sludge Treatment. *Environmental Science & Technology*, *39*(11), 3981–3989. https://doi.org/10.1021/es048550a

Hai, F. I., Li, X., Price, W. E., & Nghiem, L. D. (2011). Removal of carbamazepine and sulfamethoxazole by MBR under anoxic and aerobic conditions. *Bioresource Technology*, *102*(22), 10386–10390. https://doi.org/10.1016/j.biortech.2011.09.019

Hicks, K. A., Fuzzen, M. L. M., McCann, E. K., Arlos, M. J., Bragg, L. M., Kleywegt, S., Tetreault, G. R., McMaster, M. E., & Servos, M. R. (2017). Reduction of Intersex in a Wild Fish Population in Response to Major Municipal Wastewater Treatment Plant Upgrades. *Environmental Science & Technology*, *51*(3), 1811–1819. https://doi.org/10.1021/acs.est.6b05370

Inyang, M., Flowers, R., McAvoy, D., & Dickenson, E. (2016). Biotransformation of trace organic compounds by activated sludge from a biological nutrient removal treatment system. *Bioresource Technology*, *216*, 778–784. https://doi.org/10.1016/j.biortech.2016.05.124

Joss, A., Keller, E., Alder, A. C., Göbel, A., McArdell, C. S., Ternes, T., & Siegrist, H. (2005). Removal of pharmaceuticals and fragrances in biological wastewater treatment. *Water Research*, *39*(14), 3139–3152. https://doi.org/10.1016/j.watres.2005.05.031

Kaiser, E., Prasse, C., Wagner, M., Bröder, K., & Ternes, T. A. (2014). Transformation of Oxcarbazepine and Human Metabolites of Carbamazepine and Oxcarbazepine in Wastewater Treatment and Sand Filters. *Environmental Science & Technology*, *48*(17), 10208–10216. https://doi.org/10.1021/es5024493

Kennes-Veiga, D. M., Vogler, B., Fenner, K., Carballa, M., & Lema, J. M. (2021). Heterotrophic enzymatic biotransformations of organic micropollutants in activated sludge. *Science of The Total Environment*, 146564. https://doi.org/10.1016/j.scitotenv.2021.146564

Khunjar, W. O., Mackintosh, S. A., Skotnicka-Pitak, J., Baik, S., Aga, D. S., & Love, N. G. (2011). Elucidating the Relative Roles of Ammonia Oxidizing and Heterotrophic Bacteria during the Biotransformation of 17α-Ethinylestradiol and Trimethoprim. *Environmental Science & Technology*, *45*(8), 3605–3612. https://doi.org/10.1021/es1037035

Lakshminarasimman, N., Quiñones, O., Vanderford, B. J., Campo-Moreno, P., Dickenson, E. V., & McAvoy, D. C. (2018). Biotransformation and sorption of trace organic compounds in biological nutrient removal treatment systems. *Science of The Total Environment*, *640–641*, 62–72. https://doi.org/10.1016/j.scitotenv.2018.05.145

Li, T., Liu, J., Bai, R., & Wong, F. S. (2008). Membrane-Aerated Biofilm Reactor for the Treatment of Acetonitrile Wastewater. *Environmental Science & Technology*, *42*(6), 2099–2104. https://doi.org/10.1021/es702150f

Maeng, S. K., Choi, B. G., Lee, K. T., & Song, K. G. (2013). Influences of solid retention time, nitrification and microbial activity on the attenuation of pharmaceuticals and estrogens in membrane bioreactors. *Water Research*, *47*(9), 3151–3162. https://doi.org/10.1016/j.watres.2013.03.014

Mazioti, A. A., Stasinakis, A. S., Pantazi, Y., & Andersen, H. R. (2015). Biodegradation of benzotriazoles and hydroxy-benzothiazole in wastewater by activated sludge and moving bed biofilm reactor systems. *Bioresource Technology*, *192*, 627–635. https://doi.org/10.1016/j.biortech.2015.06.035

Mehdi, H., Dickson, F. H., Bragg, L. M., Servos, M. R., & Craig, P. M. (2018). Impacts of wastewater treatment plant effluent on energetics and stress response of rainbow darter (Etheostoma caeruleum) in the Grand River watershed. *Comparative Biochemistry and Physiology Part B: Biochemistry and Molecular Biology*, *224*, 270–279. https://doi.org/10.1016/j.cbpb.2017.11.011

Mei, X., Wang, Y., Yang, Y., Xu, L., Wang, Y., Guo, Z., Shen, W., Zhang, Z., Ma, M., Ding, Y., Xiao, Y., Yang, X., Yin, C., Guo, W., Xu, K., & Wang, C. (2020). Enhanced treatment of nitroaniline-containing wastewater by a membrane-aerated biofilm reactor: Simultaneous nitroaniline degradation and nitrogen removal. *Separation and Purification Technology*, 117078. https://doi.org/10.1016/j.seppur.2020.117078

Miao, X.-S., Yang, J.-J., & Metcalfe, C. D. (2005). Carbamazepine and Its Metabolites in Wastewater and in Biosolids in a Municipal Wastewater Treatment Plant. *Environmental Science & Technology*, *39*(19), 7469–7475. https://doi.org/10.1021/es050261e

Murray, K. J., Parker, W. J., Bragg, L. M., & Servos, M. R. (2017). Fate of selected pharmaceutically active compounds in the integrated fixed film activated sludge process. *Water Science and Technology*, *75*(11), 2680–2691. https://doi.org/10.2166/wst.2017.100

Nikel, K. E., Tetreault, G. R., Marjan, P., Hicks, K. A., Fuzzen, M. L. M., Srikanthan, N., McCann, E. K., Dhiyebi, H., Bragg, L. M., Law, P., Celmer-Repin, D., Kleywegt, S., Cunningham, J., Clark, T., McMaster, M. E., & Servos, M. R. (2023). Wild fish responses to wastewater treatment plant upgrades in

the Grand River, Ontario. *Aquatic Toxicology*, *255*, 106375. https://doi.org/10.1016/j.aquatox.2022.106375

Ogunlaja, O. O., & Parker, W. J. (2015). Assessment of the removal of estrogenicity in biological nutrient removal wastewater treatment processes. *Science of The Total Environment*, *514*, 202–210. https://doi.org/10.1016/j.scitotenv.2015.01.100

Oulton, R. L., Kohn, T., & Cwiertny, D. M. (2010). Pharmaceuticals and personal care products in effluent matrices: A survey of transformation and removal during wastewater treatment and implications for wastewater management. *Journal of Environmental Monitoring*, *12*(11), 1956–1978. https://doi.org/10.1039/C0EM00068J

Parker, W. J., Pileggi, V., Seto, P., Chen, X., Ogunlaja, M., Van Der Kraak, G., & Parrott, J. (2014). Impact of activated sludge configuration and operating conditions on in vitro and in vivo responses and trace organic compound removal. *Science of The Total Environment*, *490*, 360–369. https://doi.org/10.1016/j.scitotenv.2014.05.023

Patel, M., Kumar, R., Kishor, K., Mlsna, T., Pittman, C. U., & Mohan, D. (2019). Pharmaceuticals of Emerging Concern in Aquatic Systems: Chemistry, Occurrence, Effects, and Removal Methods. *Chemical Reviews*, *119*(6), 3510–3673. https://doi.org/10.1021/acs.chemrev.8b00299

Petrie, B., Barden, R., & Kasprzyk-Hordern, B. (2015). A review on emerging contaminants in wastewaters and the environment: Current knowledge, understudied areas and recommendations for future monitoring. *Water Research*, *72*, 3–27. https://doi.org/10.1016/j.watres.2014.08.053

Pomiès, M., Choubert, J.-M., Wisniewski, C., & Coquery, M. (2013). Modelling of micropollutant removal in biological wastewater treatments: A review. *Science of The Total Environment*, *443*, 733–748. https://doi.org/10.1016/j.scitotenv.2012.11.037

Puranik, Y. G., Birnbaum, A. K., Marino, S. E., Ahmed, G., Cloyd, J. C., Remmel, R. P., Leppik, I. E., & Lamba, J. K. (2013). Association of carbamazepine major metabolism and transport pathway gene polymorphisms and pharmacokinetics in patients with epilepsy. *Pharmacogenomics*, *14*(1), 35–45. https://doi.org/10.2217/pgs.12.180

Radjenovic, J., Petrovic, M., & Barceló, D. (2007). Analysis of pharmaceuticals in wastewater and removal using a membrane bioreactor. *Analytical and Bioanalytical Chemistry*, *387*(4), 1365–1377. https://doi.org/10.1007/s00216-006-0883-6

Radjenović, J., Petrović, M., & Barceló, D. (2009). Fate and distribution of pharmaceuticals in wastewater and sewage sludge of the conventional activated sludge (CAS) and advanced membrane bioreactor (MBR) treatment. *Water Research*, *43*(3), 831–841. https://doi.org/10.1016/j.watres.2008.11.043

Sanchez-Huerta, C., Fortunato, L., Leiknes, T., & Hong, P.-Y. (2022). Influence of biofilm thickness on the removal of thirteen different organic micropollutants via a Membrane Aerated Biofilm Reactor (MABR). *Journal of Hazardous Materials*, *432*, 128698. https://doi.org/10.1016/j.jhazmat.2022.128698

Sanchez-Huerta, C., Medina, J. S., Wang, C., Fortunato, L., & Hong, P.-Y. (2023). Understanding the role of sorption and biodegradation in the removal of organic micropollutants by membrane aerated biofilm reactor (MABR) with different biofilm thickness. *Water Research*, 119935. https://doi.org/10.1016/j.watres.2023.119935

Schwarzenbach, R. P., Escher, B. I., Fenner, K., Hofstetter, T. B., Johnson, C. A., von Gunten, U., & Wehrli, B. (2006). The Challenge of Micropollutants in Aquatic Systems. *Science*, *313*(5790), 1072–1077. https://doi.org/10.1126/science.1127291

Shao, Y., Chen, Z., Hollert, H., Zhou, S., Deutschmann, B., & Seiler, T.-B. (2019). Toxicity of 10 organic micropollutants and their mixture: Implications for aquatic risk assessment. *Science of The Total Environment*, *666*, 1273–1282. https://doi.org/10.1016/j.scitotenv.2019.02.047

Stamm, C., Räsänen, K., Burdon, F. J., Altermatt, F., Jokela, J., Joss, A., Ackermann, M., & Eggen, R. I. L. (2016). Chapter Four - Unravelling the Impacts of Micropollutants in Aquatic Ecosystems: Interdisciplinary Studies at the Interface of Large-Scale Ecology. In A. J. Dumbrell, R. L. Kordas, & G. Woodward (Eds.), *Advances in Ecological Research* (Vol. 55, pp. 183–223). Academic Press. https://doi.org/10.1016/bs.aecr.2016.07.002

Suarez, S., Lema, J. M., & Omil, F. (2010). Removal of Pharmaceutical and Personal Care Products (PPCPs) under nitrifying and denitrifying conditions. *Water Research*, *44*(10), 3214–3224. https://doi.org/10.1016/j.watres.2010.02.040

Taşkan, B., Casey, E., & Hasar, H. (2019). Simultaneous oxidation of ammonium and tetracycline in a membrane aerated biofilm reactor. *Science of The Total Environment*, *682*, 553–560. https://doi.org/10.1016/j.scitotenv.2019.05.111

Ternes, T. A. (1998). Occurrence of drugs in German sewage treatment plants and rivers1. *Water Research*, *32*(11), 3245–3260. https://doi.org/10.1016/S0043-1354(98)00099-2

Tran, N. H., Urase, T., & Kusakabe, O. (2009). The characteristics of enriched nitrifier culture in the degradation of selected pharmaceutically active compounds. *Journal of Hazardous Materials*, *171*(1), 1051–1057. https://doi.org/10.1016/j.jhazmat.2009.06.114

Verlicchi, P., Al Aukidy, M., & Zambello, E. (2012). Occurrence of pharmaceutical compounds in urban wastewater: Removal, mass load and environmental risk after a secondary treatment—A review. *Science of The Total Environment*, *429*, 123–155. https://doi.org/10.1016/j.scitotenv.2012.04.028

Vieno, N. M., Tuhkanen, T., & Kronberg, L. (2005). Seasonal Variation in the Occurrence of Pharmaceuticals in Effluents from a Sewage Treatment Plant and in the Recipient Water. *Environmental Science & Technology*, *39*(21), 8220–8226. https://doi.org/10.1021/es051124k

Vieno, N., Tuhkanen, T., & Kronberg, L. (2007). Elimination of pharmaceuticals in sewage treatment plants in Finland. *Water Research*, *41*(5), 1001–1012. https://doi.org/10.1016/j.watres.2006.12.017

Wijekoon, K. C., Hai, F. I., Kang, J., Price, W. E., Guo, W., Ngo, H. H., & Nghiem, L. D. (2013). The fate of pharmaceuticals, steroid hormones, phytoestrogens, UV-filters and pesticides during MBR treatment. *Bioresource Technology*, *144*, 247–254. https://doi.org/10.1016/j.biortech.2013.06.097

Zhang, Y., Geißen, S.-U., & Gal, C. (2008). Carbamazepine and diclofenac: Removal in wastewater treatment plants and occurrence in water bodies. *Chemosphere*, *73*(8), 1151–1161. https://doi.org/10.1016/j.chemosphere.2008.07.086

Zwiener, C., & Frimmel, F. H. (2003). Short-term tests with a pilot sewage plant and biofilm reactors for the biological degradation of the pharmaceutical compounds clofibric acid, ibuprofen, and diclofenac. *Science of The Total Environment*, *309*(1), 201–211. https://doi.org/10.1016/S0048-9697(03)00002-0

Chapter 6 – Conclusions

6.1 Summary of conclusions

The main conclusions drawn in each of the research chapters in this dissertation are summarized below.

Chapter 2 – Long term performance evaluation of a full-scale hybrid membrane aerated biofilm reactor (MABR) facility

- The MABR process enabled year-round nitrification in the plant with low effluent NH_4-N concentrations below 1 mg-N/L and 5 mg-N/L in summer and winter conditions, respectively. The MABR upgrade doubled the TN removal in the plant with high denitrification efficiencies (80-92%).
- The MABR nitrification rate can be limited by the thickness control provided by the airflow. The MABR nitrification rate had a low sensitivity to operational temperature with a 22% decrease in nitrification rate for an average temperature differential of 6 ℃ between warm and cold weather operations.
- The denitrification efficiency in the MABR tank was insensitive to wastewater temperature, loading, and MABR airflow. The DNR and associated oxygen credit through anoxic carbon removal were limited by the nitrification rate in the MABR.
- The volumetric electricity consumption for plantwide aeration decreased by 50% after the MABR upgrade because of substantial loading reduction achieved in that MABR that had higher aeration efficiency and reduced aeration requirements for the conventional diffused aeration that had a relatively lower aeration efficiency.

Chapter 3 – Characterizing the biofilm thickness, microbial community, and functionality in a full-scale hybrid MABR

- The arrangement of MABR cassettes in a single row within a plug flow tank resulted in a longitudinal thickness gradient with biofilms in the front cassette atleast twice as thick as the ones in the rear end.
- Biofilm thickness was variable depending on the MABR process airflow that provided thickness control. The rear cassettes at lower airflow setting at Phase 3 (4.5 NL m^{-2} hr^{-1}) had a higher average thickness of 819 ± 69 μm when compared to Phases 1 and 4 where the average range was 285-667 μm under a higher airflow (6 NL m^{-2} hr^{-1}).
- Examination of the Bray-Curtis dissimilarity index revealed the variability in community composition followed similar trends as biofilm thickness. The microbial community profile along

the full-length membrane were more similar to each other. However, the community composition varied along the length of the full-scale MABR tank. Changing operating conditions with respect to MABR airflow and temperature also resulted in different community compositions between phases.

- Thicker biofilms had a higher relative abundance of microbes with anaerobic functionalities such as fermentation and sulfur reduction. Biofilm samples collected from all the locations and operating conditions showed presence of microbes with nitrite denitrification function suggesting a widespread prevalence of short cut N removal in the biofilms.
- Biofilm thickness and MABR nitrification rate were strongly correlated with the microbial community composition of the samples.

Chapter 4 – An improved model to investigate the dynamics of nitrous oxide emissions from a full-scale hybrid MABR facility

- The AOO activity in the innermost layer of the biofilm was a significant source of N_2O which then diffused to both the lumen gas and the outer biofilm layers.
- The middle and outer layers of the biofilm and the bulk mixed liquor where denitrification was active resulted in a net consumption of N_2O through the heterotrophic denitrification pathway.
- The decreasing longitudinal substrate concentrations along the MABR tank decreased the N_2O bioconversions in both the biofilm and suspended sludge.
- Comparing N_2O in the gas streams entering and leaving the MABR bulk showed that there was substantial N_2O scrubbing (55-70%) into the MABR mixed liquor.
- The model predicted a low N_2O emission factor of $0.18 \pm 0.01\%$ while achieving up to 60% removal of the influent N loading demonstrating that hybrid MABRs are a low emission alternative for intensification of wastewater treatment processes.

Chapter 5 – Do full-scale hybrid MABRs enhance the removal of organic micropollutants?

- Of the 16 target compounds, 12 OMPs showed a decreased concentration after the MABR upgrade demonstrating its presence can improve effluent quality.
- A comparison of removal efficiency before and after the upgrade under warm weather conditions, showed that highly removable compounds such as acetaminophen, ibuprofen, and naproxen, and recalcitrant compounds such as carbamazepine were not impacted by MABR addition.
- Six OMPs were moved from the poorly removed group to the moderately removed group with the upgrade.

- The enhanced removal after MABR upgrade was influenced by seasonality, with compounds such as atorvastatin, p-hydroxy atorvastatin, and gemfibrozil showing a significantly higher removal during warm weather conditions.
- The role of the hybrid MABR process in overall removal was highly variable and compound specific with a wide range of responses such as complete biotransformation, partial biotransformation to apparent formation of target compounds from unmeasured precursors.

6.2 Impact of the research

This study successfully achieved all six of its research objectives. The main contributions and their impacts for each of the objectives are listed below.

O1. Compare key performance indicators related to carbon and nitrogen removal and electricity consumption at a full-scale WRRF before and after an MABR upgrade.

The relative benefits of upgrading a CAS process with a hybrid MABR have so far been investigated using process modeling tools. This study systematically monitored the carbon and nitrogen removal, and the associated electricity consumption before and after the upgrade at full-scale and reported the improvement in performance based on measured data. The findings from this research will be a useful case study for other municipal utilities interested in intensifying their treatment processes.

O2. Evaluate the impact of MABR airflow, influent loading, and wastewater temperature on the nitrification and denitrification performance of a full-scale hybrid MABR.

The data gathered to address this research objective spanned over 20 months of monitoring a full-scale hybrid MABR treating real wastewater under various operational conditions. Analysis of this large dataset has yielded practical recommendations for optimizing the MABR process airflow to achieve desired nitrification rates under different seasonal and loading conditions. Moreover, the findings on MABR impacts on downstream aeration tanks are noteworthy as they provide practically relevant insights to operate the hybrid MABR-CAS configuration optimally and realize the full process benefits of this novel technology.

O3. Characterize spatial and operational variations in biofilm thickness in a full scale MABR to obtain insights into factors affecting process performance.

Biofilm thickness is a critical parameter in modeling MABR processes. Modeling studies so far have assumed biofilm thickness values based on observations from co-diffusional biofilm systems or from smaller-scale MABRs that are not necessarily representative of the full-scale MABR systems. The biofilm thickness measurements obtained at different locations and operating conditions are a significant contribution of this work as this type of information is not currently available in the literature. The findings on longitudinal thickness gradient hold important implications for better MABR modeling practice as it is common to assume a uniform biofilm thickness. Observed trends in thickness also highlight the need for better biofilm thickness control design in full-scale MABR cassettes to further push the nitrification capacity of the process.

O4. Characterize the microbial community in the MABR biofilm as a function of location and operating conditions and correlate the community profile with MABR performance.

The microbial community dynamics has not been characterized in full-scale MABR processes before. Investigating the full-scale MABR biofilm community profile and their functionalities in relation to their thickness is a key contribution of this research. Moreover, the microbial community data obtained in this study complemented the long-term MABR nitrification performance dataset and provided insights for optimizing biofilm thickness control in full-scale systems from a microbial ecology standpoint.

O5. Develop and validate an improved model to describe the spatial and diurnal dynamics of N_2O emissions from a full-scale hybrid MABR process.

The improved N_2O model developed in this study includes liquid-gas transfer processes that are commonly overlooked in full-scale MABR modeling. To the best of our knowledge, this is the most comprehensive N_2O model available in the literature for full-scale MABR applications. The improved N_2O model will be useful for wastewater treatment practitioners to assess effects of any changes in MABR operations on the N_2O emissions. The improved model can also be used to investigate the impacts of adding the MABR process in different process configurations.

O6. Evaluate whether upgrading a full-scale WRRF with a hybrid MABR enhanced removal of OMPs during different seasons.

Very few studies have investigated the removal of organic micropollutants in MABR processes and none of them have been at full-scale or with real wastewater. This study addressed this knowledge gap and demonstrated the removal of select micropollutants by full-scale treatment plants with MABRs. The findings on enhanced removal of OMPs by hybrid MABRs will be of interest to risk assessors, government regulators, and conservation authorities that are responsible for protection of inland water quality and ecosystem health.

6.3 Recommendations for future research

Based on the lessons learned from this research, the following recommendations have been made for future MABR technology research.

- The performance evaluation in this study was done when the plant was operating with an aeration tank SRT of 5 days throughout the year. It would be beneficial to study the process performance at even lower SRTs (2-3 days) to further evaluate the potential of nitrifier seeding in the aeration tank.
- This study evaluated the impact of higher airflow (6 NL m^{-2} hr^{-1}) during warm and cold weather conditions. However, the impact of lower airflow (4.5 NL m^{-2} hr^{-1}) was only investigated during cold weather conditions which resulted in lower nitrification rates. It would be worthwhile to observe the MABR nitrification at the lower airflow under warm weather conditions to further understand the interactive effect of temperature and biofilm thickness.
- This study developed an improved model for investigating the N_2O emissions from hybrid MABR process and validated the model using short term, grab sample data. Future studies could validate the model using long-term, continuously monitored diurnal N_2O data.
- The N_2O model considered two main biokinetic pathways of N_2O formation namely the autotrophic denitrification and heterotrophic denitrification for a simplified approach. Other studies in literature have considered generation of N_2O from hydroxylamine pathway as well. Future N_2O modeling activities in MABR could include the third pathway and evaluate its significance in the overall emission.
- Assessing the removal of organic micropollutants from the full-scale hybrid MABR-CAS plant showed interesting results with a wide range of behavior. However, the mass balance approach was only able to fractionate the removal in terms of MABR and aeration tank. The specific biotransformation capabilities of the MABR biofilm and the suspended sludge in MABR could not be clearly delineated. Bench scale biotransformation studies with MABR biofilm and the anoxic suspended sludge in separate reactors will help us understand the removal mechanisms better.
- This study has demonstrated several process benefits of full-scale MABR adoption. However, MABR technology is not without its limitations. Currently, there is limited knowledge of the impact of inorganic fouling on the MABR performance. Future studies should examine long-term oxygen transfer with MABRs to investigate whether scaling or precipitation of inorganic minerals such as calcium, iron, manganese, etc is significant.

References

Alvarino, T., Lema, J., Omil, F., & Suárez, S. (2018). Trends in organic micropollutants removal in secondary treatment of sewage. *Reviews in Environmental Science and Bio/Technology*, *17*(3), 447–469. https://doi.org/10.1007/s11157-018-9472-3

Bunse, P., Orschler, L., Agrawal, S., & Lackner, S. (2020). Membrane aerated biofilm reactors for mainstream partial nitritation/anammox: Experiences using real municipal wastewater. *Water Research X*, *9*, 100066. https://doi.org/10.1016/j.wroa.2020.100066

Corsino, S. F., & Torregrossa, M. (2022). Achieving complete nitrification below the washout SRT with hybrid membrane aerated biofilm reactor (MABR) treating municipal wastewater. *Journal of Environmental Chemical Engineering*, *10*(1), 106983. https://doi.org/10.1016/j.jece.2021.106983

Downing, L. S., & Nerenberg, R. (2008). Total nitrogen removal in a hybrid, membrane-aerated activated sludge process. *Water Research*, *42*(14), 3697–3708. https://doi.org/10.1016/j.watres.2008.06.006

Hibiya, K., Terada, A., Tsuneda, S., & Hirata, A. (2003). Simultaneous nitrification and denitrification by controlling vertical and horizontal microenvironment in a membrane-aerated biofilm reactor. *Journal of Biotechnology*, *100*(1), 23–32. https://doi.org/10.1016/S0168-1656(02)00227-4

IESO. (2018). *Market Characterization & Conservation Potential for Ontario's Drinking Water & Wastewater Treatment Plants*. http://www.ieso.ca/en/Sector-Participants/IESO-News/2019/02/Water-and-wastewater-treatment-report. Accessed on: May 10, 2023

Jenkins, D., & Wanner, J. (2014). *Activated Sludge – 100 Years and Counting*. IWA Publishing. https://doi.org/10.2166/9781780404943

Kampschreur, M. J., Temmink, H., Kleerebezem, R., Jetten, M. S. M., & van Loosdrecht, M. C. M. (2009). Nitrous oxide emission during wastewater treatment. *Water Research*, *43*(17), 4093–4103. https://doi.org/10.1016/j.watres.2009.03.001

Knowles, G., Downing, A. L., & Barrett, M. J. (1965). Determination of Kinetic Constants for Nitrifying Bacteria in Mixed Culture, with the Aid of an Electronic Computer. *Microbiology*, *38*(2), 263–278. https://doi.org/10.1099/00221287-38-2-263

Lackner, S., Terada, A., Horn, H., Henze, M., & Smets, B. F. (2010). Nitritation performance in membrane-aerated biofilm reactors differs from conventional biofilm systems. *Water Research*, *44*(20), 6073–6084. https://doi.org/10.1016/j.watres.2010.07.074

Long, Z., Oskouie Ali K., Kunetz Thomas E., Peeters Jeff, Adams Nick, & Houweling Dwight. (2020). Simulation of Long-Term Performance of an Innovative Membrane-Aerated Biofilm Reactor. *Journal of Environmental Engineering*, *146*(6), 04020041. https://doi.org/10.1061/(ASCE)EE.1943-7870.0001705

Mehrabi, S., Houweling, D., & Dagnew, M. (2020). Establishing mainstream nitrite shunt process in membrane aerated biofilm reactors: Impact of organic carbon and biofilm scouring intensity. *Journal of Water Process Engineering*, *37*, 101460. https://doi.org/10.1016/j.jwpe.2020.101460

Metcalf and Eddy Inc., George Tchobanoglous, H. Stensel, Ryujiro Tsuchihashi, & Franklin Burton. (2014). *Wastewater Engineering: Treatment and Resource Recovery* (5th Edition). McGraw Hill.

Peeters, J., Adams, N., Long, Z., Côté, P., & Kunetz, T. (2017). Demonstration of innovative MABR low-energy nutrient removal technology at Chicago MWRD. *Water Practice and Technology*, *12*(4), 927–936. https://doi.org/10.2166/wpt.2017.096

Ravishankar, H., Nemeth, A., Massons, G., Puig, D., Zardoya, D., Carpi, N., Lens, P. N. L., & Heffernan, B. (2022). Factors impacting simultaneous nitrification and denitrification in a membrane aerated biofilm reactor (MABR) system treating municipal wastewater. *Journal of Environmental Chemical Engineering*, *10*(5), 108120. https://doi.org/10.1016/j.jece.2022.108120

Stamm, C., Räsänen, K., Burdon, F. J., Altermatt, F., Jokela, J., Joss, A., Ackermann, M., & Eggen, R. I. L. (2016). Chapter Four - Unravelling the Impacts of Micropollutants in Aquatic Ecosystems: Interdisciplinary Studies at the Interface of Large-Scale Ecology. In A. J. Dumbrell, R. L. Kordas, & G. Woodward (Eds.), *Advances in Ecological Research* (Vol. 55, pp. 183–223). Academic Press. https://doi.org/10.1016/bs.aecr.2016.07.002

Terada, A., Yamamoto, T., Igarashi, R., Tsuneda, S., & Hirata, A. (2006). Feasibility of a membrane-aerated biofilm reactor to achieve controllable nitrification. *Biochemical Engineering Journal*, *28*(2), 123–130. https://doi.org/10.1016/j.bej.2005.10.001

Uri-Carreño, N., Nielsen, P. H., Gernaey, K. V., & Flores-Alsina, X. (2021). Long-term operation assessment of a full-scale membrane-aerated biofilm reactor under Nordic conditions. *Science of The Total Environment*, *779*, 146366. https://doi.org/10.1016/j.scitotenv.2021.146366
